2011

THE CHARACTERIZATION OF GROUND ICE DEPOSITS USING GROUND-PENETRATING RADAR TECHNIQUES

Laura I. Thomson

THE CHARACTERIZATION OF GROUND ICE DEPOSITS USING GROUND-PENETRATING RADAR TECHNIQUES

(Spine title: Radar Investigations of Ground Ice Dielectrics)

(Thesis format: Integrated Article)

by

Laura I. Thomson

Graduate Program in Earth Science
(Geophysics and Planetary Science)

A thesis submitted in partial fulfillment
of the requirements for the degree of
Master of Science

The School of Graduate and Postdoctoral Studies

The University of Western Ontario
London, Ontario, Canada

THE UNIVERSITY OF WESTERN ONTARIO
SCHOOL OF GRADUATE AND POSTDOCTORAL STUDIES

CERTIFICATE OF EXAMINATION

Supervisor	Examiners
Dr. Gordon Osinski	Dr. Gerhard Pratt
Supervisory Committee	Dr. Philip Stooke
Dr. Gerhard Pratt	Dr. Robert Shcherbakov

The thesis by

Laura I. Thomson

entitled:

THE CHARACTERIZATION OF GROUND ICE DEPOSITS USING GROUND-PENETRATING RADAR TECHNIQUES

is accepted in partial fulfilment of the
requirements for the degree of
Master of Science

Date_____

Dr. Cameron J. Tsujita
Chair of the Thesis Examination Board

ABSTRACT

This study explores the capabilities of ground-penetrating radar (GPR) in the task of characterizing ground ice and the role this instrument can play in understanding the geomorphology of the cryosphere. The first article investigates the dielectric permittivity of ground ice using on-ice common-midpoint (CMP) GPR surveys conducted over massive stratified segregation ice, non-stratified segregation ice, and polygon ice wedges located on Ellesmere and Devon Islands, Nunavut. In comparison with ice cores, it was found that the dielectric permittivity of ground ice is most influenced by the volumetric ice content. This relationship appears to follow a modified complex refractive index (CRIM) dielectric mixing model. The second study applies the Brewster angle of incidence method to determine the dielectric permittivity of ground ice using endfire CMP surveys conducted atop the active layer. This method was able to predict dielectric permittivities within one dielectric unit of those established in the first article.

Keywords: ground-penetrating radar, ground ice, periglacial geomorphology, Mars geomorphology, analogue studies

ACKNOWLEDGEMENTS

First, thank you to my supervisor, Dr. Osinski, for making this project possible in many ways, for supporting my studies in both my undergraduate and Masters thesis, and for introducing me to the Canadian Arctic three years ago. The field studies component of this thesis became a success thanks to the mentorship and support of W. Pollard and C. Omelon during studies on Ellesmere Island, and the assistance and companionship of T. Unrau, A. Singleton, C. Marion, and J. McCutcheon on Devon Island. I owe these folks a great debt of gratitude for their patience and good humor through the days of wind, cold, and mud. Thank you also to Dr. Pratt who helped me in a pinch when the GPR system was broken, and for being a sounding board on all things "Geophysics" over the past few years. A special thanks goes to Dr. G. Southam for allowing me to conduct all of my ice core analysis in his laboratory and for talking me through analysis techniques. Thanks also to Dr. S. Hicock for sharing his sediment scale, to K. Law for helping me gain access to the department freezers where I sectioned the ice cores, and to B. Price for your patience as I was learning to use the GPR system and for helping in preparing the system for the field. Finally, a sincere thank you goes to the friends, family, and teachers, who have shown a humbling amount of support through all of my academic endeavors.

TABLE OF CONTENTS

LIST OF TABLES

LIST OF FIGURES

1 INTRODUCTION

The nature of ice, with regards to its physical and chemical properties, holds the clues to the climate and environmental conditions at its time of formation. On Earth, ice at the surface reveals annual temperature cycles; in the winter we can observe the growth of sea ice and the accumulation of snow over polar regions and their glaciers, while summer months lead to the total or partial melt of both. Over centuries, the trends in the ebb and flow of these ice masses indicate changes in our global climate. Beneath the soils of Arctic, Antarctic, and high elevation regions where permafrost conditions prevail, these seasonal and long-term climate cycles are similarly recorded in the ice deposits of the frozen ground. Active ice-wedges, forming branching polygonal networks, grow each year with the influx of snowmelt through fractures in the permafrost, whereas subsurface deposits of segregation ice indicate a distinct change in climate as permafrost conditions advance into ground water reserves [*French*, 2007]. The study of periglacial features on Earth has enabled us to spatially and temporally map the growth and retreat of continental ice sheets as well as the onset and demise of continuous permafrost, thus providing the scientific community with proxy information on the climate history of a region.

In 1784 astronomer William Herschel, upon recognizing the two white blemishes at the poles and the similar polar inclinations of Mars and Earth, became the first to postulate the presence of snow and ice on Mars [*Herschel*, 1784]. Unbeknownst to Herschel, his comparisons of Mars and Earth may be considered to be one of the foundations for a contemporary sub-discipline of the Planetary Sciences. Comparative Planetology and analogue studies, ideas that consider the similarities between Earth and other planetary bodies, utilize sites with analogous geological, climatological, or even biological conditions, as a parallel laboratory for

investigations that we cannot yet conduct on other planets. By better understanding the physical processes that define environments on Earth, we can constrain our theories of past and present conditions on other terrestrial bodies, and perhaps even speculate the future of our own planet. In the past ten years, the scientific potential of the Canadian North has come to light for the discipline of planetary analogue research [*Osinski et al.*, 2006]. In particular, the climate and terrain of the arctic have been recognized as effective analogues to regions of Mars thought to be rich in subsurface ice deposits – namely the Northern Plains of the red planet [*Carr and Schaber*, 1977]. The majority of these analogue mission projects have been developed through the Canadian Space Agency's Canadian Analogue Research Network (CARN), and through NASA/CSA's Haughton–Mars Project on Devon Island, NU [*Lee and Osinski*, 2005].

Centuries after Herschel's discovery, the existence of ice on Mars is undoubted in the scientific community and present day theories now question the nature of this ice with respect to its age, the process of emplacement, and the climate conditions at the time of its formation. Indeed, theories of glacial, sea, lake, and ground ice have all been presented as potential explanations for geomorphic features observed on Mars. One means of constraining theories about the origins of ice within landscapes on Mars is to physically characterize the nature of the ice within these landscapes. This idea encompasses the motivation for the following thesis, which explores the hypothesis that the propagation velocity of a ground-penetrating radar (GPR) wave may be used to reveal the physical and chemical nature of ground ice and hereby be used to determine the nature of the ice present.

To test the capabilities of GPR in this task, field studies have been conducted over four ground ice deposits in permafrost environments on Ellesmere Island and Devon Island, Nunavut. Permafrost, broadly, refers to ground perpetually frozen for two or more years [*French*, 2007].

The specifics of sediment grain size, composition, and water content (as ice) of the frozen ground are limitless in variability. Furthermore, the nature of the ice component in frozen ground can vary greatly according to the mode of origin, being one of several forms of congelation, sedimentary, or metamorphic ice, and according to the types of ice inclusions (viz. gases, water, salts, and solid inclusions) [*Shumskii*, 1964]. Of the four sites investigated in this study, stratified segregation ice, non-stratified segregation ice, and ice wedges have been targeted.

As an integrated article formatted thesis, the chapter following this introduction presents background literature for the two articles and covers the nature and occurrence of ice on Earth and Mars, followed by an overview of ground-penetrating radar theory, survey design, and the dielectric properties of ice.

The first article, entitled "Factors controlling the dielectric signature of terrestrial ground ice and considerations for planetary exploration using ground-penetrating radar," compares remotely gathered dielectric measurements, derived from GPR velocity surveys, with validation data including the chemistry and sediment content of ground ice from stratified segregation ice on the Fosheim Peninsula of Ellesmere Island, non-stratified segregation ice and an ice wedge in the vicinity of Thomas Lee Inlet, Devon Island, and an ice wedge hosted in impact melt breccia within the Haughton impact structure on Devon Island. Specifically, common-midpoint surveys were conducted within trenches excavated over the ice deposits using a high-frequency (450 MHz) system. Following the surveys ice cores from each study site were collected and analyzed according to the acidity, conductivity, and the ratio of sediment present. Correlations were then drawn between the dielectric properties observed and the ice core properties to determine the physio-chemical parameters controlling the dielectric properties of ground ice. It was found that the volumetric fraction of ice to sediment present in ground ice deposits plays the greatest role in

defining the dielectric properties of the deposit and that the relationship follows a modified complex refractive index method (CRIM) dielectric mixing model. On the other hand, parameters including pH and conductivity were not statistically correlated to the dielectric properties at the sites considered.

The second article, "Radar wave velocity structure of an ice wedge polygon hosted in segregation ice determined by the reflection coefficient, Thomas Lee Inlet, Devon Island, Nunavut," utilizes GPR surveys conducted atop the active layer (the thawed sediment layer overlying the permafrost table during summer months) rather than within excavated trenches. Though more practical for conventional surveying objectives, the active layer adversely effects signal propagation to the ice deposits and impairs the quality of the resulting GPR data. In an effort to overcome these challenges, the second study of this thesis tests an unconventional cross-polar and endfire mode common-midpoint surveying method presented by Reppert et al. (2000) as a means of determining the dielectric properties of ice deposits from atop the active layer. Unlike traditional CMP velocity analysis methods, the Reppert et al. (2000) technique utilizes the Brewster angle of incidence, indicated by a 90° phase shift in the hyperbolic features of CMP surveys collected in parallel endfire orientation, to determine the dielectric properties of the ice deposits. Comparison of dielectric measurements acquired using the Reppert et al. (2000) method from the active layer with the dielectric properties observed from the on-ice radar surveys in the first article showed that the Reppert method could constrain the dielectric properties of the ground ice within one dielectric unit.

From this Masters thesis there are several positive implications for the application of GPR in a broad range of northern scientific studies including glacial and periglacial history, planetary analogue sciences, and the potential to aid in northern infrastructure development. The

concluding chapter summarizes these results and presents recommendations for future studies involving GPR in permafrost environments, be they on Earth or elsewhere in our solar system. Three appendices follow which summarize the parameters for each of the GPR surveys conducted, the laboratory methods used for ice core analysis, and the processing protocol used for the CMP radargrams.

1.1 BIBLIOGRAPHY

Carr, M. H., and G. G. Schaber (1977), Martian Permafrost Features, *J. Geophys. Res.*, *82*(28), 4039-4054.

French, H., M. (2007), *The Periglacial Environment*, 3 ed., 458 pp., John Wiley & Sons Ltd, West Sussex, England.

Herschel, W. (1784), On the remarkable Appearances at the Polar Regions of the Planet Mars, the Inclination of its Axis, the Position of its Poles, and its spheroidical Figure; with a few Hints relating to its real Diameter and Atmosphere, *Philosophical Transactions of the Royal Society of London 74*, 41.

Lee, P., and G. R. Osinski (2005), The Haughton-Mars Project: Overview of science investigations at the Haughton impact structure and surrounding terrains, and relevance to planetary studies, *Meteoritics & Planetary Science, 40*(12), 1755-1758.

Osinski, G., R. Léveillé, A. Berinstain, M. Lebeuf, and M. Bamsey (2006), Terrestrial Analogues to Mars and the Moon: Canada's Role, *Geoscience Canada, 33*(4), 175-188.

Shumskii, P., A. (1964), *Principles of Structural Glaciology*, Dover Publications, Inc., New York.

2 LITERATURE REVIEW

The following section provides a review of studies concerning ice deposits on Earth and Mars, as well as an overview of ground penetrating radar as a geophysical technique, its application to ice, and the dielectric properties of ice.

2.1 THE NATURE AND OCCURRENCE OF ICE

2.1.1 ICE ON EARTH

Ice comprises 1.7% of the global volume of water, with 68.7% of Earth's freshwater being contained in glacial ice and continental ice sheets, and 0.86% bound in ground ice in permafrost regions, together constituting ~20% of Earths' land surface [*Shumskii*, 1964; *Gleick*, 1996]. With additional contributions from seasonal snow and ice on land, and sea and drift ice over the oceans, ice can comprise 30-50% of the global surface area [*Shumskii*, 1964].

Ice is formed naturally under several different environments on, and under, the surface of the Earth and these differing environments host unique ice formation processes. Shumskii [1964] provides what is likely the most detailed description of natural ice and its many forms in his book "Principles of Structural Glaciology." His approach to ice begins with considering the ice compound to behave as any other rock in geology, which can be categorized as igneous, sedimentary, or metamorphic. For example, ice forming from the freezing of standing water at the surface (e.g., lake or sea ice) would be considered igneous, while glacial ice, formed as a result of multi-year accumulations of snow and eventually lithified under its own pressure, would be considered sedimentary. Metamorphic ice is restricted to regions deep within glaciers where the pressure forces are great enough to restructure the crystal lattice of the formerly sedimentary

ice. Each of these forms of ice are recognizable by their crystal lattice and the amount and type of inclusions within them. Syngenetic ice inclusions are those which are incorporated penecontemporaneously with the ice at the time of formation, such as air bubbles released and captured by the ice during the freezing process (autogenous), or air bubbles incorporated into the ice due to turbulence during the freezing process (xenogenous). Epigenetic inclusions in ice are incorporated after the ice has formed and can be hypogenous or hypergenous in nature. Hypogenous inclusions are those that embed themselves between ice crystals after the ice has fully formed. These may include water formed as a result of increased pressure to the system, or salts precipitated from briney water inclusions as a result of lowered temperatures. Hypergenous inclusions are those which intrude into the ice formation through cracks and fissures, and may be any combination of air, water, or sediment. Both syngenetic and epigenetic inclusions of air, water, and sediment are possible for each type of ice deposit, be it igneous, sedimentary, or metamorphic.

Following from Shumski's "Genetic Classification of Fresh Ice Rock" and "The world of underground ice" by Ross Mackay (1972), the ground ice deposits investigated in this study can be generalized as follows:

(1) Segregation Ice (igneous) – (e.g., stratified segregation ice studied at South Slidre Fiord, Ellesmere Island, NU, and non-stratified segregation ice at Thomas Lee Inlet, Devon Island, NU). Segregation ice is formed *in situ* under slow freezing conditions due to the aggradation of frozen conditions in the subsurface. Ice crystals, which are generally prismatic-granular, hypidiomorphic-granular, or allotrimorphic-granular, can have orientations ranging from being normal to the freezing front, or random. Air bubble

inclusions are rare in segregation ice and sedimentary inclusions are commonly oriented to align with the host sediment.

(2) Perennial vein ice (igneous) – (e.g., ice wedges studied at Thomas Lee Inlet, and Haughton impact structure, Devon Island, NU). Ice wedges are formed due to the intrusion of surface water into thermal contraction cracks and the subsequent freezing of the water as it enters into the permafrost layer. The surface expression of these features can result in extensive polygonal networks of troughs, under which lie the ice wedge deposits. Due to seasonal heat flux variations, the contraction cracks may re-open yearly leading to annual growth of the ice wedges. Sediment drawn into the cracks during melt water entry can lead to vertical stratification in the ice wedges. Ice crystals in wedge ice are commonly allotrimorphic-granular or platy hypidiomorphic-granular, and are oriented parallel to the heat flux gradient or random. Air inclusions of intersertal autogenous and xenogenous nature can make up to 60% of the ice volume.

Ice existing on Mars can be categorized similarly according to Shumski's definitions, whether it be glacial ice, sea ice, or ice-hosting periglacial formations. A summary of studies proposing these types of deposits on Mars follows.

2.1.2 ICE ON MARS

Theories for the existence of ice deposits on Mars, formed under natural hydrological and cryospheric systems similar to those of Earth, range from glacial deposits (both ancient and active), preserved sea and lake ice, and ground-ice incorporated in periglacial features (Figure 3.1).

Glacial Ice

The most significant evidence of ice on Mars lies in the two great polar ice caps. These are present day examples of continental-scale ice sheets on the planet. Already, radar investigations of these deposits have revealed internal layering and a present day thickness of ~300 km and are composed of both frozen carbon dioxide and water ice, with water ice dominating the volume of the northern ice cap, and an 8 m thick rind of permanent frozen carbon dioxide blanketing underlying water ice at the southern pole, as determined by spacebourne radar measurements [*Nunes and Phillips*, 2006; *Phillips et al.*, 2008; *Plaut et al.*, 2007; *Putzig et al.*, 2009; *Seu et al.*, 2007]. It has been proposed that similarly massive ice sheets existed at, or extended to, lower latitudes on the planet during periods of low obliquity. For example, Hiesinger and Head [2000] suggest that the removal or retreat of a continental scale ice sheet, comparable in size to the Laurentide ice sheet on Earth, may have caused enough tectonic disturbance, in the form of brittle deformation during isostactic rebound, to tectonically form the giant polygons observed throughout the Utopia basin in the northern hemisphere of Mars. In addition to ice sheets, many have suggested the occurrence of smaller-scale glacial activity in the lower latitudes of Mars occurring as recently as the late-Amazonian era (viz. the last billion years). In studies of a fan-shaped deposits on the western slopes of Arsia Mons, one of the three Tharsis Montes volcanoes, Head and Marchant [2003], and Shean et al. [2007] conclude that moraine-like features and hummocky terrain interpreted as a sublimation tills are evidence of a former cold-based mountain glacier formed during the Amazonian era. Similarly, lobate piedmont-like glaciers observed using the European Space Agency's High Resolution Stereo Camera (HRSC) have been proposed to flow near the base of Olympus Mons, the highest volcano on the planet, and within the caldera and on the flanks of Hecates Tholus [*Hauber et al.*,

2005; *Head et al.*, 2005; *Neukum et al.*, 2004]. Some glacial features even suggest the existence of complex valley networks similar to those seen flowing from ice fields on Earth [*Head et al.*, 2006]. It is thought that the high elevations of these volcanoes and other mountainous terrains, such as the eastern rim of Hellas basin, provided accumulation alcoves for snowfall during periods of obliquity favoring such climates [*Forget et al.*, 2006; *Head et al.*, 2005]. Further evidence for presence of ice in the subsurface of the Hellas Basin and Deuteronilus Mensae is provided by the SHARAD (Shallow Radar) instrument on board the Mars Reconnaissance Orbiter (MRO) [*Holt et al.*, 2008; *Plaut et al.*, 2009]. In addition to buried or debris covered glaciers, rock glaciers have been suggested as an explanation for martian flow features. The rheology of ice-rock mixtures have been modeled by Colaprete and Jakosky [1998] under Mars conditions that would have favored the size and extent of features observed on the surface. Given the climate implications it would hold, there is great excitement surrounding glacier related landforms on Mars. However, Whalley and Azizi [2003] provide a cautionary paper which communicates the importance of vigilance when classifying proglacial features and that, for example, it is very possible that prolatus lobes and ramparts associated with snow fall incorporations into sediment could be misinterpreted as moraine deposits in glacial foregrounds.

Sea and Lake Ice

Under present conditions on Mars, the standing water required to form igneous type sea or lake ice could not exist. However, several scientists have suggested that in Mars' past streams flowed, lakes formed, and massive oceans covered large regions of the planet, as introduced by Parker et al. [1989] and summarized by Clifford and Parker [2001]. A thermodynamical explanation of such conditions and the subsequent implications leading to stream and lake

formation was presented by Carr [1983]. Twenty years later, Carr put forth an argument for the existence and demise of a large ocean covering the northern plains of the planet [*Carr and Head*, 2003], a theory which has been supported by many including Kreslavsky and Head [2002], and Parker et al. [2003]. While it is believed that much of the water reserves from this ocean are now held up in the polar ice caps, some theorists have proposed that sea ice from this frozen ocean has been preserved under a thin veneer of debris. For instance, Murray et al. [2005] provide evidence for a small sea or large lake in the viscinity of southern Elysium, a theory stemming from the presence of plate like terrain that uncannily resembles fractured sea ice seen on Earth. Further support for the existence of floating ice follows from a study of scour marks in the Kasei Valles system and in Echus Chasma, believed to be formed as the keel of icebergs scrape across the underlying sediments [*Woodworth-Lynas and Guigne*, 2003].

Ground Ice in Periglacial Environments

Landscapes in the cryosphere are surface evidence for the presence and nature of subsurface ice deposits. A detailed explanation of terrestrial periglacial features and their thermodymaical, mechanical, and hydrological processes is best presented by French [2007]. For Mars, reviews identifying analogous ground ice features have been provided by both Carr and Schaber [1977], and Rossbacher and Judson [1981]. With the onset of modern spaceborne imagery techniques and the Phoenix robotic lander mission to the high latitudes of Mars, the scientific community is literally beginning to scratch the surface of ground ice studies. The presence of polygonal networks have been interpreted as sublimation polygons, which are formed due to the degradation of a continuous icy mantle [*Lefort et al.*, 2009; *Levy et al.*, 2009] or ice wedge polygons, which are formed as the result of water infiltration and freezing in

thermal contraction cracks into permafrost [*Seibert and Kargel*, 2001; *Yoshikawa*, 2000]. Thermokarst features, collapse depressions formed due to the degradation of subsurface ice, have been observed throughout the northern plains and have been postulated as being formed due to the degradation of ancient frozen thermokarst lakes in the region [*Soare et al.*, 2008; *Ulrich et al.*, 2010; *Warner et al.*, 2010]. Finally, others have identified possible ice-cored mounds in the Utopia basin and believe them to be similar to pingos, a common periglacial feature throughout the Canadian Western Arctic as well as Siberia [*Burr et al.*, 2009; *de Pablo and Komatsu*, 2009].

2.2 GROUND PENETRATING RADAR AND ITS APPLICATION TO ICE

Following the great success of the Mars Exploration Rover (MER) missions, the application of ground-penetrating radar in future planetary exploration for ice prospecting objectives has been proposed in several studies [*Arcone et al.*, 2002; *Barfoot et al.*, 2003; *Barfoot et al.*, 2010; *Leuschen et al.*, 2003; *Olhoeft*, 1998; *Stillman and Olhoeft*, 2004]. The recognized potential of GPR has likely motivated the WISDOM (Water Ice and Subsurface Deposit Observations on Mars) team of the European Space Agency to include in their ExoMars mission suite a 500 MHz to 3 GHz GPR system with cross-polarimetric capabilities [*Hamran et al.*, 2007; *Plettemeier et al.*, 2009a; *Plettemeier et al.*, 2009b; *Plettemeier et al.*, 2009c].

2.2.1 BASIC PRINCIPLES OF GROUND-PENETRATING RADAR

Ground penetrating radar is an active geophysical technique that responds to inhomogeneities in the dielectric properties of a medium. The dielectric permittivity of a material refers to the ability of molecules in the material to become polarized in the presence of an electromagnetic field. Typically, GPR systems utilize two antennas: a transmitter (Tx), which

generates an EM field by propagating a current through a coil; and the receiver (Rx), which is a passive loop which detects wave-fronts reflected from a favorable orientation (Figure 2.1).

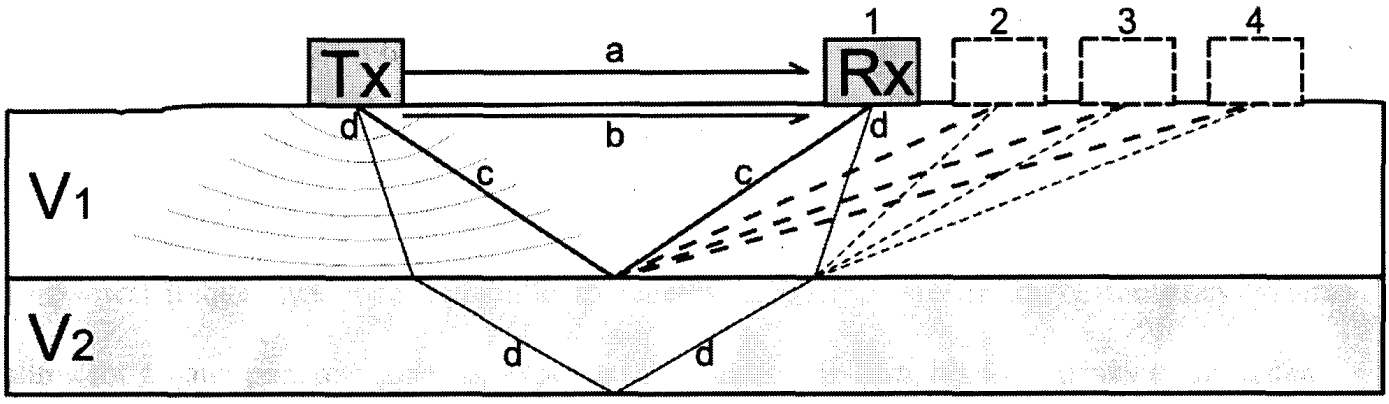

Figure 2.1. Schematic of radar wave propagation through the subsurface, where $V_1 < V_2$.

As depicted in Figure 2.1, the radar signal propagates from the transmitter (Tx) in a conical wavefront. The first wave to arrive at the receiver (Rx) is the airwave (a), which is followed by the direct wave (b). Both of these waves have linear wave paths. Waves propagating downwards at the correct incident angle (c) meet a horizontal boundary, such as that between V1 and V2, part of the wave reflects upwards to the receiver (Rx), which is symmetrically positioned around a common mid-point. Wave scattering occurs at these boundaries, such that adjusting the Rx to positions 2, 3, or 4, enables wide angle reflections to be received. Waves are also refracted (d) at boundaries. With favorable geometry and adequate signal strength, the refracted waves can reflect off lower boundaries and be received at the surface. The depth of penetration of a GPR system is dependent on the signal strength, dielectric permittivity of the subsurface materials, and the degree of signal loss associated with scattering and attenuation effects, the latter of which is heightened in high-conductivity materials.

Several parameters in the GPR system may be changed for the purpose of resolving a desired target, the first of these being the frequency of the electromagnetic wave that the instrument produces (see Reynolds, [1997]). In all cases, lower frequency waves require larger antenna and vice versa for high frequency waves. The minimum thickness of a layer that can be resolved is commonly accepted to be ¼ λ where the wavelength (λ) is defined as velocity (m/s) divided by frequency (1/s or Hz). In turn, the depth of penetration is a function of frequency, with lower frequency signals being able to penetrate deeper. However, lower frequency systems allow for greater penetration at the expense of resolution. In turn, high frequency systems can detect finer structures in the subsurface, but the signal may not be able to detect deeper features. On glacial ice, operating with frequencies of 12.5-200 MHz have enabled resolving the base of glaciers over 150 m thick [*Shean and Marchant*, 2010]. A similarly wide range of frequencies has been applied in permafrost regions (50-800 MHz) according to the depth of the target material [*Brandt et al.*, 2007; *Judge et al.*, 1991].

2.2.2 SURVEY DESIGN

Altering the separation and orientation of the antenna may also be used to exploit signal returns from the subsurface. Common-offset surveys, where the Tx and Rx are kept at fixed distances as they are moved together across a target, are the most popular survey design for GPR profiling. Application of these techniques have enabled glaciologists to resolve sub-glacial lakes, internal layering, and the peizometric boundary (the transition between cold and temperate ice) within glaciers [*Bingham and Siegert*, 2007; *Bogorodsky et al.*, 1985; *Gudmandsen*, 1975; *Woodward and Burke*, 2007]. In periglacial environments GPR profiling has enabled users to

map the extent of buried glacial ice, ice lenses, ice wedges, and internal sediment layers within the ice [*Brandt et al.*, 2007; *De Pascale*, 2008; *Hinkel et al.*, 2001; *Judge et al.*, 1991].

For common midpoint surveys (CMP) the two antennae are centred about a mid-point above the target, and then moved apart from one another in steps, the size of which is dependent on the operating frequency (higher frequencies require smaller steps). As the antenna move away from one another, the time for the radar wave to arrive at Rx increases as a function of the survey geometry and the unique radar wave velocity associated with the material through which the wave passes. Corrections must be applied to CMP survey results collected over dipping horizons, and these procedures can be found in most Applied Geophysics texts (e.g., Reynolds, [1997]). Though used less commonly in practice, CMP surveys enable the user to determine dielectric permittivity of the subsurface medium K_r according to

$$K_r = (c/v)^2 \tag{2.1}$$

where c = speed of light and v = radar wave velocity. In this way the user can determine the dielectric properties of the subsurface rather than using empirical dielectric values, which is typical of common-offset surveys.

Similar to the CMP method, wide-angle (WA) surveys involve increasing the separation of the antenna but, in this case, the transmitter remains stationary and the receiver moves away from it in predefined steps. The radar data acquired from wide-angle surveys are similar to those of CMP surveys in that they can be used to determine the radar-wave velocities.

In addition to the geometric progression of the antenna through the survey, the orientation of the antenna relative to one another and to the survey line alters the signal returned to the receiver. As noted in the following section on the dielectric properties of ice, GPR is sensitive to isotropic effects induced by the crystal lattice of ice such that various antenna orientations yield

differing results in the radargram. As part of the field procedures, CMP surveys were conducted in perpendicular broadside, parallel endfire, and cross-polar orientations (Figure A1-2).

2.2.3 THE DIELECTRIC PERMITTIVITY OF ICE

A detailed study of the electrical properties of ice is presented in "Physics of Ice," by Petrenko and Whitworth [1993]. The response of ice to an electromagnetic (EM) field introduced by GPR systems is defined by the dielectric permittivity of the ice, which dictates the speed of the radar wave and the reflective and refractive paths of the signal. "Dielectric" refers to the ability of a medium to become polarized in the presence of an EM field. Inherently, this is a property of electrical insulators – those materials that cannot conduct charge. "Permittivity" refers to the ability of a material to resist an external EM field by means of becoming polarized with an internal dipole moment that counteracts that of the introduced field, following from Lenz's Law of induction [*Young and Freedman*, 2004]. As such, materials with a high permittivity are best able to resist signal propagation by becoming polarized more readily and, subsequently, these materials cause lower radar wave velocities.

The polarization of ice can occur as a result of two possible processes [*Petrenko and Whitworth*, 1993]. Firstly, in the presence of an EM field the electron cloud surrounding the nuclei of the individual atoms within the molecules of the ice will shift into an orientation that counteracts the EM field direction. Secondly, the reorientation of dipolar molecules (e.g., H_2O) to align in a vector opposing the external EM field can lead to a net polarization of the material. While this is the general rule, the crystal lattice of a material may constrain the direction of the induced dipole such that it may not be oriented in the exact opposite direction of the primary EM field. This isotropic effect has been observed in GPR studies of first year sea ice, known to have

a horizontal c-axis crystal orientation causing the ice to be transparent (no reflections) in perpendicularly oriented antenna configurations and reflective for parallel oriented antennae [*Lalumiere*, 2006]. In the presence of an EM field, both of aforementioned processes can contribute to the polarization of ice, though it is this second reorientation of water molecules that holds the greatest effect following from the inherent dipole moment of the H_2O molecule in ice [*Glen and Paren*, 1975].

Given that it is the reorientation of H_2O molecules that induces a dipole moment in ice, how is it possible for these molecules to reorient while bound in the ice lattice? The following explanation is a summary of that presented by Glen and Paren [1975]. In the simplest case, the H_2O molecules in ice follow the Bernal-Fowler rules which state that (1) every oxygen atom is covalently bound to two hydrogen atoms, such that water is not ionic, and (2) that a hydrogen atom exists between the oxygen bonds between two H_2O molecules, the rule which keeps H_2O molecules drawn to one another as required by their inherent dipole moment (hydrogen bonding). If the first of the Bernal-Fowler rules are broken, this is referred to as an ionic defect. There are two types of ionic defects, one where H^+ is produced, and one where OH^- is produced. If the second Bernal-Fowler rule is broken, then the space between oxygen atoms may have either two hydrogen atoms between them, or, no hydrogen atoms between them. These are referred to as Bjerrum 'D' (double) or 'L' (vacant) defects, respectfully. As a result, there are four possible ways in which the Bernal-Fowler rules may be broken, thereby enabling the mobilization of H_2O molecules for reorientation. While it seems intuitive that ionic defects go hand in hand, such that for every H^+ produced there is a corresponding OH^-, the presence of soluable inclusions in ice can skew the chemistry to favor an imbalance in ratios (see example of HF inclusions from Glen and Paren [1975]. Similarly, fractures and fissures in ice can interrupt

and unbalance Bjerrum defects depending on whether the fissure is in-filled with a medium that draws or repels hydrogen atoms to, or from, the fractured surface. Locations in the ice lattice at which any one of the Bernal-Fowler rules is broken are referred to as "point defects." The coexistence and balance between positive and negative ionic point defects, and between L and D Bjerrum defects, indicates that even pure ice without chemical inclusions or physical disturbances can become polarized in the presence of an EM field. However, inclusions in ice provide greater opportunities for Bernal-Fowler rules to be broken and as such, generally increases the ability for the material to become polarized.

The dipole moment induced in ice in the presence of an EM field does not appear or disappear instantaneously when the field is turned on or off. As explained by Petrenko [1993], this time-dependence explains why the dielectric properties of ice can be frequency dependent. For example, at lower frequencies polarization is dominated by molecular polarization (process 2 above) and, to a significantly lesser extent, atomic polarization (process 1). However, the Debye relaxation time, being the time it takes for the material to polarize to a strength that acts as a perfect capacitor – for molecular polarization lags behind the signal period at higher frequencies such that atomic polarization, having a more rapid Debye relaxation time – is the dominant process dictating the dielectric properties. At the 10-1000 MHz range, which includes most GPR operating frequencies, the dielectric permittivity of ice is dominated by molecular polarization alone [*Petrenko*, 1993]. Thus, in this thesis we consider there to be no perturbations associated with frequency in the dielectric permittivities derived.

2.3 BIBLIOGRAPHY

Arcone, S. A., M. L. Prentice, and A. J. Delaney (2002), Stratigraphic profiling with ground-penetrating radar in permafrost: A review of possible analogs for Mars, *J. Geophys. Res.*, *107*(E11), 5108.

Barfoot, T., G. M. T. D'Eleuterio, and A. P. Annan (2003), Subsurface surveying by a rover equipped with ground-penetrating radar, paper presented at Intelligent Robots and Systems, 2003. (IROS 2003). Proceedings. 2003 IEEE/RSJ International Conference on, 27-31 Oct. 2003.

Barfoot, T., P. T. Furgale, G. R. Osinski, N. Ghafoor, and K. K. Williams (2010), Field testing of robotic technologies to support ground ice prospecting in martian polygonal terrain, *Planetary and Space Science*, *58*(4), 671-681.

Bingham, R. G., and M. J. Siegert (2007), Radio-Echo Sounding over Polar Ice Masses, *Journal of Environmental and Engineering Geophysics*, *12*(1), 16.

Bogorodsky, V. V., C. R. Bentley, and P. E. Gudmandsen (1985), *Radioglaciology*, D. Reidel Publishing Company, Dordrecht, Holland.

Brandt, O., K. Langley, J. Kohler, and S.-E. Hamran (2007), Detection of buried ice and sediment layers in permafrost using multi-frequency Ground Penetrating Radar: A case examination on Svalbard, *Remote Sensing of Environment*, *111*(2-3), 212-227.

Burr, D. M., K. L. Tanaka, and K. Yoshikawa (2009), Pingos on Earth and Mars, *Planetary and Space Science*, *57*(5-6), 541-555.

Carr, M. H. (1983), Stability of streams and lakes on Mars, *Icarus*, *56*(3), 476-495.

Carr, M. H., and G. G. Schaber (1977), Martian Permafrost Features, *J. Geophys. Res.*, *82*(28), 4039-4054.

Carr, M. H., and J. W. Head, III (2003), Oceans on Mars: An assessment of the observational evidence and possible fate, *J. Geophys. Res.*, *108*(E5), 5042.

Clifford, S., and T. J. Parker (2001), The Evolution of the Martian Hydropshere: Implications for the Fate of a Primordial Ocean and the Current State of the Northern Plains, *Icarus*, *154*(1), 40.

Colaprete, A., and B. M. Jakosky (1998), Ice flow and rock glaciers on Mars, *J. Geophys. Res.*, *103*(E3), 5897-5909.

de Pablo, M. Á., and G. Komatsu (2009), Possible pingo fields in the Utopia basin, Mars: Geological and climatical implications, *Icarus*, *199*(1), 49-74.

De Pascale, G. P., Pollard, W. H, Williams, K. K. (2008), Geophysical mapping of ground ice using a combination of capacitive coupled resistivity and ground-penetrating radar, Northwest Territories, Canada, *Journal of Geophysical Research, 113*.

Forget, F., R. M. Haberle, F. Montmessin, B. Levrard, and J. W. Head (2006), Formation of Glaciers on Mars by Atmospheric Precipitation at High Obliquity, *Science, 311*(5759), 368-371.

French, H., M. (2007), *The Periglacial Environment*, 3 ed., 458 pp., John Wiley & Sons Ltd, West Sussex, England.

Gleick, P. H. (1996), Water Resources. In *Encyclopedia of Climate and Weather*, ed. by S. H. Schneider, Oxford University Press, New York, vol. 2, pp.817-823.

Glen, J. W., and G. J. Paren (1975), The Electrical Properties of Snow and Ice, *Journal of Glaciology, 15*(73), 24.

Gudmandsen, P. E. (1975), Layer Echos in Polar Ice Sheets, *Journal of Glaciology, 15*(73), 7.

Hamran, S. E., T. Berger, L. Hanssen, M. J. Oyan, V. Ciarletti, C. Corbel, and D. Plettemeier (2007), A prototype for the WISDOM GPR on the ExoMars mission, paper presented at Advanced Ground Penetrating Radar, 2007 4th International Workshop on, 27-29 June 2007.

Hauber, E., et al. (2005), Discovery of a flank caldera and very young glacial activity at Hecates Tholus, Mars, *Nature, 434*(7031), 356-361.

Head, J. W., and D. R. Marchant (2003), Cold-based mountain glaciers on Mars: Western Arsia Mons, *Geology, 31*(7), 641-644.

Head, J. W., D. R. Marchant, M. C. Agnew, C. I. Fassett, and M. A. Kreslavsky (2006), Extensive valley glacier deposits in the northern mid-latitudes of Mars: Evidence for Late Amazonian obliquity-driven climate change, *Earth and Planetary Science Letters, 241*(3-4), 663-671.

Head, J. W., et al. (2005), Tropical to mid-latitude snow and ice accumulation, flow and glaciation on Mars, *Nature, 434*(7031), 346-351.

Hiesinger, H., and J. W. Head, III (2000), Characteristics and origin of polygonal terrain in southern
Utopia Planitia, Mars: Results from Mars Orbiter Laser Altimeter and Mars Orbiter Camera data, *J. Geophys. Res., 105*(E5), 11999-12022.

Hinkel, K. M., J. A. Doolittle, J. G. Bockheim, F. E. Nelson, R. Paetzold, J. M. Kimble, and R. Travis (2001), Detection of subsurface permafrost features with ground-penetrating radar, Barrow, Alaska, *Permafrost and Periglacial Processes, 12*(2), 179-190.

Holt, J. W., et al. (2008), Radar Sounding Evidence for Buried Glaciers in the Southern Mid-Latitudes of Mars, *Science*, *322*(5905), 1235-1238.

Judge, A. S., C. M. Tucker, J. A. Pilon, and B. J. Moorman (1991), Remote Sensing of Permafrost by Ground-Penetrating Radar at Two Airports in Arctic Canada, *Arctic 44*(1), 9.

Kreslavsky, M., and J. W. Head (2002), Fate of outflow channel effluents in the northern lowlands of Mars: The Vastitas Borealis Formation as a sublimation residue from frozen ponded bodies of water, *Journal of Geophysical Research*, *107*(E125121), 25.

Lalumiere, L. (2006), Ground Penetrating Radar for Helicopter Snow and Ice Surveys*Rep.*, 48 pp, Bedford Institude of Oceanography, Dartmouth, Nova Scotia.

Lefort, A., P. S. Russel, N. Thomas, A. S. McEwen, C. M. Dundas, and R. L. Kirk (2009), Observations of periglacial landforms in Utopia Planitia with the High Resolution Imaging Science Experiment (HiRISE), *Journal of Geophysical Research*, *114*(E04005), 18.

Leuschen, C., P. Kanagaratnam, K. Yoshikawa, S. Arcone, and P. Gogineni (2003), Design and field experiments of a ground-penetrating radar for Mars exploration, *J. Geophys. Res.*, *108*(E4), 8034.

Levy, J. S., J. W. Head Iii, and D. R. Marchant (2009), Thermal contraction crack polygons on Mars: Classification, distribution, and climate implications from HiRISE observations, *Journal of Geophysical Research*, *114*, 19.

Murray, J. B., et al. (2005), Evidence from the Mars Express High Resolution Stereo Camera for a frozen sea close to Mars' equator, *Nature*, *434*(7031), 352-356.

Neukum, G., et al. (2004), Recent and episodic volcanic and glacial activity on Mars revealed by the High Resolution Stereo Camera, *Nature*, *432*(7020), 971-979.

Nunes, D. C., and R. J. Phillips (2006), Radar subsurface mapping of the polar layered deposits on Mars, *Journal of Geophysical Research*, *111*, 16.

Olhoeft, G. (1998), Ground Penetrating Radar on Mars, paper presented at Seventh International Conference on Ground Penetrating Radar, Lawrence, Kansas, USA, May 27-30, 1998.

Parker, T. J., et al. (1989), Transitional morphology in West Deuteronilus Mensae, Mars: Implications for modification of the lowland/upland boundary, *Icarus*, 82(1), 111-145.

Petrenko, V. F. (1993), Electrical Properties of Ice, *Rep.*, 81 pp, US Army Corps of Engineers, Cold Regions Research & Engineering Laboratory.

Phillips, R. J., et al. (2008), Mars North Polar Deposits: Stratigraphy, Age, and Geodynamical Response, *Science*, *320*(5880), 1182-1185.

Plaut, J. J., A. Safaeinili, J. W. Holt, R. J. Phillips, J. W. Head, III, R. Seu, N. E. Putzig, and A. Frigeri (2009), Radar evidence for ice in lobate debris aprons in the mid-northern latitudes of Mars, *Geophys. Res. Lett.*, *36*(2), L02203.

Plaut, J. J., et al. (2007), Subsurface Radar Sounding of the South Polar Layered Deposits of Mars, *Science*, 1139672.

Plettemeier, D., V. Ciarletti, S. Hamran, C. Corbel, S. Linke, and W. Benedix (2009a), Design and Performance of the WISDOM Antenna System aboard the ExoMars Rover, paper presented at European Geosciences Union General Assembly, Vienna, Austria, 19 – 24 April, 2009.

Plettemeier, D., S. Balling, W. S. Benedix, V. Ciarletti, S. E. Hamran, C. Corbel, and S. Linke (2009b), Ultra light-weight antenna system for full polarimetric GPR applications, paper presented at EUROCON 2009, EUROCON '09. IEEE, 18-23 May 2009.

Plettemeier, D., V. Ciarletti, S. E. Hamran, C. Corbel, P. Cais, W. S. Benedix, K. Wolf, S. Linke, and S.
Roddecke (2009c), Full polarimetric GPR antenna system aboard the ExoMars rover, paper presented at Radar Conference, 2009 IEEE, 4-8 May 2009.

Putzig, N. E., R. J. Phillips, B. A. Campbell, J. W. Holt, J. J. Plaut, L. M. Carter, A. F. Egan, F. Bernardini, A. Safaeinili, and R. Seu (2009), Subsurface structure of Planum Boreum from Mars Reconnaissance Orbiter Shallow Radar soundings, *Icarus*, *204*(2), 443-457.

Reynolds, J. (1997), *An Introduction to applied and environmental geophysics*, John Wiley & Sons, Inc., West Sussex, England.

Reppert, P. M., F. D. Morgan, and M. N. Toksöz (2000), Dielectric constant determination using ground-penetrating radar reflection coefficients, *Journal of Applied Geophysics*, *43*(2-4), 189-197.

Rossbacher, L. A., and S. Judson (1981), Ground ice on Mars: Inventory, distribution, and resulting landforms, *Icarus*, *45*(1), 39-59.

Seibert, N. M., and J. S. Kargel (2001), Small‐scale Martian polygonal terrain: Implications for liquid surface water, *Geophys. Res. Lett.*, *28*(5), 899-902.

Seu, R., et al. (2007), Accumulation and Erosion of Mars' South Polar Layered Deposits, *Science*, *317*(5845), 1715-1718.

Shean, D. E., and D. R. Marchant (2010), Seismic and GPR surveys of Mullins Glacier, McMurdo Dry Valleys, Antarctica: ice thickness, internal structure and implications for surface ridge formation, *Journal of Glaciology*, *56*, 48-64.

Shean, D. E., J. W. Head, III, J. L. Fastook, and D. R. Marchant (2007), Recent glaciation at high elevations on Arsia Mons, Mars: Implications for the formation and evolution of large tropical mountain glaciers, *J. Geophys. Res.*, *112*(E3), E03004.

Shumskii, P., A. (1964), *Principles of Structural Glaciology*, Dover Publications, Inc., New York.

Soare, R. J., G. R. Osinski, and C. L. Roehm (2008), Thermokarst lakes and ponds on Mars in the very recent (late Amazonian) past, *Earth and Planetary Science Letters*, *272*(1-2), 382-393.

Stillman, D., and G. Olhoeft (2004), GPR and Magnetic Minerals at Mars Temperatures, paper presented at Tenth International Conference on Ground Penetrating Radar, Delft, The Netherlands, 21-24 June, 2004.

Ulrich, M., A. Morgenstern, F. Günther, D. Reiss, K. E. Bauch, E. Hauber, S. Rössler, and L. Schirrmeister (2010), Thermokarst in Siberian ice-rich permafrost: Comparison to asymmetric scalloped depressions on Mars, *J. Geophys. Res.*, *115*(E10), E10009.

Warner, N., S. Gupta, J.-R. Kim, S.-Y. Lin, and J.-P. Muller (2010), Hesperian equatorial thermokarst lakes in Ares Vallis as evidence for transient warm conditions on Mars, *Geology*, *38*(1), 71-74.

Whalley, W. B., and F. Azizi (2003), Rock glaciers and protalus landforms: Analogous forms and ice sources on Earth and Mars, *J. Geophys. Res.*, *108*(E4), 8032.

Woodward, J., and M. J. Burke (2007), Applications of Ground-Penetrating Radar to Glacial and Frozen Materials, *Journal of Environmental and Engineering Geophysics*, *12*(1), 17.

Woodworth-Lynas, C., and J. Guigne (2003), Ice Keel Scour Marks on Mars: Evidence for Floating and Grounding Ice Floes in Kasei Valles, *Oceanography*, *16*(4), 8.

Yoshikawa, K. (2000), Contraction cracking and ice wedge polygons in Mars, paper presented at The Second international Conference on Mars Polar Science and Exploration, Reykjavik, Iceland, August 21-25, 2000.

Young, H. D., and R. A. Freedman (2004), *Sears and Zemansky's University Physics with Modern Physics*, 11 ed., Pearson Education, Inc. as Addison Wesley, San Francisco.

3

FACTORS CONTROLLING THE DIELECTRIC SIGNATURE OF TERRESTRIAL GROUND ICE AND COSIDERATIONS FOR PLANETARY EXPLORATION USING GROUND-PENETRATING RADAR

Laura I. Thomson[1], Gordon R. Osinski[1], and Wayne Pollard[2]

[1]Departments of Earth Sciences and Physics and Astronomy, University of Western Ontario, London, ON, Canada N6A 5B7.

[2]Department of Geography, McGill University, Montreal, QC, H3A 2K6

Abstract

The presence of polar ice caps, in addition to proposed glacial and periglacial landforms on the surface of Mars, advocates for the exploration of these features that may, as they do on Earth, reveal the ancient climate conditions and provide information as to the history of water on the planet. Given numerous recommendations suggesting that ground-penetrating radar (GPR) applications should play a role in understanding the nature of these features, we have explored the dielectric properties of stratified segregation ice, non-stratified segregation ice, and polygon ice wedge deposits in the Canadian Arctic using common-midpoint velocity methods with a 450 MHz GPR. In comparison with ice cores collected from these sites, we have found that the volumetric fraction of ice to sediment present in ground ice deposits plays the greatest role in defining the dielectric properties of the deposit and that the relationship follows a modified complex refractive index method (CRIM) mixing model. On the other hand, parameters including pH and conductivity were not statistically correlated to the dielectric properties at the sites considered. Following from our modified CRIM model, we provide values of the expected dielectric permittivity for several ground ice deposits on Earth according to ice content and

provide estimates for similar features on Mars using laboratory derived and theoretical values of permittivity for Martian sediments.

1. Introduction

On Earth, the relationship between ice and climate is clear. We recognize the ebb and flow of both glacial termini and sea ice extents to be indicators of our presently changing climate. In addition, periglacial and glacial landscapes can reveal the paleoclimate and geological histories of entire regions [*Mackay*, 1972].

Motivated by the geomorphic evidence available from spaceborne observation initiatives over the past several decades, numerous studies proposing the existence of ice deposits in the Martian subsurface have arisen [*Carr and Schaber*, 1977; *Mangold and Allemand*, 2001; *Rossbacher and Judson*, 1981]. As the quality of this imagery improves with continued missions (e.g., High Resolution Imaging Science Experiment (HiRISE) and the High Resolution Stereo Camera (HRSC)), the level of detail available for geomorphic interpretation has enabled planetary scientists to speculate the role, and ultimately the nature, of ice incorporated in landforms across the planet. These observations have motivated theories predicting the existence of glacial ice [*Colaprete and Jakosky*, 1998; *Forget et al.*, 2006; *Hauber et al.*, 2005; *Head and Marchant*, 2003; *Head et al.*, 2006; *Head et al.*, 2005; *Neukum et al.*, 2004; *Shean et al.*, 2007], sea and lake ice [*Baker et al.*, 1991; *Carr*, 1983; *Carr and Head*, 2003; *Clifford and Parker*, 2001; *Murray et al.*, 2005; *Parker et al.*, 1993] and periglacial ice deposits on Mars [*Burr et al.*, 2009; *Lefort et al.*, 2009; *Levy et al.*, 2009; *Soare et al.*, 2008] (Figure 3.1).

Discovering the nature and distribution of the ice present within the landscapes identified in the above studies, according to physical and chemical properties, is the key to confirming the validity of, and resolving conflicts between, geomorphic theories surrounding ice-related

features. For the exploration of Mars, many geophysical, geochemical, and isotopic techniques have been suggested to accomplish this task [*Berthelier et al.*, 2003; *Del Vento and Vannaroni*, 2005; *Lacelle et al.*, 2008; *Singleton et al.*, 2010; *Trautner et al.*, 2003].

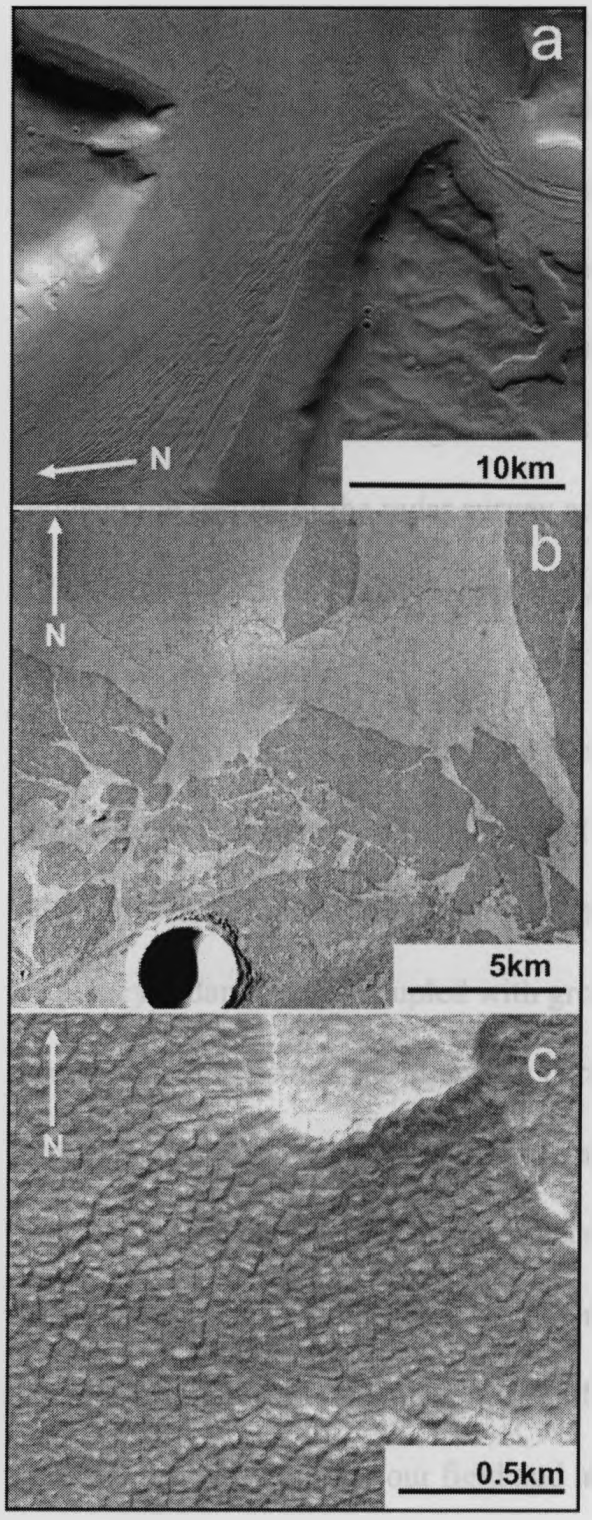

Figure 3.1. Ice-hosting landforms on Mars: a) proposed glacial features in Deuteronilus–Protonilus Mensae area (THEMIS_V03070003) [*Head et al.*, 2006]; b) proposed sea ice features (THEMIS_V27265033) proposed by [*Murray et al.*, 2005]; c) thermokarst scarp formations with high- and low-centred polygons (HIRISE_PSP_002560_1335) [*Levy et al.*, 2009].

Ground-penetrating Radar (GPR), an active geophysical prospecting technique which exploits inhomogeneities in the dielectric properties of the subsurface, has been proposed numerous times as a planetary exploration technique for mapping the spatial extent and abundance of ice [*Arcone et al.*, 2002; *Barfoot et al.*, 2003; *Barfoot et al.*, 2010; *Leuschen et al.*, 2003; *Olhoeft*, 1998; *D. Stillman and Olhoeft*, 2004]. These studies may, in part, have motivated the decision to include a radar system onboard the upcoming ESA ExoMars mission. The WISDOM (Water Ice and Subsurface Deposit Observations on Mars) radar system will operate at 500 MHz to 3 GHz with cross-polarimetric capabilities [*Hamran et al.*, 2007; *Plettemeier et al.*, 2009a; *Plettemeier et al.*, 2009b; *Plettemeier et al.*, 2009c]. As the mission is also equipped with a drill capable of drawing 2 m cores, the potential exists for correlations to be drawn between the results of the radar survey and core analysis. With mission plans already in place for GPR studies of ice on Mars, an appreciation for the dielectric nature of ground ice, in its many formations, is essential.

It is the authors' hope that the results of this study, which explores the dielectric properties of numerous terrestrial ground ice deposits, will aid in the interpretation of the WISDOM radar results and future GPR hosting exploration rovers by providing data from high-frequency radar surveys coupled with ground ice cores on Earth. In turn, we hope that our results, which constrain the dielectric permittivity of ground ice deposits of various origins in the Canadian Arctic, will encourage further applications of GPR as a relatively inexpensive and non-destructive tool for both scientific and economic exploration of northern territories. With this consideration, we have explored the potential high-frequency GPR systems offer for determining the bulk-physical and -chemical nature of ice through the application of radar wave velocity analysis. We will describe our field and laboratory approaches for relating the dielectric

permittivity to the physical and chemical properties of ground ice, and reveal the utility of correlations found between permittivity and volumetric ice content for future GPR investigations of permafrost environments.

2. Terrestrial applications of GPR on ice

Several studies have explored the dielectric properties of ice both experimentally and in the natural environment. Radar applications on glaciers, commonly referred to as radio-echo soundings (RES), were developed through the 1960s and 1970s by glaciologists aiming to understand the dielectric properties of snow and ice and exploit the changes in electrical properties to determine and detect ice thickness and internal horizons within glaciers and ice sheets [*Evans*, 1965; *Fitzgerald*, 1975; *Glen and Paren*, 1975; *Gudmandsen*, 1975; *Oswald*, 1975; *Page and Ramseier*, 1975; *Plewes and Hubbard*, 2001; *Robin*, 1975a; b]. It was these studies that laid the foundation for the development of GPR in other geological investigations [*Annan*, 2002]. The factors controlling the dielectric permittivity of glacial ice, according to the physical and chemical nature of ice sheets, have been explored thoroughly by Fujita et al. [2000], Moore [1993], Moore and Fujita [1993], and Wolff [2000]. Following from both theoretical studies and field-based observations the glaciology community has broadly constrained a dielectric permittivity of 3.2271 (v = 0.167m/ns) for cold and 4 (v = 0.15 m/ns) for temperate glacial ice [*Woodward and Burke*, 2007].

Practical applications of GPR over sea and lake ice have largely focused on resolving ice thickness [*Campbell and Orange*, 1974]. Additionally, experimental and theoretical studies of radar wave propagation have explored the influence of salinity on signal losses [*Iizuka et al.*, 1988], and the relationship between ice crystal orientation and anisotropy of radar signal propagation [*Kovacs and Morey*, 1978].

Ground ice investigations employing GPR have been conducted in the Arctic, Antarctic, and alpine permafrost regions of our planet. Most commonly, these applications use GPR for detecting and spatially mapping the extent of ice deposits associated with geomorphic features such as polygon ice wedges [*Fortier and Allard*, 2004; *Hinkel et al.*, 2001], segregated ice [*De Pascale*, 2008], debris covered glaciers and rock-glaciers [*Brandt et al.*, 2007; *Degenhardt and Giardino*, 2003; *Fukui et al.*, 2007], and pingos [*Yowhikawa et al.*, 2006]. In these cases, the dielectric properties of the ice are rarely measured *in situ*. Instead, they are typically assumed using the empirical dielectric standards for glacial ice, K≈3 [*Davis and Annan*, 1989]. In recognition of this deficiency, we have conducted a series of common-midpoint GPR surveys over ground ice deposits in the Canadian Arctic with the objective of generating an understanding of dielectric properties for subsurface ice of differing origins.

3. Field sites

This study uses the results from four ground ice-bearing permafrost sites in the Canadian Arctic that target horizontally stratified segregation ice, non-stratified segregation ice, and two polygon ice wedges (Figure 3.2).

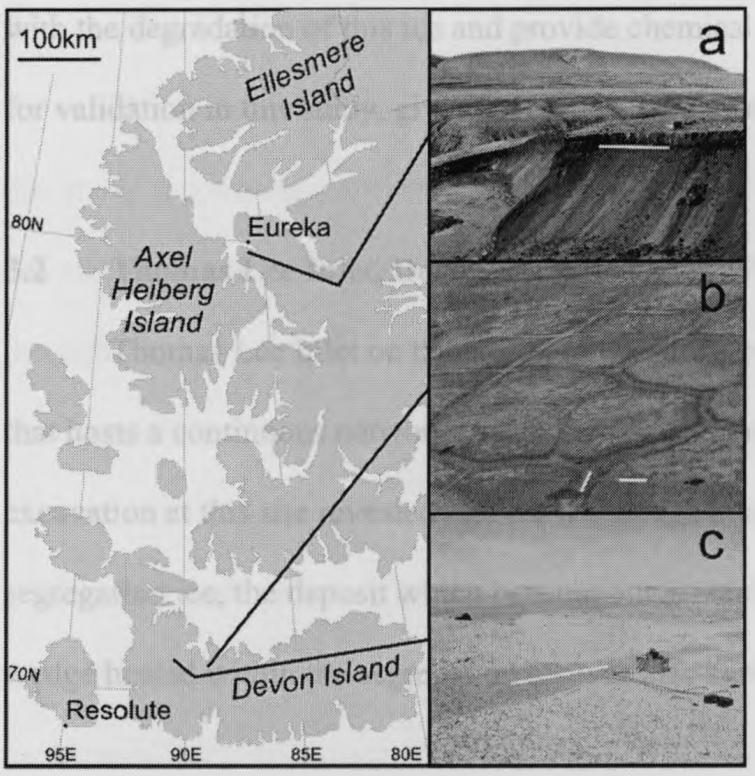

Figure 3.2. Locations of field sites in this study: a) Massive ice thaw slump feature near the southern shore of Slidre Fiord, Ellesmere Island; b) Ice wedges hosted in non-stratified segregation ice, Thomas Lee inlet, Devon Island; c) Ice wedges hosted in impact melt rocks, Haughton impact structure, Devon Island. Survey lines measuring 3 m in length are indicated by white lines in each photograph.

3.1 South Slidre Fiord, Ellesmere Island – 79°55'43"N, 86°01'58"W

The first site of study hosted horizontally stratified segregation ice located at a thaw slump feature on the Fosheim Peninsula in an area south of Slidre Fiord, Ellesmere Island, near the Environment Canada High Arctic Weather Station (HAWS) in Eureka. Studies of the history, nature, and extent of ground ice deposits in the area indicate that the largest deposits were formed during the mid- to late-Holocene, that they are intrasedimental in nature, and that ~30% of the near-surface (<6 m) permafrost is host to ground ice deposits including massive segregation ice, ice lenses, ice wedges, and pore ice [*Couture and Pollard*, 1998; *Pollard*, 2000; *Pollard and Bell*, 1998]. Studies by Barry [1992] highlight slump feature processes associated

with the degradation of this ice and provide chemical and physical data of the ice which are used for validation in this study, given that no ice cores were able to be collected from this site.

3.2 **Thomas Lee Inlet, Devon Island** – 75°21'29" N, 88°40'52" W

Thomas Lee Inlet on the Northern coast of Devon Island ends in a broad outwash plain that hosts a continuous network of ice wedge polygons with no ice exposures present. Shallow excavation at this site revealed that the ice wedge in question lay adjacent to clay- and silt-rich segregation ice, the deposit which became our second target [*Singleton et al.*, 2010]. An ice wedge hosted within the segregation ice was also surveyed as the third target of this study.

3.3 **Haughton impact structure, Devon Island** – 75°22'06" N, 89°31'33" W

The fourth site, located in the Haughton impact structure, is also part of a polygon network, this one being situated atop a 15 metre high plateau of clast-rich impact melt rock formed during a cratering event ~39 million years ago [*Osinski et al.*, 2005]. The primary target at this site is the trough of one of the polygons, approximately 20 metres from the edge of the plateau. Impressive gullies have formed at the point where the troughs of these polygons intersect the cliff-face.

4. Methods and Analysis

Ground-penetrating radar surveys were the primary objective of field operations in this study. As a means of ground-truthing, these surveys were accompanied by sampling of the subsurface via excavation and ice core extraction at the Devon Island sites.

4.1 GPR Field Methods

The Sensors and Software Pulse EKKO 1000 ground-penetrating radar system used in this study is comprised of a main consol, the transmitter and receiver electronics, the transmitter and receiver shielded antenna (450 MHz), a power source, and a main console that is controlled through an external laptop computer. It is common for GPR investigations on ice to utilize common-offset (CO) survey designs, which are those for which the transmitter (Tx) and receiver (Rx) are kept at a fixed separation and moved together across the target thus returning a spatial profile of the subsurface. If the velocity of the radar signal in the subsurface is known then the depth to subsurface reflectors can be determined. In the CO survey mode, this velocity can be determined from diffraction hyperbola off point-reflectors in the subsurface, as demonstrated by [*Brandt et al.*, 2007], or by using the two-way travel time and depth to a known reflector. Velocity may also be acquired by conducting common-midpoint (CMP) or wide-angle (WA) surveys. In this type of survey design the distance separating Tx and Rx is increased incrementally either about a common centre point (CMP), or with Tx remaining stationary and Rx moving away in predefined step sizes (WA). By definition, the radar wave velocity in non-magnetic environments is a function of the dielectric properties (see derivation by Greaves et al. [1996]) and can be calculated from survey geometry according to

$$v = c / [(\mu_r * K_r)^{1/2}] = xt^{-1} \text{ or, } = 2\{[d^2+(0.5x)^2]^{1/2}\}t^{-1}. \quad (3.1)$$

The first term of (3.1) shows radar propagation velocity v as it has been derived from Maxwell's equation (see Greaves et al., 1996) where c is the speed of light, μ_r is the relative magnetic permeability, K_r is the relative dielectric permittivity (K hereafter). The dielectric permittivity is complex, having both real and imaginary parts in the time and frequency domains, respectively. By assuming that frequency dependent variances in the dielectric permittivity are negligible for

frequencies of 10-1000 MHz [*Davis and Annan*, 1989], we can treat our velocity-derived measurements of K as real hereafter. The remaining two terms in (3.1) express velocity according to the travel time and the path length of the radar signal. The second term of (3.1) describes velocity as it can be calculated for the direct-wave path, which travels in the near-subsuface, and the third term describes the velocity according to a path to and from a subsurface reflector located at the midpoint between Tx and Rx. In these latter terms, t represents travel time from Tx to Rx (that is, two-way travel time for term 3), x is antenna separation, and d is the depth to a reflector. In non-magnetic materials, as is the case for target sites in this study, $\mu_r = 1$ and thus that term may be removed from (3.1). The time-distance relationship is linear for the ground wave (also known as the direct wave), and hyperbolic for the reflected wave (see results).

At each of our field sites, both CMP and WA surveys were conducted over the target ice deposit. An initial survey conducted on top of the active layer revealed that signal loss, likely due to a high conductivity environment caused by the presence of water in the fine-grained overburden, inhibited penetration below the permafrost table. To avoid these adverse effects on our measurements of the ground ice dielectric properties, we excavated a trench beyond the length of the survey line (>3 m) down to the ice surface, a depth which was equivalent to the active layer-permafrost boundary (~0.9 m). Each survey reached a maximum Tx-Rx separation of 3 m, with antenna separation increasing in 0.05 m increments. Signal stacking, which refers to multiple pulses being emitted by the transmitter, was used to improve the signal to noise ratio. We collected 64 stacks at each position along the survey line. For most surveys, fiducial marks were taken every metre to ensure that the recorded transect spacing was in agreement with the on-ground geometry.

In conventional GPR surveys, the transmitter and receiver antenna are parallel along the antenna long axis (a.k.a. parallel broadside), such that the signal is being received in the same orientation as it is transmitted. However, [*Kovacs and Morey*, 1978] have shown that the crystal lattice of a medium through which the radar wave propagates may promote polarization in a specific direction. To explore the effect of ice lattice on the propagation of radar waves we tested four antenna orientations during the CMP surveys: 1) Tx and Rx parallel along the antenna long axis (common design, Ori1); 2) Rx rotated 90° to Tx (Ori2); 3) Tx rotated 90° to Rx (Ori3); and 4) both Tx and Rx rotated to be parallel along the antenna short axis (Ori4).

4.2 Ice Sampling

Following GPR surveys on Devon Island, an ice core was collected from the non-stratified ground ice and ice wedge at Thomas Lee Inlet, and the ice wedge in the Haughton impact structure. Cores were drawn from the midpoint of the on-ice CMP transects (1.5 m along the 3 m survey line) after the excavation of the active layer and GPR surveys were conducted. Cores were collected using the US Snow, Ice, and Permafrost Research Establishment (SIPRE) designed core auger, which is comprised of a 1 m core barrel, equipped with removable and replaceable carbide tip cutting bits, which attaches to a gas powered drive motor. Each core measured 0.10 m in diameter and approximately one metre in length. Immediately following extraction, the cores were sealed in sample bags and packed in coolers for transportation south.

4.3 Ice-core Analysis

Ice cores were sectioned into 5 cm long segments, weighed, and melted. The meltwater was filtered using 1.2 micron glass fibre microfilters and measured for pH and conductivity. From each core one sample was further filtered to 0.45 microns and tested for cation and anion

concentrations using ICP-AES and IC methods, respectively. Sediment inclusions from each segment were kiln dried and weighed so that the volume fraction of ice could be determined according to methods described for excess ice in clay and silt by Pollard and French [1980]

$$fV_i = V_i/(V_i+V_s) \qquad \text{for} \qquad V_i = W + (0.09\ W) \qquad (3.2)$$

$$V_s = \gamma_d/P_s$$

where fV_i is the volume fraction of ice, V_i is the volume of ice derived from W the volume of water, and V_s is the volume of sediment derived from γ_d, the dry soil weight, and P_s, the particle density. P_s values used in this study are derived from those of Pollard and French (1980) and clay to silt ratios of 1:1 for the non-stratified segregation ice, 1:0 for the ice wedge at Thomas Lee Inlet, and 3:1 for the ice wedge in Haughton Crater. While cores could not be collected from the South Slidre Fiord site, the ice properties reported by Barry [1992] are used as bulk representations for the ice deposit.

5. Results

5.1 GPR Analysis

The approach taken to prepare the GPR data for comparison with the ice cores is illustrated in Figure 3.3, which shows CMP results collected in conventional antenna orientation (Ori1) from the non-stratified segregation ice deposit at Thomas Lee Inlet as an example. For each of the four sites and antenna orientations the survey radargrams were post-processed and analyzed using the Sensors & Software Ltd. EKKO_View Deluxe processing software. In a statistical assessment of GPR surveys, Jacob and Hermance [2004] indicate that the accuracy of a CMP velocity is +/- 0.001 m/ns, which is considered to be the smallest detectable velocity change in this study. Post processing of the radargrams involved a high-pass filter (DeWOW) to

remove low frequency signal components that cause signal saturation. The need for further adjustments through gain functions was minimal as the direct wave and hyperbolic diffraction features were clear after applying a Dewow function to the data. Direct wave measurements were acquired by computing the slope of the first arrivals. In accordance with Pallavi et al. [2009] the penetration depth of a GPR direct wave signal is related to the operating frequency and can be approximated as one-quarter of the signal wavelength (¼λ=v/4*f*). For surveys collected in Ori1 the direct wave results of CMP surveys range from 0.113 m/ns to 0.155 m/ns which, for a central operating frequency of 450 MHz, suggests direct wave penetration depths of 0.063 – 0.086 m. In turn, these depths translate to a near-surface time horizon of ~0.5ns.

Velocities from the reflected wave paths were picked from hyperbolic features using an internal velocity-picking tool provided by the Sensors & Software EKKO_View2 software package which determines the velocity according to normal moveout (NMO) associated with the increasing offset between Tx and Rx. These measurements gave RMS velocities of 0.113 – 0.155 m/ns between the four sites. The two-way travel time to a depth of 1 m (approximate core depth) for such velocities ranges from 17.7 – 12.9 ns for a zero Tx-Rx offset, and 31.9 – 23.3 ns for a 3 m Tx-Rx offset. Therefore, only hyperbolic features earlier than the 31.9 ns time horizon have been considered when we compare the surveys to the ice cores. As is the case in seismic CMP surveys, the RMS velocity (v_N) for a given layer is a function of the internal velocities (V_N) for the overlying layers with the two-way travel time of each layer (t_N) according to

$$v_N = [\Sigma(V_N^2\, t_N)/\, \Sigma t_N]^{1/2}. \qquad (3.3)$$

As such, the observed RMS velocities picked from the software ought not to be used to calculate the dielectric permittivity without applying a corrective for the overlying layers. To do this, we have utilized a method by Tillard and Dubois [1995], which demonstrates that the seismic Dix equation (3.4) can be applied to GPR data such that

$$V_N^2 = [(t_N v_N^2) - (t_{N-1} v_{N-1}^2)] / (t_N - t_{N-1}) \quad (3.4)$$

may be used to determine the interval velocity within layer *N* (Figure 3, Equation A). An iterative script was created to correct the layers in succession, including the ¼λ layer associated with the direct wave. The corrected velocity measurements were then converted to relative dielectric permittivity using (3.1) (Figure 3.3, Equation B) and the reasonable assumption that μ_r is comparable to the magnetic permeability of free space (μ_o) in the absence of metallic materials. To generate a vertical profile of the dielectric permittivity the time arrivals of the hyperbolic features were converted to depths using the RMS velocities. The thickness (*Th*) of each dielectric layer was calculated via

$$Th = [(t_N - t_{N-1}) v_N] / 2 \quad (3.5)$$

and used to determine the dielectric boundaries within the ice cores (Figure 3.3, Equation C).

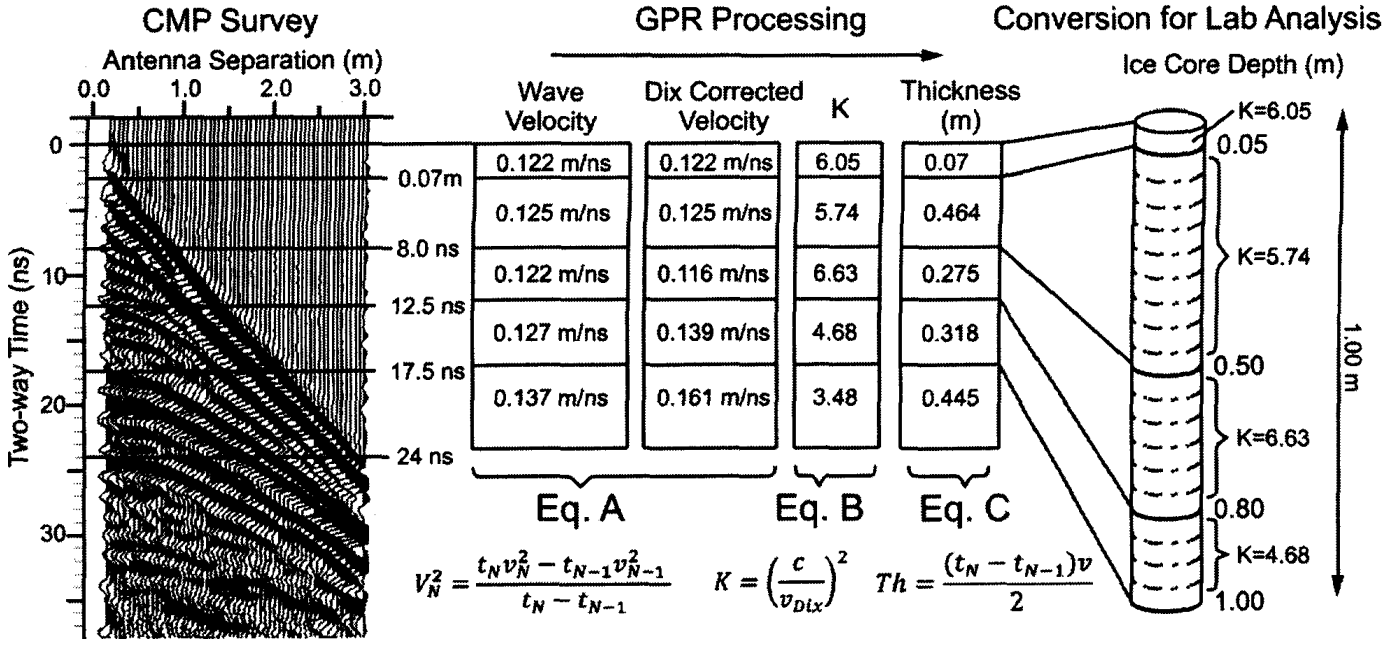

Figure 3.3. Schematic of the post-processing method used to prepare GPR data for comparison with ice core results. In equation A, V refers to the Dix corrected velocity for layer $_N$; v and t are the observed velocities and time horizons for layer $_N$ and the overlying layer $_{N-1}$. Equation B allows dielectric permittivity, K, to be calculated from the Dix velocity (v_{Dix}) and radar wave propagation in free space (c = 0.3 m/ns). Finally, equation C allows the thickness (Th) of layer $_N$ to be calculated using the difference between two-way time horizons ($t_N - t_{N-1}$) and the wave velocity of $_N$.

Calculating the reflection coefficient (RC) between adjacent dielectric units can provide confirmation that observed changes in dielectric permittivity are true and not artefacts of noise

$$RC = [(K_{r1})^{1/2} - (K_{r2})^{1/2}] / [(K_{r1})^{1/2} + (K_{r2})^{1/2}]. \quad (3.6)$$

As stated by Annan [1996], the RC between adjacent units with permittivities of K_{r1} and K_{r2} should be greater than 0.10 for unstacked data, or RC > 0.10/[(# of stacks)$^{1/2}$]. Thus, for our surveys collected with 64 stacks, the RC must be greater than 0.0125 as was the case for all of the horizons we detected between hyperbolic features.

While CMP and WA surveys gave similar velocities, we found that CMP surveys generally portrayed stronger reflectors, better clarity, and superior correlation with the ice core data. This finding can likely be attributed to the favourable geometry of CMP surveys that

focuses the vertex of each reflected signal along a vertical profile corresponding to where the ice core was collected. As such, all of the results we present here, except for the rare cases where CMP survey results were of considerable lesser quality, are derived from CMP surveys. Similarly, surveys conducted in cross-polar orientations showed lower quality profiles and the few velocities that were apparent varied little from those collected in Ori1. For this reason the results that follow are derived from surveys conducted in conventional antenna orientation.

5.2 Ice Core Analysis

Once the GPR results were converted into a vertical dielectric profile for each site, ice core data was averaged according to the dielectric horizons identified in Figure 3c and plotted against dielectric permittivity (Figure 4, Ori1 results). As only an averaged measure pH and volumetric ice content was available from the stratified segregation ice at South Slidre Fiord these values, representing the top metre of the deposit, have been plotted against a weighted average of the observed dielectric properties for a time horizon equivalent to 1 m depth. Figure 3.4 illustrates the variation of observed dielectric permittivity with these chemical and physical measurements at each of the four sites, with dielectric values from CMP surveys conducted in Ori1. The error associated with manual velocity picking (0.001 m/ns accuracy) lead to a mean error in dielectric permittivity of 0.146±0.057.

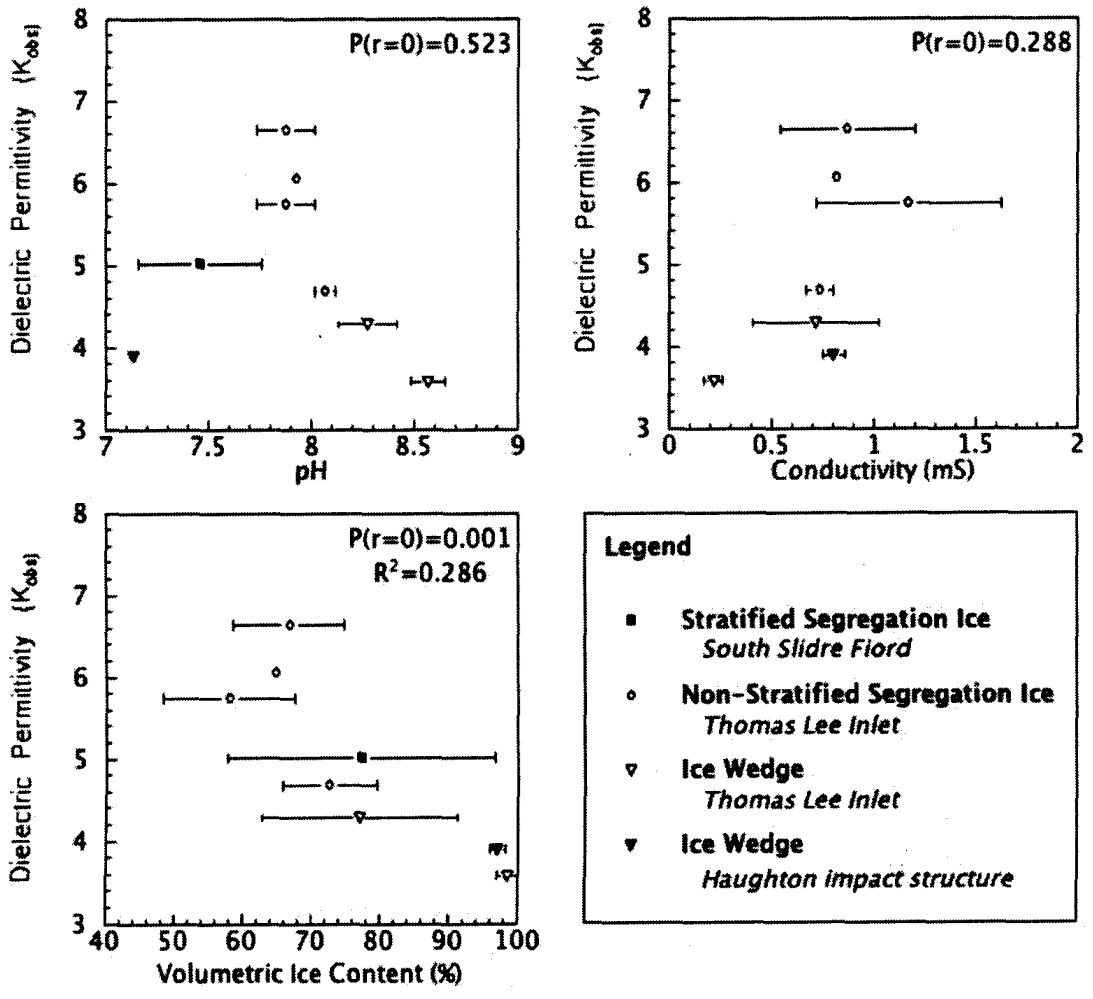

Figure 3.4. Scatter plots of the observed dielectric permittivity for CMP surveys collected in Ori1. Errors for ice core properties are derived from the variation of the property within the dielectric layers, as defined in Figure 3. The statistical correlations presented for each plot are based on linear regressions.

5.3 Data Integration

Polynomial regressions of the data indicate that there are no statistically significant correlations between the observed dielectric properties and the ice core pH and conductivity measurements (P(r=0)>0.05, Figure 3.4a and 3.4b). The effect of acidity on the dielectric properties of ice, a relationship of particular interest in the study of volcanic event horizons in continental ice sheets, has been explored experimentally by Fujita et al. [2000]. By increasing acid concentrations in ice from 1.6 x 10^{-2} to 4.9 x 10^{-2} M, they observed a linear rise from 3.0 to 4.6 in dielectric permittivity values. The correlation lacking between pH and K_r in this study is

very likely associated with the extremely low concentrations of acidic solutes in the ice cores, on the order of 10^{-8} M, which would lead to nominal changes in K_r. Fujita et al. [2000] also studied the effect of conductivity and found conductivity to be dependent on pH and independent of the type of acid, suggesting that the lack of correlation between K_r and conductivity is linked to the low concentrations of acids in the core melt water.

6.0 Discussion

6.1 Dielectric permittivity and volumetric ice content: A modified CRIM model

Though we are unable to detect the relationship between K_r and ice chemistry shown by Fujita et al. [2000], we did find a statistically significant correlation between K_r and the volumetric ice content (fV_i) (Figure 3.4c). A first order regression shows that changes in fVi explain ~30% of the variation in K_r (P(r=0)=0.0014). While empirically this expression relates fV_i to K_r, in practice the dielectric properties of the sediment included in ice deposits must also dictate the effective permittivity of the mixture as a whole. For the purposes of this study, the complex refractive index method (CRIM) developed by Schlumberger [1991] is a favourable dielectric mixing model both for its simplicity and for its primary application as a mixing model for unfrozen saturated sediments; a near parallel to our saturated sediment targets in permafrost environments. As noted by Greaves et al. [1996], the CRIM model is only suitable in low-loss environments; otherwise, the imaginary component of dielectric permittivity must be incorporated so that the frequency dependent component of the permittivity may be accounted for. Being in a low-loss environment, we have adapted the effective permittivity, K_e, as determined by the CRIM model

$$\sqrt{K_e} = \varphi\sqrt{K_w} + (1 - \varphi)\sqrt{K_s}, \qquad (3.7)$$

where K_e is the effective permittivity of the mixture, φ is porosity, and K_w and K_s are the permittivities of water and the host sediment), to suit a frozen environment by substituting the porosity with our fraction of volumetric ice content, *fVi*, and the dielectric permittivity of water with that of ice (K_i)

$$\sqrt{K_e} = fVi\sqrt{K_i} + (1 - fVi)\sqrt{K_s}. \quad (3.8)$$

If we make the assumption that the sediment included in ground ice is dielectrically similar to that of the overlying active layer sediments, we can use CMP velocities of the active layer to determine K_s. In Thomas Lee Inlet, CMP surveys of the active layer over the non-stratified segregation ice and ice wedge yielded velocities of 0.083 m/ns and 0.060 m/ns and subsequent K_s values of 13 and 25, which are in agreement with observed dielectric values of silts and clays, respectively [*Davis and Annan*, 1989]. Integrating the values of K_s and *fVi* values from our ice cores into our adapted CRIM model, we find theoretically derived effective permittivites of 5.78 and 3.38 for the non-stratified segregation ice and ice wedge respectively, which vary by -0.03 and -0.27 to our observed dielectric permittivities of 5.81 and 3.65. Bringing data together from each site, statistical correlation tests indicate that 82% of the variance in the observed permittivity can be accounted for by changes in *fVi*, following the relationship established in the adapted CRIM model.

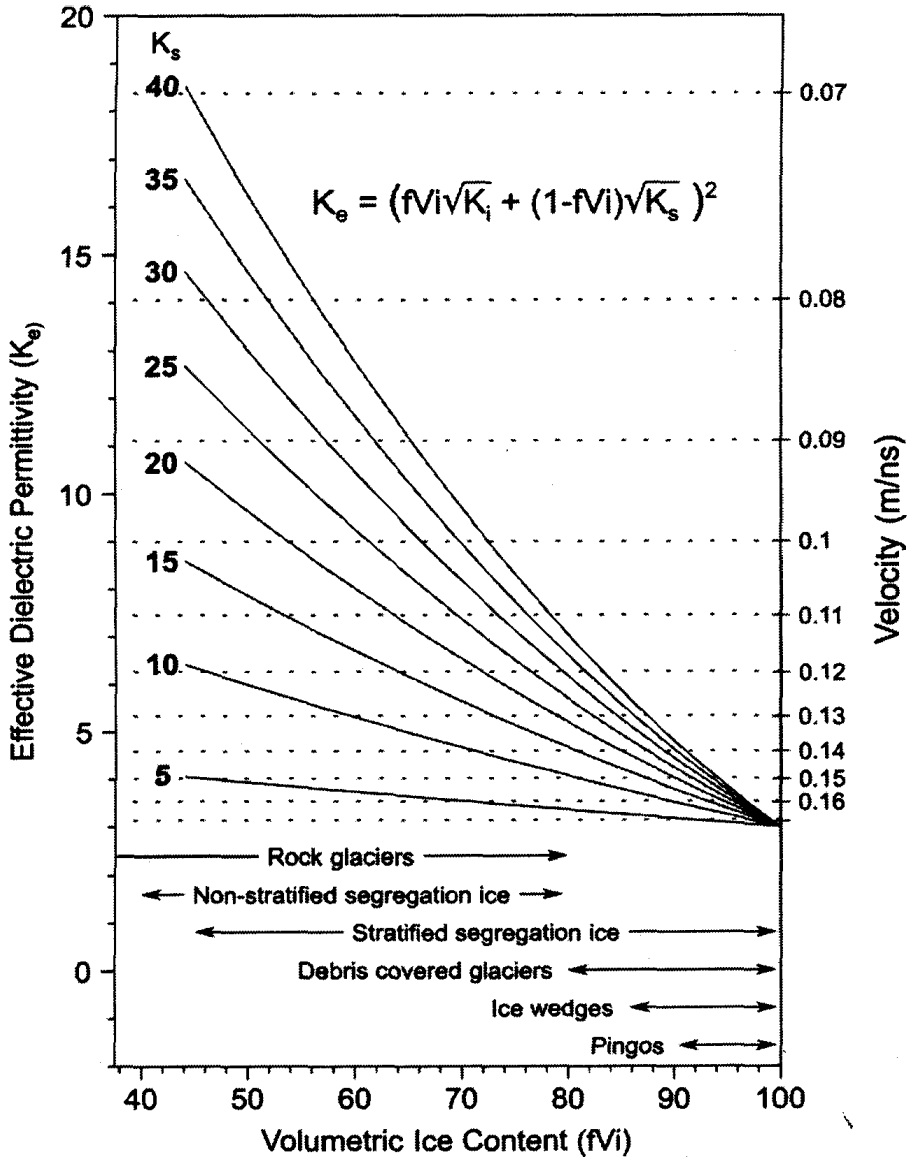

Figure 3.5. Dielectric permittivities of saturated ice deposits derived from the adapted CRIM model for K_s values ranging from 5 to 40 (bold values). The volumetric ice content values for the ground ice deposits listed are derived from the studies noted in Table 3.1.

Projections of the expected effective dielectric permittivity values for ice-rich (saturated) terrestrial ground ice deposits are illustrated in Figure 3.5 for a range of sediment permittivity values (K_s = 5 – 40) using a dielectric permittivity value of 3 for ice. It is clear that as Ks values approach Ki (Ki=3 in Figure 3.5), the contrast in dielectric permittivity is lessened. However, as ice provides a relatively fast medium for radar wave propagation, these small changes in permittivity will likely be discernable in velocity measurements.

Assuredly, ice content alone does not define the dielectric properties of an ice deposit, though it does appear to play a significant role and in dilute solutions of ground ice especially. We expect that as the amount of sediment present in a ground ice deposit decreases, the role of other parameters such as air bubble inclusions, temperature, ice chemistry, and density variations will play a greater role, as has been exhibited in polar ice sheets [*Ackley and Keliher*, 1979; *Fujita et al.*, 2000; *Moore et al.*, 1989]. The lack of variation between the CMP velocities observed from those derived from cross-polarimetric surveys indicate that changes in crystal lattice are not significant in the dielectric properties of ground ice deposits. Further evidence of this follows from Ackley and Keliher [1979] who reported changes in crystal lattice can contribute a ~0.0037 change in dielectric properties. Even for the ice wedge at Thomas Lee Inlet which contained 96.8% ice by volume resulting in K_{obs} = 3.65, a 0.0037 change in the dielectric constant would only cause a -0.0001 m/ns change in the signal speed which is an order of magnitude below the accuracy required for CMP velocities [*Jacob and Hermance*, 2004]. The minute effects of parameters influencing K_{obs} derived from ice sheet studies [*David Stillman and Olhoeft*, 2008; *Fujita et al.*, 2000; *Moore and Fujita*, 1993] further support that sediment content will overshadow changes in dielectric properties derived from density, air bubble orientation, and temperature.

At present, the modified CRIM model presented here allows for the mixing of two dielectrically heterogeneous substances, however, it would be interesting to explore multi-component mixtures such as bubble rich ground ice deposits. For example, the K_{ice} of bubble rich ice deposits in the Tuktoyaktuk region of the Northwest Territories has been reported as being as low as 2.6 [*Annan and Davis*, 1976]. It should be noted that the adapted CRIM model here is considered to be applicable for saturated ground ice deposits exclusively where the ice

content exceeds the porosity of the host sediments such that the pore spaces are in-filled with ice. The presence of bubbles in ice should not be mistaken for air cavities in pore spaces. Rather, bubble formation in ground ice is a result and indicator of the environmental conditions during the freezing process [*Shumskii*, 1964].

6.2 Implications for Mars exploration using GPR

Can the adapted CRIM model be applied to ice-hosting features on Mars? Laboratory measurements of a Mars soil simulant (JSC Mars-1) with properties similar to that of oxidized volcanic ash [*Allen et al.*, 1998], were found to be $K_s = 3.57$ [*Leuschen*, 1999]. This permittivity falls within the range of theoretical dielectric values of sedimentary units in the near surface such as air rich eolien sediments predicted to have Ks = 2.8, while more compact indurated sediments have Ks = 5.8 [*Leuschen et al.*, 2001]. By considering ice deposit bearing sediments on Mars to have a similar dielectric values those in the Leuschen studies, we have estimated the expected dielectric permittivity of ground ice deposits on Mars according to the adapted CRIM model (6) and the fractional volume of ice for ground ice deposits following values reported by studies noted in Table 3.1.

Feature	*fVi* (%)	K_{CRIM}		
		$K_s = 2.8$	$K_s = 3.57$	$K_s = 5.8$
Ice Wedges[A]	85-100	2.97 – 3	3.08 – 3	3.36 – 3
Stratified Segregation Ice[B]	45-100	2.89 – 3	3.31 – 3	4.42 – 3
Non-stratified Seg. Ice[A]	40-80	2.88 – 2.96	3.34 – 3.11	4.57 – 3.49
Ice-assisted talus creep[C]	20-30	2.84 – 2.86	3.45 – 3.39	5.27 – 4.86
Rock-glaciers[D]	30-80	2.86 – 2.96	3.39 – 3.11	4.86 – 3.49
Debris covered glaciers[E]	8-100	2.96 – 3	2.96 – 3	3.49 – 3
Pingos[F]	90-100	2.98 – 3	3.05 – 3	3.24 – 3

[A] This study
[B] Barry, 1992; Pollard and French, 1980;
[C] Squyres, 1978, 1979
[D] Mangold et al., 2002
[E] Head et al., 2006a, 2006b
[F] Lagerbäck and Rodhe, 1985

Table 3.1. Theoretical dielectric permittivities derived from the modified CRIM model for a range of ground ice deposits with volumetric ice contents corresponding to the references noted in the footnotes. The dielectric permittivity values considered for martian host sediments (K_s) follow from the studies of Allen et al. [1998], Leuschen [1999], and Leuschen et al. [2001].

Findings from the Mars Odyssey Gamma-Ray Spectrometer, sensitive to a surface depth of 1 m, note the presence of a hydrogen rich layer below the surface that supports the existence of an ice rich mantle with 40-70% ice by volume for ice-filled pore spaces, increasing with latitude [*Boynton et al.*, 2002]. These volumetric ice content estimates are derived under the assumption that host sediments in these regions have similar porosities to sediments present at the Viking 1 Lander site. Under similar logic, if we assume that the host sediments have a similar dielectric permittivity to the compacted drift material at the Viking 1site (K_s=2.6), the proposed ice deposits in regions of observed hydrogen enrichment detected by the Gamma-Ray Spectrometer ice deposits should give effective dielectric permittivities between 2.76 and 2.88, respectively. Based on the range of K_{CRIM} values listed in Table 3.1, it would be difficult to state the volumetric ice content of a given glacial or periglacial feature Mars without a better constraint on the dielectric properties of the material. In particular, given that the CRIM model assumes filled pore spaces, it would be beneficial to have an experimentally derived measure of dielectric permittivity for a Mars stimulant at the saturation point (where fraction of water is equivalent to porosity). The limitations of the CRIM model could also be constrained through wave propagation modeling to determine the threshold at for the microgeometry of sedimentary inclusions must be considered, as is accounted for in the Hanai-Bruggeman model for dielectric mixtures.

For future studies, further knowledge of the volume fraction of ice in periglacial and glacial features on both Earth and Mars would benefit science and exploration prospects. As noted by Plaut et al. [2009], the amount of ice within present-day lobate debris aprons is still uncertain. Modelled results of these rock glacier-like features suggest that ice content exceeding 80% would be required to cause the extent of flow observed [*Colaprete and Jakosky*, 1998]. It

has been note by Paterson [1994] that soluble impurities (HF, NH_3, and HCl) present on the order of parts per million could increase the deformation rates of these features and thus decrease the amount of ice content required to explain the extent of LDAs. While our findings suggest that GPR is not sensitive to sparse chemical impurities in the presence of significant sediment load, GPR derived observations of low ice content – less than the 80% required by the Colaprete and Jakosky model [1998] – might indicate that such impurities are present and playing a role in the rheology of ice on Mars.

Beyond the specific task of constraining a dielectric signature to determine the nature of ice rich deposits, CMP survey data collected from future GPR missions would provide critical radar wave velocity information for converting two-way time horizons in common-offset surveys into true depth. For exploration purposes, the benefits of the CMP velocity methods lay in the fact that they can discern changes in dielectric properties between horizontal boundaries, whereas velocities picked from diffraction hyperbola in common-offset surveys require point scatterers in the subsurface which may, or may not, align with dielectric horizons. Moreover, it is highly unlikely that velocities will be able to be calculated according to the travel time to a reflector of known depth given the exploratory nature and purpose of rover-hosted GPR systems. The merits of CMP survey capable systems are, however, compromised by the mechanical requirements to move the transmitter and receiver of the system independently.

In addition to CMP survey capabilities, GPR instruments designed for exploration would benefit from system capabilities that enabled information on antenna ground coupling, power output, and transmission wave characteristics to be assessed and accessed since knowledge of these parameters would assist in constraining both dielectric and conductivity profiles (Moore, 1988). Coupling a conductivity system with GPR instruments would provide more robust

geophysical results and could aid in determining the frequency dependence of target materials (which influences the imaginary part of complex dielectric permittivity). This might have interesting prospects for unveiling the volcanic history of Mars from radar investigations of the polar ice caps given findings by Fujita et al. [2000] that the imaginary part of the dielectric constant is sensitive to peaks in ice acidity that are, in turn, indicative of volcanic events in terrestrial ice sheets [*Hammer et al.*, 1980; *Millar*, 1982]. On a more practical note, conductivity measurements coupled with GPR data would assist in post-processing methods since radar data must account for the attenuation effects materials with conductivities below 10 mS/m [*Davis and Annan*, 1989; *Pettinelli et al.*, 2007].

6. Conclusions

For the assessment of dielectric properties targeting sub-surface ice deposits using ground-penetrating radar, we found that common-midpoint surveys have proven superior to wide-angle methods and that cross-polar methods do not improve upon the correlation between the dielectric and physio-chemical data. Thus, we have the greatest confidence in CMP surveys collected in the conventional orientation which resulted in radar wave velocities of 0.134 m/ns, 0.124 m/ns, and 0.157-0.152 m/ns for stratified segregation ice, non-stratified segregation ice, and ice wedges, which correspond to dielectric permittivities of 5.01, 5.81, and 3.65-3.90, respectively. Chemical changes in the pH and conductivity of the ice could not be statistically correlated to variations in K_{obs}. However, a modified CRIM model relating the effective permittivity, K_e, of a dielectrically heterogeneous mixture to the volumetric ice content, fVi, of the ground ice was able to explain 82% of the variance in the observed permittivity, K_{obs}, for the

topmost metre of the four deposits we investigated. Future CMP radar investigations of ice-rich deposits with known volumetric ice content would help to affirm this relationship.

For future applications of GPR in permafrost environments, the projections in Figure 3.5 may provide helpful velocity constraints for converting time horizons to true depth in future GPR profiling studies of the ice-hosting geomorphic features noted. In turn, we suggest that CMP velocity analysis over the noted features may be used to estimate the volumetric ice content in these features when drilling proves to be both impractical and expensive. In consideration of our findings, we believe that GPR systems capable of conducting CMP surveys could successfully constrain the ice content of the proposed glacial and periglacial features on Mars with the accuracies of these measurements being dependent on the confidence in the dielectric properties of host sediment. These sediment properties, in turn, may be also be derived from CMP surveys if a lag of significant thickness (>¼ λ) exists as overburden over the deposit.

Ultimately, we hope that velocities derived from the adapted CRIM model, as well as the direct measurements of dielectric permittivities over ground ice deposits, will provide helpful baseline values for common-offset GPR prospecting in permafrost environments and have encouraged future radar investigations on this planet and the next.

Acknowledgements. This study would not have been financially possible without support from the Department of Indian and Northern Affairs Northern Training Grant Program (LIT), NSERC Discovery Grant Northern Supplement (GRO), and the ACUNS Canadian Northern Studies Trust Research Support Opportunity (LIT), nor without the logistical support of the Polar Continental Shelf Project. We thank those field companions who helped immensely with the

excavation and coring process, as well as Dr. Gordon Southam, Dr. Steven Hicock, and Dr. R. Gerhard Pratt for sharing their laboratory facilities, equipment, and expertise.

References

Allen, C. C., K. M. Jager, R. V. Morris, D. J. Lindstrom, M. M. Lindstrom, and J. P. Lockwood (1998), Martian soil stimulant available for scientific, educational study, *EOS, Transactions American Geophysical Union, 79*(34).

Annan, A. P. (1996), Transmission Dispersion and GPR, *Journal of Environmental and Engineering Geophysics, 1*(B), 125-136.

Annan, A. P. (2002), GPR - History, Trends, and Future Developments, *Subsurface Sensing Technologies and Applications, 3*(4), 18.

Annan, A. P., and J. L. Davis (1976), Impulse radar sounding in permafrost, *Radio Sci., 11*(4), 383-394.

Arcone, S. A., M. L. Prentice, and A. J. Delaney (2002), Stratigraphic profiling with ground-penetrating radar in permafrost: A review of possible analogs for Mars, *J. Geophys. Res., 107*(E11), 5108.

Baker, V. R., R. G. Strom, V. C. Gulick, J. S. Kargel, G. Komatsu, and V. S. Kale (1991), Ancient oceans, ice sheets and the hydrological cycle on Mars, *Nature, 352*(6336), 589-594.

Barfoot, T., G. M. T. D'Eleuterio, and A. P. Annan (2003), Subsurface surveying by a rover equipped with ground-penetrating radar, paper presented at Intelligent Robots and Systems, 2003. (IROS 2003). Proceedings. 2003 IEEE/RSJ International Conference on, 27-31 Oct. 2003.

Barfoot, T., P. T. Furgale, G. R. Osinski, N. Ghafoor, and K. K. Williams (2010), Field testing of robotic technologies to support ground ice prospecting in martian polygonal terrain, *Planetary and Space Science, 58*(4), 671-681.

Barry, P. (1992), Ground ice characteristics in permafrost on the Fosheim Peninsula, Ellesmere Island, N.W.T. A study utilizing ground probing radar and geomorphological techniques, McGill University, Montreal, Quebec, Canada.

Berthelier, J. J., et al. (2003), GPR, a ground-penetrating radar for the Netlander mission, *J. Geophys. Res., 108*(E4), 8027.

Boynton, W. V., et al. (2002), Distribution of Hydrogen in the Near Surface of Mars: Evidence for Subsurface Ice Deposits, *Science, 297*(5578), 81-85.

Brandt, O., K. Langley, J. Kohler, and S.-E. Hamran (2007), Detection of buried ice and sediment layers in permafrost using multi-frequency Ground Penetrating Radar: A case examination on Svalbard, *Remote Sensing of Environment*, *111*(2-3), 212-227.

Burr, D. M., K. L. Tanaka, and K. Yoshikawa (2009), Pingos on Earth and Mars, *Planetary and Space Science*, *57*(5-6), 541-555.

Campbell, K. J., and A. S. Orange (1974), A continuous profile of sea ice and freshwater ice thickness by impulse radar, *Polar Record*, *17*(106), 11.

Carr, M. H. (1983), Stability of streams and lakes on Mars, *Icarus*, *56*(3), 476-495.

Carr, M. H., and G. G. Schaber (1977), Martian Permafrost Features, *J. Geophys. Res.*, *82*(28), 4039-4054.

Carr, M. H., and J. W. Head, III (2003), Oceans on Mars: An assessment of the observational evidence and possible fate, *J. Geophys. Res.*, *108*(E5), 5042.

Clifford, S., and T. J. Parker (2001), The Evolution of the Martian Hydropshere: Implications for the Fate of a Primordial Ocean and the Current State of the Northern Plains, *Icarus*, *154*(1), 40.

Colaprete, A., and B. M. Jakosky (1998), Ice flow and rock glaciers on Mars, *J. Geophys. Res.*, *103*(E3), 5897-5909.

Couture, N., and W. Pollard (1998), An assessment of ground ice volume near Eureka Northwest Territories, in *Seventh International Permafrost Conference*, edited by A. G. Lewkowicz and M. Allard, pp. 195-200, Université Laval, Centre d' études nordiques, Collection Nordicana, Yellowknife, NWT.

Davis, J. L., and A. P. Annan (1989), Ground-penetrating radar for high-resolution mapping of soil and rock stratigraphy, *Geophysical Prospecting*, *37*(5), 531-551.

De Pascale, G. P., Pollard, W. H, Williams, K. K. (2008), Geophysical mapping of ground ice using a combination of capacitive coupled resistivity and ground-penetrating radar, Northwest Territories, Canada, *Journal of Geophysical Research*, *113*.

Degenhardt, J. J., Jr., and J. R. Giardino (2003), Subsurface investigation of a rock glacier using ground-penetrating radar: Implications for locating stored water on Mars, *J. Geophys. Res.*, *108*(E4), 8036.

Del Vento, D., and G. Vannaroni (2005), Evaluation of a mutual impedance probe to search for water ice in the Martian shallow subsoil, *Review of Scientific Instruments*, *76*(084504), 8.

Evans, S. (1965), Dielectric properties of ice and snow - A Review, *Journal of Glaciology*, *5*(42), 20.

Head, J. W., et al. (2005), Tropical to mid-latitude snow and ice accumulation, flow and glaciation on Mars, *Nature*, *434*(7031), 346-351.

Hinkel, K. M., J. A. Doolittle, J. G. Bockheim, F. E. Nelson, R. Paetzold, J. M. Kimble, and R. Travis (2001), Detection of subsurface permafrost features with ground-penetrating radar, Barrow, Alaska, *Permafrost and Periglacial Processes*, *12*(2), 179-190.

Iizuka, K., A. Freundorfer, D. Wilson, G. Tsang, and W. Haras (1988), Measurement of saline ice thickness using a step frequency radar, *Cold Regions Science and Technology*, *15*(1), 23-32.

Jacob, R. W., and J. F. Hermance (2004), Assessing the Precision of GPR Velocity and Vertical Two-way Travel Time Estimates, *Journal of Environmental and Engineering Geophysics*, *9*(3), 143-153.

Kovacs, A., and R. M. Morey (1978), Radar Anisotropy of Sea Ice Due to Preferred Azimuthal Orientation of the Horizontal c Axes of Ice Crystals, *J. Geophys. Res.*, *83*(C12), 6037-6046.

Lacelle, D., D. Fisher, I. Clark, and A. Bernstain (2008), Distinguishing between vaour- and liquid-formed ground ice in the northern martian regolith and potential for biosignatures preserved in ice bodies, *Icarus*, *197*, 12.

Lefort, A., P. S. Russel, N. Thomas, A. S. McEwen, C. M. Dundas, and R. L. Kirk (2009), Observations of periglacial landforms in Utopia Planitia with the High Resolution Imaging Science Experiment (HiRISE), *Journal of Geophysical Research*, *114*(E04005), 18.

Leuschen, C. (1999), Analysis of the complex permittivity and permeability of a Martian soil simulant from 10 MHz to 1 GHz, paper presented at Geoscience and Remote Sensing Symposium, 1999. IGARSS '99 Proceedings. IEEE 1999 International, 1999.

Leuschen, C., S. P. Gogineni, S. M. Clifford, and R. K. Raney (2001), Simulation and design of ground-penetrating radar for Mars exploration, paper presented at Geoscience and Remote Sensing Symposium, 2001. IGARSS '01. IEEE 2001 International, 2001.

Leuschen, C., P. Kanagaratnam, K. Yoshikawa, S. Arcone, and P. Gogineni (2003), Design and field experiments of a ground-penetrating radar for Mars exploration, *J. Geophys. Res.*, *108*(E4), 8034.

Levy, J. S., J. W. Head Iii, and D. R. Marchant (2009), Thermal contraction crack polygons on Mars: Classification, distribution, and climate implications from HiRISE observations, *Journal of Geophysical Research*, *114*, 19.

Mackay, J. R. (1972), The World of Underground Ice, *Annals of the Association of American Geographers*, *62*(1), 1-22.

Mangold, N., and P. Allemand (2001), Topographic analysis of features related to ice on Mars, *Geophys. Res. Lett.*, *28*(3), 407-410.

Millar, D. H. M. (1982), Acidity levels in ice sheets from radio echo-sounding, *Annals of Glaciology*, *3*, 5.

Moore, J. C. (1993), High-resolution dielectric profiling of ice cores, *Journal of Glaciology*, *39*(132), 4.

Moore, J. C., and S. Fujita (1993), Dielectric Properties of Ice Containing Acid and Salt Impurity at Microwave and Low Frequencies, *J. Geophys. Res.*, *98*(B6), 9769-9780.

Murray, J. B., et al. (2005), Evidence from the Mars Express High Resolution Stereo Camera for a frozen sea close to Mars' equator, *Nature*, *434*(7031), 352-356.

Neukum, G., et al. (2004), Recent and episodic volcanic and glacial activity on Mars revealed by the High Resolution Stereo Camera, *Nature*, *432*(7020), 971-979.

Olhoeft, G. (1998), Ground Penetrating Radar on Mars, paper presented at Seventh International Conference on Ground Penetrating Radar, Lawrence, Kansas, USA, May 27-30, 1998.

Osinski, G. R., P. Lee, J. G. Spray, J. Parnell, D. S. S. Lim, T. E. Bunch, C. S. Cockell, and B. Glass (2005), Geological overview and cratering model for the Haughton impact structure, Devon Island, Canadian High Arctic, *Meteoritics & Planetary Science*, *40*(12), 1759-1776.

Oswald, G. K. A. (1975), Investigation of sub-ice bedrock characteristics by radio-echo sounding, *Journal of Glaciology*, *15*(73), 13.

Page, D. F., and R. O. Ramseier (1975), Application of radar techniques to ice and snow studies, *Journal of Glaciology*, *15*(73), 14.

Pallavi, B., H. Saito, and M. Kato (2009), Application of GPR ground wave to monitor seasonal variations of surface moisture contents at a kanto loam field site, *Technical report of IEICE. SANE*, *109*(219), 91-95.

Parker, T. J., D. S. Gorsline, R. S. Saunders, D. C. Pieri, and D. M. Schneeberger (1993), Coastal Geomorphology of the Martian Northern Plains, *J. Geophys. Res.*, *98*(E6), 11061-11078.

Paterson, W. S. B. (1994), *The physics of glaciers, Ed. 3*, Pergamon Press, Oxford, New York.

Pettinelli, E., P. Burghignoli, A. R. Pisani, F. Ticconi, A. Galli, G. Vannaroni, and F. Bella (2007), Electromagnetic Propagation of GPR Signals in Martian Subsurface Scenarios Including Material Losses and Scattering, *Geoscience and Remote Sensing, IEEE Transactions on*, *45*(5), 1271-1281.

Plaut, J. J., A. Safaeinili, J. W. Holt, R. J. Phillips, J. W. Head, III, R. Seu, N. E. Putzig, and A. Frigeri (2009), Radar evidence for ice in lobate debris aprons in the mid-northern latitudes of Mars, *Geophys. Res. Lett.*, *36*(2), L02203.

Plettemeier, D., V. Ciarletti, S. Hamran, C. Corbel, S. Linke, and W. Benedix (2009a), Design and Performance of the WISDOM Antenna System aboard the ExoMars Rover, paper presented at European Geosciences Union General Assembly, Vienna, Austria, 19 – 24 April, 2009.

Plettemeier, D., S. Balling, W. S. Benedix, V. Ciarletti, S. E. Hamran, C. Corbel, and S. Linke (2009b), Ultra light-weight antenna system for full polarimetric GPR applications, paper presented at EUROCON 2009, EUROCON '09. IEEE, 18-23 May 2009.

Plettemeier, D., V. Ciarletti, S. E. Hamran, C. Corbel, P. Cais, W. S. Benedix, K. Wolf, S. Linke, and S. Roddecke (2009c), Full polarimetric GPR antenna system aboard the ExoMars rover, paper presented at Radar Conference, 2009 IEEE, 4-8 May 2009.

Plewes, L. A., and B. Hubbard (2001), A review of the use of radio-echo sounding in glaciology, *Progress in Physical Geography*, *25*(2), 203-236.

Pollard, W. (2000), Ground ice aggradation on Fosheim Peninsula, Ellesmere Island, Nunavut,*Rep.*, 325-333 pp, Geological Survey of Canada, Ottawa, Ontario, Canada.

Pollard, W., and H. M. French (1980), A first approximation of the volume of ground ice, Richards Island, Pleistocene Mackenzie delta, Northwest Territories, Canada, *Canadian Geotechnical Journal*, *17*(4), 8.

Pollard, W., and T. Bell (1998), Massive Ice Formation in the Eureka Sound Lowlands: A Landscape Model, in *Permafrost. Proceedings Seventh International Conference.*, edited by A. G. Lewkowicz and M. Allard, pp. 903-907, Yellowknife, Canada.

Robin, G. Q. (1975a), Radio-Echo Sounding: Glaciological Interpretations and Applications, *Journal of Glaciology*, *15*(73), 16.

Robin, G. Q. (1975b), Velocity of Radio Waves in Ice by means of a Bore-hold Interferometric Technique, *Journal of Glaciology*, *15*(73), 9.

Rossbacher, L. A., and S. Judson (1981), Ground ice on Mars: Inventory, distribution, and resulting landforms, *Icarus*, *45*(1), 39-59.

Shean, D. E., J. W. Head, III, J. L. Fastook, and D. R. Marchant (2007), Recent glaciation at high elevations on Arsia Mons, Mars: Implications for the formation and evolution of large tropical mountain glaciers, *J. Geophys. Res.*, *112*(E3), E03004.

Schlumberger, (1991), Log interpretation principles/Applications: Schlumberger Educational Services, Houston, TX.

Shumskii, P., A. (1964), *Principles of Structural Glaciology*, Dover Publications, Inc., New York.

Singleton, A. C., G. R. Osinski, C. Samson, M.-C. Williamson, and S. Holladay (2010), Electromagnetic characterization of polar ice-wedge polygons: Implications for periglacial studies on Mars and Earth, *Planetary and Space Science*, *58*(4), 472-481.

Soare, R. J., G. R. Osinski, and C. L. Roehm (2008), Thermokarst lakes and ponds on Mars in the very recent (late Amazonian) past, *Earth and Planetary Science Letters*, *272*(1-2), 382-393.

Stillman, D., and G. Olhoeft (2004), GPR and Magnetic Minerals at Mars Temperatures, paper presented at Tenth International Conference on Ground Penetrating Radar, Delft, The Netherlands, 21-24 June, 2004.

Stillman, D., and G. Olhoeft (2008), Frequency and temperature dependence in electromagnetic properties of Martian analog minerals, *J. Geophys. Res.*, *113*(E9), E09005.
Tillard, S., and J.-C. Dubois (1995), Analysis of GPR data: wave propagation velocity determination, *Journal of Applied Geophysics*, *33*(1-3), 77-91.

Trautner, R., R. Grard, and M. Hamelin (2003), Detection of subsurface ice and water deposits on Mars with a mutual impedance probe, *Journal of Geophysical Research*, *108*(E108047), 5.

Wolff, E. W. (2000), Electrical stratigraphy of polar ice cores: priciples, methods, and findings, paper presented at International Symposium on Physics of Ice Core Records, Hokkaido University Press, Shikotsukohan, Hokkaido, Japan, September 14-17, 1998.

Woodward, J., and M. J. Burke (2007), Applications of Ground-Penetrating Radar to Glacial and Frozen Materials, *Journal of Environmental and Engineering Geophysics*, *12*(1), 17.

Yowhikawa, K., C. Leuschen, A. Ikeda, K. Harada, P. Gogineni, P. Hoekstra, L. Hinzman, Y. Sawada, and N. Matsuoka (2006), Comparison of geophysical investigations for detection of massive ground ice (pingo ice), *Journal of Geophysical Research*, *1111*(E06S19).

4

RADAR WAVE VELOCITY STRUCTURE OF AN ICE WEDGE POLYGON HOSTED IN SEGREGATION ICE DETERMINED BY THE REFLECTION COEFFICIENT, THOMAS LEE INLET, DEVON ISLAND, NUNAVUT

Laura I. Thomson[1], and Gordon R. Osinski[1]

[1]Departments of Earth Sciences and Physics and Astronomy, University of Western Ontario, London, ON, Canada N6A 5B7.

Abstract

This study explores the use of common-midpoint (CMP) survey methods in the application of ground-penetrating radar over permafrost targets. CMP surveys offer an effective and non-intrusive method for determining the radar wave velocities and subsequent dielectric properties of subsurface units; however, the results of common-midpoint surveys may be complicated or rendered unusable due to penetration depriving attenuation effects in the thawed active layer. To address these potential problems, we test whether the dielectric properties of the underlying permafrost may be revealed according to the nature of the reflection coefficient between it and the overlying active layer. The study targets two adjacent ground ice deposits, non-stratified segregation ice and wedge ice, in the region of Thomas Lee Inlet, Devon Island, Nunavut. CMP surveys conducted on the active layer overlying these deposits were run using a 450 MHz GPR with cross-polar capabilities. In analysis of the data, we utilize the Brewster angle of incidence, indicated by a 90° phase shift in the hyperbolic features of CMP radargrams, collected in parallel orientation, to determine the dielectric properties of the ice deposits below the active layer and find that the technique provides solutions that are in agreement to those acquired from on-ice CMP surveys.

1. Introduction

Ground-penetrating radar (GPR) is a popular technique for resolving the spatial extent of ice deposits in permafrost environments [*Moorman et al.*, 2003]. These techniques have proven to be particularly helpful in identifying appropriate sites for infrastructure development in the North [*Andersland and Ladanyi*, 1994]. GPR systems equipped with independent transmitting and receiving antenna give the user the ability to conduct common-midpoint (CMP) surveys that provide information on the electromagnetic velocity, and thus, in non-magnetic settings, the dielectric permittivity of structures in the subsurface. In previous work, it has been show that for ice rich deposits (>45% volumetric ice content) the dielectric permittivity of an ice deposit in permafrost can be attributed primarily to the sediment content of the ground ice according to a modified CRIM model [Chapter 3]. Understanding the subsurface ice content of permafrost environments has implications for both our understanding of periglacial geomorphic processes and for future development of northern territories. This is especially true as warming temperatures destabilize the permafrost environment leading to the subsidence or collapse of ice rich landforms [*Nelson et al.*, 2001; *Smith et al.*, 2010].

Radargrams resulting from CMP surveys contain a linear air wave, which represents signal travel between the antenna above the ground, a linear direct wave that travels in the near subsurface at a depth of one-quarter of the signal wavelength [*Pallavi et al.*, 2009], and hyperbolic features which indicate horizons where there is a contrast in the dielectric permittivity of subsurface materials. The arrival times of the semi-hyperbolic structures resulting from CMP surveys indicate the depth of these horizons, and the shape of the hyperbola indicates the radar wave velocity in the above-lying layer where shallow dipping features indicate high velocity materials and vice versa for steeply dipping features [*Moorman et al.*, 2003; *Reynolds*, 1997].

For multilayer targets, the velocity of the overlying layers affects the observed velocity in deeper layers, however, this influence can be corrected for using the Dix equation as demonstrated by Tillard et al.[1995].

Given the inherently difficult nature of working in northern territories, the majority of both research and development campaigns take place during the summer months when the active layer temperature is above zero. For those with aspirations to conduct GPR surveys, this thawed layer, and the subsequent moisture present in it, adversely affects the quality of the data on account of attenuation effects due to the presence of water, which creates a more conductive environment [*Salat and Junge*, 2010]. Signal attenuation, as noted by Kong (1990), weakens the radar signal amplitude to a factor of $1/e$ at a depth of the inverse of the attenuation ($1/\alpha$) independent of the system's operating frequency. This indicates that even low-frequency GPR systems, merited for their greater penetration capabilities, cannot overcome attenuation effects.

1.1 Dielectric determination from Reflection Coefficients

For CMP applications over two-layer targets with a relatively conductive upper layer, which describes many summertime permafrost targets, the adverse effects of attenuation can inhibit determining the dielectric nature of the unit directly below the active layer. This case is especially true if a basal reflector in the lower unit, which could provide a second hyperbolic feature for velocity picking, is below the limiting $1/\alpha$ depth.

In a study of perpendicular- and parallel-polarized CMP surveys, Reppert et al. [2000] demonstrate that the reflection coefficient between two dielectric units can be determined using Brewster angles and that this value may, in turn, be used to determine the dielectric properties of the lower unit. The reflection coefficient (RC) expresses the fractional amount of energy returned to the GPR system from a given reflector. Most commonly, the RC is calculated once the

dielectric properties of two adjacent units have been determined by velocity analysis of hyperbolic features. However, in a common-midpoint survey, the strength of the energy returned to the GPR system is influenced by both the contrast in dielectric properties as well as the incident angle of the signal, which, in turn, is dictated by the antenna separation. When the GPR antenna are in parallel polarization (commonly referred to as "endfire" mode), an interesting phenomenon occurs at the Brewster angle of incidence whereby the reflection coefficient goes to zero [*Reppert et al.*, 2000]. The Brewster angle, by definition, is the incident angle at which all parallel-polarized energy is transmitted into the underlying layer such that no signal is returned to the surface. In a CMP radargram, this event is indicated by a 90° phase change at the antenna separation corresponding to an incident angle (θ_i) equal to the Brewster angle (θ_B) [*Reppert et al.*, 2000]. Geometrically, the incident angle is defined by the antenna separation (x) and depth to the dielectric horizon (d), and the Brewster angle at which RC goes to zero is theoretically defined by the dielectric permittivity of the first and second layers (K_1 and K_2) according to

$$\tan \theta_i \equiv x/2d = \tan \theta_B \equiv (K_2/ K_1)^{1/2}. \quad (4.1)$$

It is important to note that (4.1) is only applicable to GPR CMP surveys collected in parallel orientation. Since both d and K_1 can be determined from velocity analysis, we can rearrange (4.1) to solve for K_2, the dielectric properties of the underlying layer:

$$K_2 = K_1(x/2d)^2 \quad (4.2)$$

In presenting the theory behind applying Brewster's angle to GPR CMP data, Reppert et al. [2000] demonstrate the success of this technique for determining the dielectric properties of a high velocity sandy silt unit below a slower, water saturated sand unit. The transition from low velocity active layer sediments to the high velocity permafrost regime represents an analogous situation to the velocity structure explored by Reppert et al. [2000]. To our knowledge, however,

this technique has yet to be applied or tested in a permafrost environment. Thus, in this study we examine the above described dielectric permittivity determination method to assess whether the reflection coefficient between active layer sediments and ice-rich permafrost can be used to determine the dielectric properties of two ground ice deposits in the Canadian Arctic.

2. Methods

At the head of Thomas Lee Inlet on the north-central coast of Devon Island, Nunavut, is a broad sedimentary basin which hosts an extensive network of ice wedge polygons, 75°21'29" N 88°40'52" W (Figure 4.1). In addition to the ice wedge deposits, previous geophysical studies of this site revealed the presence of non-stratified segregation ground ice below a trench excavated through the active layer of a polygon centre [*Singleton et al.*, 2010]. As will be demonstrated, this site provided the necessary degree of dielectric contrast between the active layer and the permafrost as well as an opportunity to test the application of the Reppert et al. [2000] method over two ground ice deposits of contrasting dielectric properties and geomorphic origins.

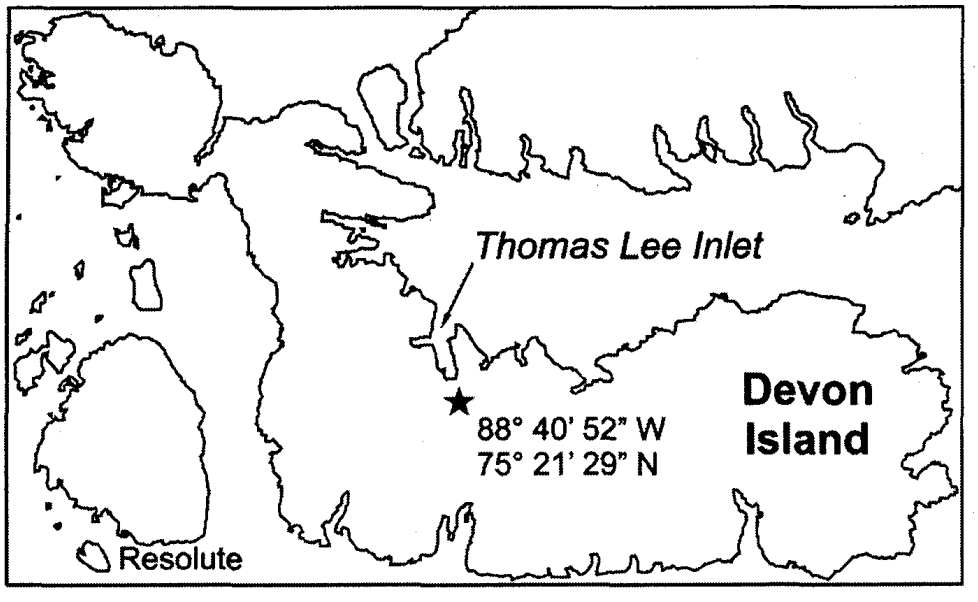

Figure 4.1. The location of the study site near Thomas Lee Inlet, Devon Island, Nunavut.

GPR surveys were carried out using the Sensors & Software Ltd. PulseEKKO 1000, which operates using 450 MHz antenna connected to a battery powered and computer commanded console. To attain a sense of spatial context, a 10 m common-offset survey collected at a 0.25 m antenna separation with a 0.05 m step size was conducted across two polygon centres, with the transect midpoint intersecting the ice wedge trough at 90° (see transect a, Figure 4.2A). Subsequent CMP surveys were conducted through the ice wedge trough (transect b, Figure 4.2A) and over the polygon centre (transect c, Figure 4.2A) for each of the antenna orientations, those being both perpendicular and parallel modes. Examples of these modes are presented in Figure 4.3.

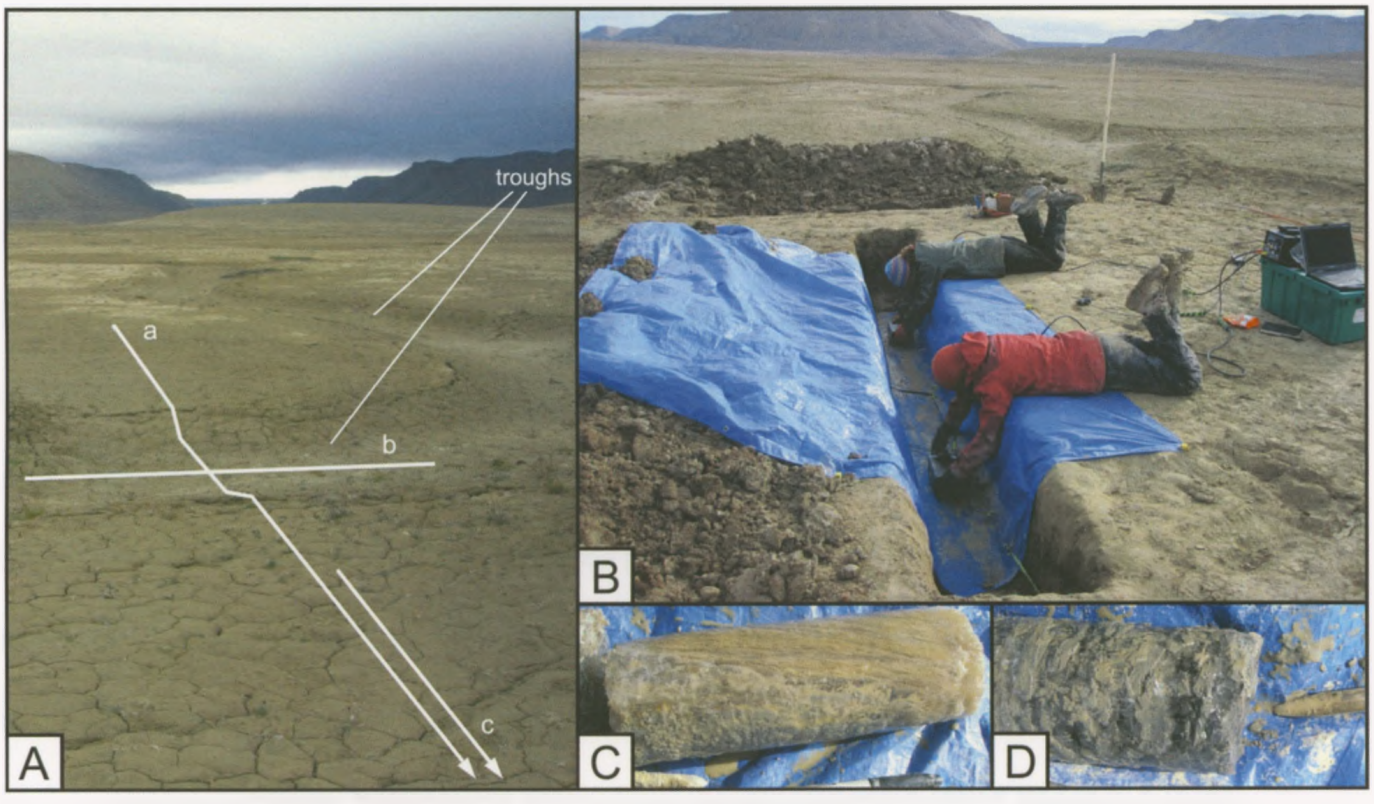

Figure 4.2. A: Field images showing the location of survey lines across the polygon network at Thomas Lee Inlet, Nunavut. Transect 'a' was conducted in common-offset mode and measured 10 metres in length while surveys 'b' and 'c' were CMP surveys measuring 3 metres in length. B: Example of on-ice survey method for collection of data on segregation ice. C: Core from ice wedge. D: Core from non-stratified segregation ice.

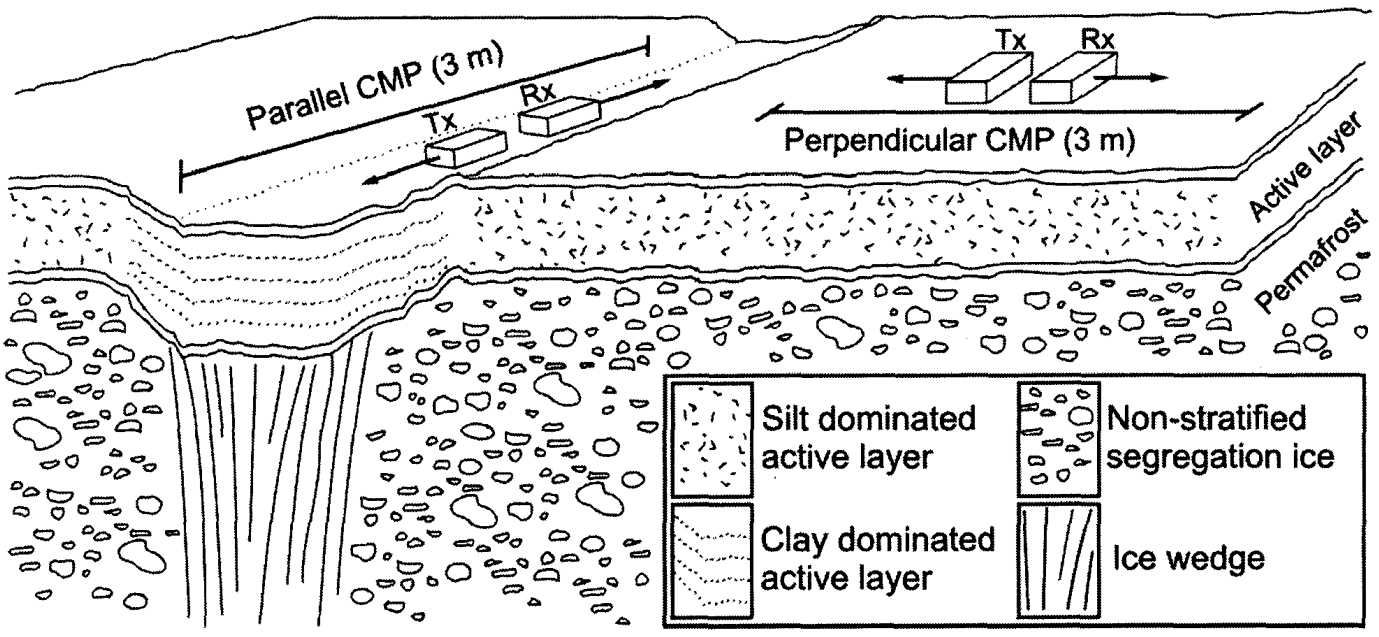

Figure 4.3. Schematic of GPR operations and the geomorphological setting. The nature of the active layer sediments and underlying ground ice deposits were observed in sediment samples and ice cores collected during a complimentary study.

Ice wedge surveys were conducted inside and parallel to the direction of the trough while polygon centre surveys were run perpendicular to the trough, so as to align with the 10 m common-offset survey (Figure 4.3). CMP surveys measured 3 m in length with each having a starting antenna separation of 0.2 metres which increased in 0.05 metre increments with every trace. To improve the signal-to-noise ratio, each trace was comprised of 128 stacks, meaning that 128 signal pulses were emitted and received for each antenna position. A coarse topographic profile of the trough was acquired by measuring the vertical distance from the ground to a rope held taught across the adjacent polygon centres. The maximum depth was 0.22 m at the centre of the 3 m wide depression. Subsequent active layer depths surveyed along transect A were determined using a permafrost probe. Beneath the polygon centre and trough the average depth to the permafrost table was 0.55 m and 0.68 m respectively.

In a complimentary study of the physical and chemical factors controlling the dielectric properties of ground ice at this site, parallel and perpendicularly-oriented CMP surveys were conducted directly on the two ground ice deposits after the active layer survey lines had been excavated by removal of the active layer. Though not the focus of this study, these on-ice surveys provide helpful validation for the dielectric properties determined from the reflection coefficient between the active layer and ice body.

3. Results

The common-offset GPR profile across the polygon centres and ice wedge trough at Thomas Lee Inlet is presented in Figure 4.4. The profile has been topographically corrected using the results of the survey noted in the methods section above and verifies that the GPR system can detect the depth to the permafrost table. There is a notable increase in this depth over the ice wedge, as indicated by the horizon evident between 15 and 20 ns. Furthermore, the strength of this reflector becomes more pronounced between 4.0 and 6.0 m suggesting that a stronger reflection coefficient exists between the active layer sediments and the ice wedge. Hyperbolic refraction patterns at 3.0 m are evident both in the active layer and below the permafrost table indicating a contrast in dielectric properties. These features are associated with transitions from silt dominated sediments to clay dominated sediments in the active layer, as determined from sediment samples collected during excavation at the site, and from non-stratified segregation ice to wedge-ice below the permafrost table, according to ice cores collected in the complimentary study noted at the beginning of this article (Figure 4.4).

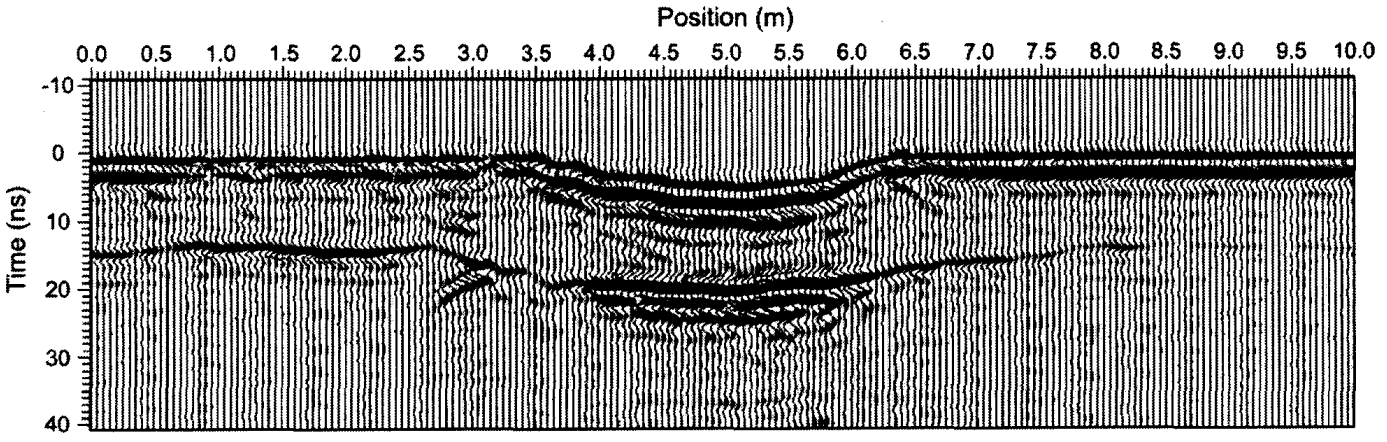

Figure 4.4. Common-offset profile across the target ice wedge trough (3.5–6.5 m) and polygon centres, Thomas Lee Inlet, Nunavut.

The increased strength of the reflection over the ice wedge is encouraging as it suggests that the GPR system is sensitive to transition between ground ice deposits, and that the nature of this the horizon may be able to reveal the dielectric properties of these deposits. The parallel oriented CMP surveys conducted to further investigate this discrepancy are presented in Figure 4.5.

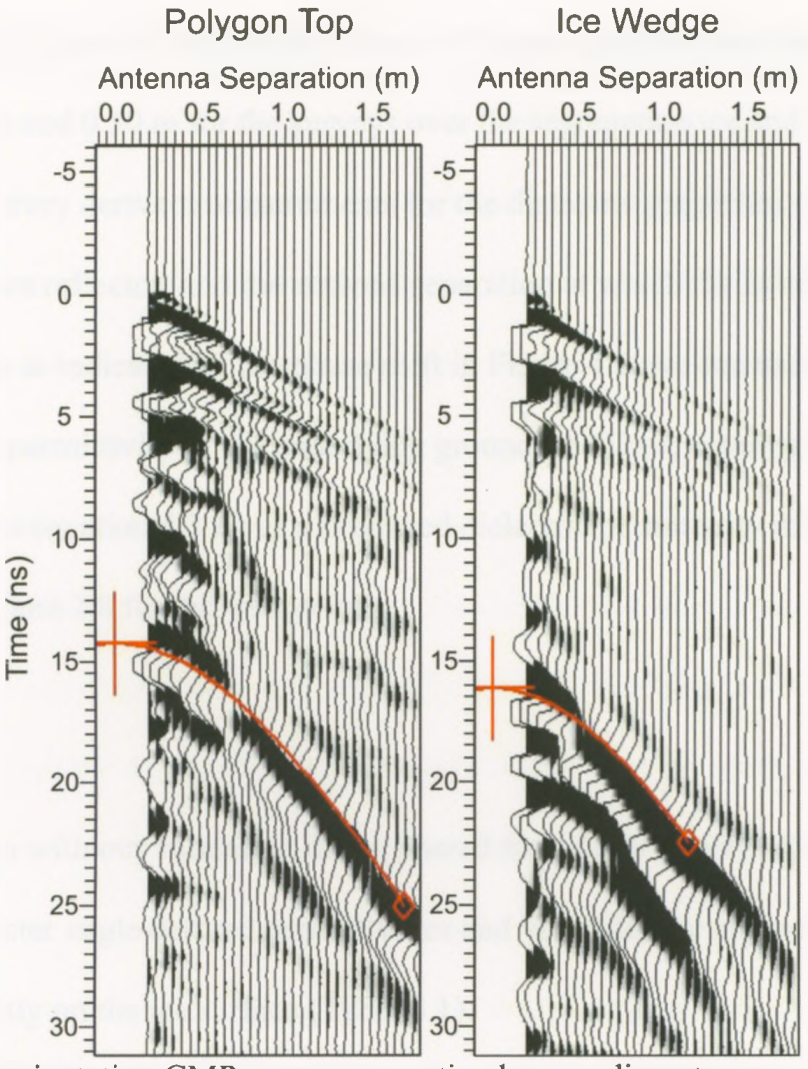

Figure 4.5. Parallel orientation CMP surveys on active layer sediments over non-stratified segregation ice and an ice wedge, Thomas Lee Inlet, Nunavut.

Velocity analysis of the parallel oriented CMP surveys of the active layer over the polygon centre and ice wedge indicated radar wave propagation speeds of 0.086 m/ns and 0.075 m/ns, which give respective dielectric permittivities of 12 and 16. Velocity analysis of the perpendicular CMP surveys gave similar values within 0.001 m/ns. In consideration of these velocities, the respective arrival times of these events translate to active layer depths of 0.56±0.05 m and 0.60±0.04 m. The error factors on these depths are equivalent to one-quarter wavelength of a radar signal travelling at the aforementioned velocities. In examining the

hyperbolic features in Figure 4.5 it is evident that a 90° phase shift exists at respective antenna separations of 0.70 m and 0.50 m for the surveys over the segregation ice and ice wedge.

With CMP survey derived measurements for the dielectric properties of the active layer, the depth of the known reflector, and the antenna separation at which the incident angle is equal to the Brewster angle as indicated by the phase shift in Figure 4.5, we can use equation 4.3 to predict the dielectric permittivity of the underlying ground ice. Thus, entering the above-mentioned values into equation 4.3 gives a predicted dielectric permittivity of 4.7 for the non-stratified ground ice, and 2.8 for the wedge ice.

4. Discussion

In comparison with our validation data gathered from CMP surveys directly on the ground ice, the Brewster angle derived permittivities and velocities are appreciably similar to those measured directly on the ice surface (Table 4.1).

Site	Parameter	Brewster angle method	On-ice CMP Validation	Residual
Segregation Ice	Dielectric Permittivity	4.7	5.8	- 1.1
	Velocity	0.14 m/ns	0.13 m/ns	+ 0.01
Ice Wedge	Dielectric Permittivity	2.8	3.7	- 0.9
	Velocity	0.18 m/ns	0.16 m/ns	+0.02

Table 4.1. Dielectric permittivities and radar wave velocities of the two ground ice deposits as derived from the Brewster angle method [*Reppert et al., 2000*] in comparison with those values acquired from CMP surveys conducted directly on the ground ice surface.

In consideration of the small deviation from the validation values (~1 dielectric unit), the method of using the Brewster angle to determine the dielectric permittivity of an underlying layer using the strength of the reflection coefficient appears to be quite effective. This precision is appreciable when considering that the dielectric permittivity can range from 5-30 for silts and 5-40 for clays [*Davis and Annan*, 1989; *Reppert et al.*, 2000]. For both cases, being over the

polygon centre and over an ice wedge, the Brewster angle method predicted dielectric permittivies that were lower than those observed in the validation studies. This effect may be due, in part, to a localized increase in conductivity over the ice wedges [*Singleton et al.*, 2010]. While the high conductivity anomalies detected by the Singleton et al. [2010] EM induction methods are primarily responding to the purer wedge ice below the polygon troughs, we believe that a slightly increased water content of the active layer over the ice wedge versus the polygon centre (16% weight content versus 15% weight content following analysis of active layer samples collected at the site) in addition to the predominantly clay-sized sediments over the ice wedges are contributing to higher active layer conductivities in the polygon troughs. A thorough explanation of the dispersive nature of water rich clays is presented by Saarenketo [1998]. The loss factor associated with the presence of conductive materials in the active layer sediments would lead to underestimation of the radar wave velocity associated with the real-part of the complex dielectric permittivity [*Reynolds*, 1997]. This would subsequently increase the dielectric contrast between the adjacent units such that, to maintain agreement with the skewed higher magnitude reflection coefficient, the predicted dielectric permittivity of the ice wedge would be forced to decrease, as is noted in the residuals in Table 4.1. Clays were also present in the active layer sediments, though to a lesser extent, above the polygon centre, which likely also explain the underestimation of the dielectric permittivity of the segregation ice.

The technique demonstrated here should translate well to GPR applications at lower frequencies since, despite the commonly larger stepsize and thus seemingly coarser resolution of incident angles tested, these systems can target deeper dielectric anomalies in the subsurface which will inherently narrow the incident angles tested, though larger antenna separations will be

required. Figure 4.6 shows the CMP antenna separation at which the phase shift associated with the Brewster angle should be observed for a range of permittivity ratios.

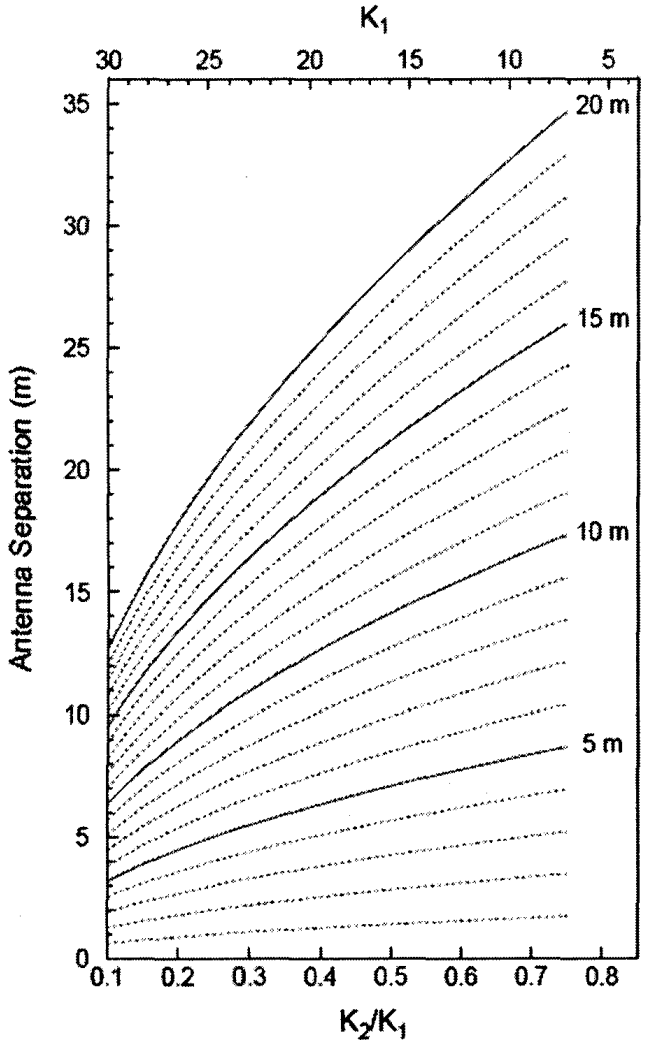

Figure 4.6. Antenna separation at which a 90° phase shift in diffraction hyperbola ought to be observed for CMP data collected in parallel endfire mode for a range of horizon depths (noted on the right) according to equation (3). K_1 and K_2 are the dielectric permittivities of the top and bottom units, respectively. The top x-axis indicates K_1 values in the case where K_2=3 (ice).

For the cases where relatively pure ice is sought (K_2=3), the upper x-axis, which provides a range of dielectrics for the ice-hosting sediment, can be used to predict the antenna separation in a CMP survey at which the phase change ought to exist. If the properties of the host sediment are unknown, this can be determined in the field from CMP velocity analysis of the horizon at the permafrost table, or they can be estimated from a thorough summary of dielectric

permittivities for materials in the natural environment as well as industrial materials, which can be found in Reynolds [1997].

5. Conclusions

Our findings show that CMP surveys conducted atop a wet and clay-rich active layer using parallel endfire antenna orientation can indeed approximate the dielectric properties of the two ground ice deposits in question using the waveform characteristics of the horizon between the units, rather than traditional velocity analysis techniques. Permittivities estimated using the Brewster angle method proposed by Reppert et al. [2000] are within one dielectric unit of validation measurements made directly on the ground ice, and within 0.020 m/ns of the validation velocities. The success in these findings is likely augmented by the strength of the reflection coefficient between the active layer and the ground ice deposits.

One of the practical merits of this technique is that it increases the potential of smaller and more portable high-frequency GPR systems. This is because this technique has the ability to constrain the dielectric properties of an underlying unit through analysis of the reflection coefficient at the upper boundary, rather than requiring a velocity to be picked from the basal boundary which may not be detectable by the GPR system due to the loss of signal strength with depth due to geometric spreading. Moreover, high-frequency systems (>400 MHz) have a greater capacity to overcome the dispersive effects in fine-grained sedimentary units with significant water content [*Saarenketo*, 1998], suggesting that such GPR systems are particularly suited to summertime permafrost targets.

Though successful at the Thomas Lee Inlet site, our confidence in the technique utilized here would benefit from further studies in other periglacial and glacial environments in the

Arctic regions of the world as it would broaden our understanding of the sort of targets best suited for this technique, and also, what else can be gained from using unconventional survey techniques. For example, the potential exists for this technique to provide clarity in discerning true dielectric horizons in the subsurface from multiples, as true horizons will be identifiable by a shift in the antenna separation at which the phase shift occurs. Similarly, just as the velocity of secondary and deeper underlying layers require correction via the Dix equation, it is possible that in a multi-layer scenario the Brewster angle is altered due to effects associated with the overlying layers. This potential obstacle ought to be examined in multi-layer settings, where the dielectric permittivities can be determined by both velocity analysis and the nature of the reflection coefficient, before application of this technique in multi-layer settings is put into practice. Also, the Thomas Lee Inlet site enabled testing of the transition from low- to high-velocity materials (high to low dielectric permittivity). However, Reppert et al. [2000] show that, in theory, a similar phase change when the reflection coefficient goes to zero should exist at the Brewster angle for high- to low-velocity transitions, though this phase signature would occur at a lower angle of incidence. As such, it would be interesting to test the application of the Brewster angle method over permafrost targets where the radar signal is capable of penetrating to the basal horizon between a ground ice deposit (high-velocity) and the underlying sediment (low-velocity) to establish whether the dielectric properties of this sediment could be determined. Indeed, in glacial environments this technique may prove ideal for determining the nature of the glacier bed and whether the high-velocity ice is adjacent with low-velocity bedrock, saturated sediments, or dry sediments. As noted by Hart and Rose [2001], characterizing the nature of the glacier bed by geophysical methods alone is not yet possible, but the greatest potential for acquiring this information lies in GPR remote sensing techniques.

While the findings of this study present a promising technique for future investigations, CMP surveys often remain an underutilized application for GPR studies on permafrost. This fact is likely due to both system design, as fixed-offset GPR transceiver units are generally more common, and the time demands of conducting CMP surveys. However, it is our hope that the findings in this paper encourage the permafrost community to explore the capabilities of radar systems described here and inspire GPR system designs that enable an easy transition from common-offset to CMP modes.

Acknowledgements. The financial contributions of the Department of Indian and Northern Affairs Northern Training Grant Program (LIT) and the ACUNS Canadian Northern Studies Trust Research Support Opportunity (LIT) have made this study possible. Funding from the NSERC Discovery Grant and Northern Research Supplement programs are also acknowledged (GRO). In addition, the Polar Continental Shelf Project provided critical logistical support and for this we offer them our sincere thanks. We thank those colleagues who helped immensely with the survey process and for their companionship in the field.

References

Andersland, O. B., and B. Ladanyi (1994), *Frozen Ground Engineering*, 352 pp., Chapman & Hall, London, England.

Davis, J. L., and A. P. Annan (1989), Ground-penetrating radar for high-resolution mapping of soil and rock stratigraphy, *Geophysical Prospecting*, *37*(5), 531-551.

Hart, J., and J. Rose (2001), Approaches to the study of glacier bed deformation, *Quaternary International*, *86*(1), 45-58.

Moorman, B. J., S. D. Robinson, and M. M. Burgess (2003), Imaging periglacial conditions with ground-penetrating radar, *Permafrost and Periglacial Processes*, *14*(4), 319-329.

Nelson, F. E., O. A. Anisimov, and N. I. Shiklomanov (2001), Subsidence risk from thawing permafrost, *Nature*, *410*(6831), 889-890.

Pallavi, B., H. Saito, and M. Kato (2009), Application of GPR ground wave to monitor seasonal variations of surface moisture contents at a kanto loam field site, *Technical report of IEICE. SANE*, *109*(219), 91-95.

Reppert, P. M., F. D. Morgan, and M. N. Toksöz (2000), Dielectric constant determination using ground-penetrating radar reflection coefficients, *Journal of Applied Geophysics*, *43*(2-4), 189-197.

Reynolds, J. (1997), *An Introduction to applied and environmental geophysics*, John Wiley & Sons, Inc., West Sussex, England.

Saarenketo, T. (1998), Electrical properties of water in clay and silty soils, *Journal of Applied Geophysics*, *40*(1-3), 73-88.

Salat, C., and A. Junge (2010), Dielectric permittivity of fine-grained fractions of soil samples from eastern Spain at 200 MHz, *Geophysics*, *75*(1), J1-J9.

Singleton, A. C., G. R. Osinski, C. Samson, M.-C. Williamson, and S. Holladay (2010), Electromagnetic characterization of polar ice-wedge polygons: Implications for periglacial studies on Mars and Earth, *Planetary and Space Science*, *58*(4), 472-481.

Smith, S. L., V. E. Romanovsky, A. G. Lewkowicz, C. R. Burn, M. Allard, G. D. Clow, K. Yoshikawa, and J. Throop (2010), Thermal state of permafrost in North America: a contribution to the international polar year, *Permafrost and Periglacial Processes*, *21*(2), 117-135.

Tillard, S., and J.-C. Dubois (1995), Analysis of GPR data: wave propagation velocity determination, *Journal of Applied Geophysics*, *33*(1-3), 77-91.

5 CONCLUSIONS

The two articles presented in this thesis investigate (1) the physical and chemical parameters dictating the dielectric permittivity of ground ice and (2) an unconventional method for determining these properties from the nature of the reflection coefficient at the horizon between the active layer and ice deposit. Both studies have demonstrated the utility of ground-penetrating radar (GPR) as a rapid, relatively inexpensive, and non-invasive tool, furthering our understanding of the dielectric nature of ground ice.

As presented in the first article, the dielectric properties of ground ice are most heavily influenced by the volumetric fraction of ice in the host sediment. Statistical analysis has shown that the relationship between this ratio and the observed dielectric permittivity of the ground ice deposit follows a complex refractive index model (CRIM) dielectric mixing model. On the other hand, statistical correlations could not be drawn between ice chemistry and dielectric permittivity. While these correlations certainly exist, as demonstrated by Fujita et al. [2000] in analysis of glacial ice cores, the relatively sediment-rich nature of ground ice appears to overshadow the dielectric properties brought on from chemical influences. An interesting continuation of this study would be to perform analysis similar to that described in the first article on a buried glacier target to determine whether internal ice horizons associated with changes in ice chemistry, density, or crystal structure are discernable beneath a sedimentary overburden. The same potential applies for buried sea ice for which both chemistry and isotropic effects, given the strong crystal lattice, are likely to play a stronger role in the presence of saline dissolved solids and reduced levels of sediment inclusions [*Kovacs and Morey*, 1978; *Lalumiere*, 2006; *Tison and Haren*, 1989].

The dielectric observations in the first study were acquired through interpretation of GPR velocities acquired using on-ice common-midpoint GPR surveys. While these findings would certainly benefit from validation using direct measurements of the dielectric permittivity in a laboratory setting, as demonstrated with artificial samples by Koh [1997], it would be difficult to gather a sample of adequate size for such analysis while preserving the environmental state of the ice (according to the temperature profile of the permafrost). However, it would be interesting to compare laboratory based dielectric measurements with simulated natural ice samples to constrain at what lower limit fraction of sediment content the effects of crystal lattice and ice chemistry begin to dictate the dielectric properties. In fact, such simulated samples could be created from the sediment and meltwater remaining from the laboratory procedures completed on the original ice cores used to determine ground ice sediment content and chemistry. Conversely, the concentration of dissolved solids required to effect the bulk dielectric permittivity in the presence of sediment-rich ground ice could also be tested by chemically doping simulated samples with salts or volcanic ash, which increases the acidity of ice [*Millar*, 1982; *Moore and Fujita*, 1993]. Undoubtedly, the potential for laboratory studies of the parameters controlling the dielectric permittivity of ground ice is limitless, as would be the value of results capable of constraining the contributing order of and limits at which parameters such as ice chemistry, crystal lattice, temperature, water content, air content, and inclusion geometry play the dominant roles. In the case that such laboratory studies are pursued in the future, the nature of the freezing process should be documented as well so as to improve our understanding of the conditions dictating the formation of various crystalline structures and inclusion geometries.

The implications of the findings in the first article will enable geomorphologists to calculate the ice content of permafrost using GPR common-midpoint survey techniques, which

may, in turn, aid in understanding the formational process of ground ice deposits. Without geophysical methods, present day estimates of ground ice content in the Arctic are based on geomorphic interpretation, coupled with manual excavation down to the permafrost table and, when funding allows, drilling of the permafrost. In comparison, GPR techniques are more rapid and representative than these methods in addition to being less destructive of the landscape [*De Pascale*, 2008]. In terms of northern community infrastructure and development, the implications of this first study suggests that GPR should be able to assess the extent, amount, and nature of ground ice beneath proposed building sites. Given that the stability of ground ice is being compromised by warming temperatures in mid- and low-Arctic communities, the consequences of building on ice rich terrain is becoming both expensive and dangerous [*Andersland and Ladanyi*, 1994]. Application of the findings of this paper could mean the difference between exposing infrastructure to rapid thermokarst and collapse vulnerable settings (e.g., in the presence of massive segregation ice) or slower subsidence settings in the presence of pore ice.

For the case of Mars, methods for characterizing buried ice using remote sensing techniques, such as that presented in the first article, is of pertinent interest to the planetary science community. Understanding the nature of the extensive reservoir of subsurface ice in the northern plains of Mars, be it glacial in origin, frozen remnants of an ancient sea, or sourced from subsurface aquifers, will have major implications for our understanding of the present and past climate conditions on the planet, and whether there is, or was, potential for life. For biological studies in permafrost, the findings of this study will provide scientists with the ability to pre-emptively characterize a component of the habitat for ice and permafrost hosted microorganisms such that, when considering where to collect a permafrost core sample for

biological analysis, GPR could help constrain site selection to areas with the most favorable conditions for life in the crysophere [*Lock*, 1990].

The findings of the first article are derived from velocity analysis of common-midpoint surveys (CMP), which reveal the radar wave velocity and subsequent dielectric properties of deposits lying *above* hyperbolic reflection signatures in the radargram. The second article in this thesis investigates a method of unraveling the dielectric properties of the unit *below* these hyperbolic features using a phase shift known to exist when the incident angle of the radar signal is equal to the Brewster angle. Application of this technique required a GPR system capable of conducting CMP surveys in a more unconventional parallel endfire antenna orientation. Using the ground ice dielectric properties derived from the first study as validation, the Brewster angle method of dielectric determination proved to be successful in predicting the dielectric properties of a basal deposit, being the deepest detectable layer in the CMP, within one dielectric unit. The success of this method in permafrost environments is encouraging for three reasons. First, in recognizing that signal loss in an attenuating active layer can inhibit the detection of the base of a ground ice deposit, thus deeming velocity analysis CMP methods unusable, an alternative method for users interested in determining the dielectric properties of the subsurface has been found to be applicable for permafrost targets. Second, this alternative method favors the use of smaller and more mobile high-frequency GPR systems, as it is only the tops of ground ice deposits and not the bases that need to be resolved for this technique to be successful. Finally, no additional equipment or data processing software are required beyond those commonly used in science or industry, given that any GPR system equipped with independently moving transmitting and receiving antenna has the potential to conduct parallel endfire oriented CMP surveys. It is believed that this technique, being capable of overcoming adverse active layer

effects, would be a particularly ideal method to use in low Arctic environments where the permafrost table is at a greater depth such that the active layer thickness is greatest here.

While proven successful in the Thomas Lee Inlet setting, our understanding of the Brewster angle technique to GPR CMP surveys would benefit from further testing over a broader range of permafrost targets. For example, article two tests this technique over a two layer model where the ground ice deposit begins at the active layer and permafrost boundary. Tests of this method over ground ice deposits originating deeper below the permafrost table (i.e. with an upper boundary of frozen sediment) would reveal whether this technique is transferable to multi-layer models.

In summary, the GPR techniques presented in this thesis has proven to be capable of:

1) Constraining the volumetric fraction of ice content in permafrost through methods using velocity analysis of CMP surveys, and
2) Determining the dielectric properties of a basal unit using parallel endfire antenna orientations and the Brewster angle of incidence.

The ability to remotely determine the ice content in permafrost will enable geomorphologists to constrain theories on the type and formation process of ground ice deposits whilst aiding in the assessment of suitable building sites in northern communities. The success of the Brewster angle of incidence method by Reppert et al. [2000] in determining the dielectric properties according to the reflection coefficient is encouraging for horizons near the penetration limit of GPR systems, though the true potential of this technique can only be realized with further studies of its application in cryosphere environments. Together, these findings demonstrate that GPR is a tool useful tool, capable of characterizing the ice content of the subsurface using small and efficient high-frequency systems. In closing, it is the author's hope that realization of these qualities will

encourage those within the periglacial and glacial scientific communities to continue experimenting with innovative and diverse GPR techniques while inspiring members of the planetary science community to foster the development of GPR systems for future exploration.

5.1 BIBLIOGRAPHY

Andersland, O. B., and B. Ladanyi (1994), *Frozen Ground Engineering*, 352 pp., Chapman & Hall, London, England.

De Pascale, G. P., Pollard, W. H, Williams, K. K. (2008), Geophysical mapping of ground ice using a combination of capacitive coupled resistivity and ground-penetrating radar, Northwest Territories, Canada, *Journal of Geophysical Research, 113.*

Fujita, S., T. Matsuoka, T. Ishida, K. Matsuoka, and S. Mae (2000), A summary of the complex dielectric permittivity of ice in the megahertz range and its applications for radar sounding of polar ice sheets, paper presented at Physics of Ice Core Records, Shikotsukohan, Hokkaido, Japan, September 14-17, 1998.

Koh, G. (1997), Dielectric properties of ice at millimeter wavelengths, *Geophys. Res. Lett.*, *24*(18), 2311-2313.

Kovacs, A., and R. M. Morey (1978), Radar Anisotropy of Sea Ice Due to Preferred Azimuthal Orientation of the Horizontal c Axes of Ice Crystals, *J. Geophys. Res.*, *83*(C12), 6037-6046.

Lalumiere, L. (2006), Ground Penetrating Radar for Helicopter Snow and Ice Surveys*Rep.*, 48 pp, Bedford Institude of Oceanography, Dartmouth, Nova Scotia.

Lock, G. S. H. (1990), *The Growth and Decay of Ice*, 434 pp., Cambridge University Press, Cambridge, England.

Millar, D. H. M. (1982), Acidity levels in ice sheets from radio echo-sounding, *Annals of Glaciology*, *3*, 5.

Moore, J. C., and S. Fujita (1993), Dielectric Properties of Ice Containing Acid and Salt Impurity at Microwave and Low Frequencies, *J. Geophys. Res.*, *98*(B6), 9769-9780.

Reppert, P. M., F. D. Morgan, and M. N. Toksöz (2000), Dielectric constant determination using ground-penetrating radar reflection coefficients, *Journal of Applied Geophysics*, *43*(2-4), 189-197.

Tison, J.-L., and J. Haren (1989), Isotopic, chemical and crystallographic characteristics of first-year sea ice from Breid Bay (Princess Ragnhild Coast - Antarctica), *Antarctic Science*, *1*(3), 8.

6 APPENDIX 1: GPR Surveys

This document provides a summary of GPR surveys and associated survey parameters for field studies conducted on ground ice deposits on Ellesmere Island and Devon Island, Nunavut, in the summer of 2010. Briefly, field surveying methods involved the following:

1) Finding and confirming the existence of a ground ice deposit according to visible ice exposures, test pits dug to the permafrost table, or probing with a permafrost probe.

2) Establishing a survey transect above the deposit and installing a survey line with knots at every 5 cm and flags at every 25 cm.

3) Conducting a common-offset (CO) survey along the 3 m transect.

4) Conducting common-midpoint (CMP) and walk-away (WA) surveys, centred at 1.5 m, along the transect line using four antenna orientations.

5) Excavating the active layer sediments along the transect, thus creating a trench ~3.5 m long, 1 m wide, and 0.5-0.8 m deep, depending on the depth to the ice deposit. A tarp was laid down in the trench (metal eyelets removed) to minimize the amount of mud in contact with the antenna. The survey line was then reinstalled inside the trench.

6) Repeating steps 3 and 4 inside the trench.

When GPR systems with different operating frequencies were available, additional surveys were conducted with these systems and generally on the overburden, rather than in the trench.

While most of the CMP surveys are analyzed and discussed in the two manuscripts of this thesis, walk-away WA surveys, cross-polar surveys, and studies conducted at two additional sites on Ellesmere Island were not included because (1) velocities derived from CMP surveys were generally more clear and self-consistent for determining the dielectric properties of ice, (2)

cross-polar data did not show any distinct variation from surveys conducted under regular orientation other than returning a weaker signal to the surface in most cases, and (3) time constraints did not allow for on-ice measurements to be made at the Wolf Slump site on Ellesmere Island, or again at higher stacking levels on Le Dump Slump. Indeed, very early in field studies it was established that signal stacking levels greater than 4 were needed to acquire signal return sufficient enough to identify hyperbolic features for velocity analysis and thus, the on-ice measurements at Le Dump Slump resulted in noisy radargrams.

Each series of surveys, listed below according to field site, is accompanied by an image of the target which, in the case of the Thomas Lee Inlet and Gully sites on Devon Island, illustrate where the surveys were conducted over the ground ice deposits. The tables identify the file name associated with the recorded data file (*.DTI), header file (*.HD), and configuration settings (*.ini) for the Sensors and Software Ekko_View and Ekko_View Deluxe software suites, as well as the date of data collection (2010), the target material which the antenna are in contact with, the survey type, the antenna orientation (see Figure A1-1), the operating frequency, the starting position of the antenna in the survey along the transect line (minimum separation for CMP), the final position of the antenna (maximum separation for CMP), the step size (referring to the net increase in antenna separation between each antenna in CMP surveys, or the increment of progression of the two antenna at a fixed separation for common-offset surveys(CO), along the transect line), antenna separation (being the fixed separation for CO surveys or the starting separation for CMP surveys), the number of stacks (DynaQ is a mode allowing for the maximum number of stacks possible while collecting CO data using an odometer), and the geographical orientation of the transect and the positioning of Tx and Rx along it.

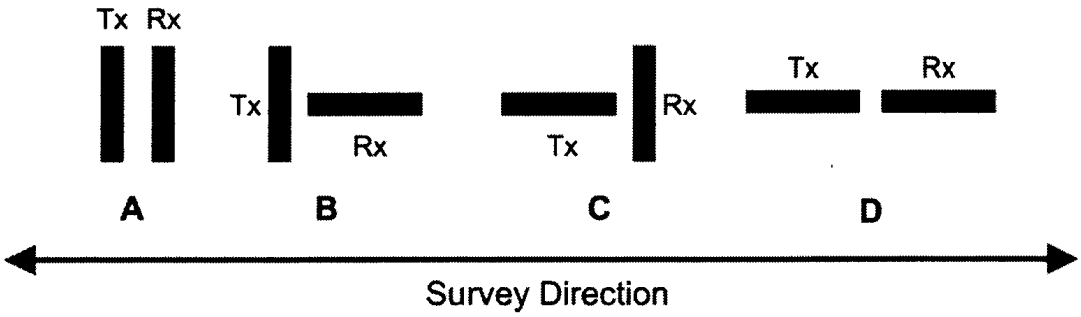

Figure A1-1. GPR antenna orientations Reg. (A), Rx 90 CW (B), Tx 90 CCW (C), and Tx and Rx (D). The rotation of the receiver and transmitter are denoted as clockwise (CW) and counter-clockwise (CCW) rotation, and the rotations were chosen in such a way to minimize the coiling and interference of cables over the transect line from the antenna to the GPR console. In scenario D, the Tx was rotated 90 degrees CCW and Rx was rotated 90 degrees CW.

Le Dump Slump, Ellesmere Island, Nunavut
79°58'53"N 85°47'16" W

File	Date	Target	Type	Orientation	Freq. (MHz)	Start Pos. (cm)	Final Pos. (cm)	Step Size (cm)	Antenna Sep. (cm)	Stacks	Compass (Tx to Rx)
SLUMP2	9-Jul	Ice	CMP	Reg.	450	25	300	5	25	4	NS
SLUMP3	9-Jul	Ice	CMP	Rx 90 CW	450	25	300	5	25	4	NS
SLUMP4	9-Jul	Ice	CMP	Tx 90 CCW	450	25	300	5	25	4	NS
SLUMP5	9-Jul	Ice	CMP	Tx and Rx	450	25	300	5	25	4	NS
DSCMP1	15-Jul	Active Layer	CMP	Reg.	450	25	300	5	25	32	NS

Figure A1-2. Exposed ice at slump feature located in the vicinity of the Eureka dump with W. Pollard for scale. Arrow indicates the location of 3 m surveys.

South Slidre Fiord, Ellesmere Island, Nunavut
79°55'43"N 86°01'58"W

File	Date	Target	Type	Orientation	Freq. (MHz)	Start Pos. (cm)	Final Pos. (cm)	Step Size (cm)	Antenna Sep. (cm)	Stacks	Compass (Tx to Rx)
SS2	11-Jul	Ice	CO	Reg.	450	25	297.5	2.5	25	4	NS
SS3	11-Jul	Ice	CMP	Multiple	450	25	82.5	5	25	16	NS
SS6	11-Jul	Ice	CO	Tx and Rx	450	25	270	5	25	32	NS
SSICE1	12-Jul	Ice	CMP	Reg.	450	25	300	5	25	32	NS
SSICE2	12-Jul	Ice	CMP	Rx 90 CW	450	25	260	5	25	32	NS
SSICE3	12-Jul	Ice	CMP	Tx 90 CCw	450	25	260	5	25	32	NS
SSICE4	12-Jul	Ice	CMP	Tx and Rx	450	25	260	5	25	32	NS
SSICE5	12-Jul	Ice	CO	Reg.	450	25	265	2.5	25	32	NS

*Test survey to assess the influence of changed survey orientations at this site.

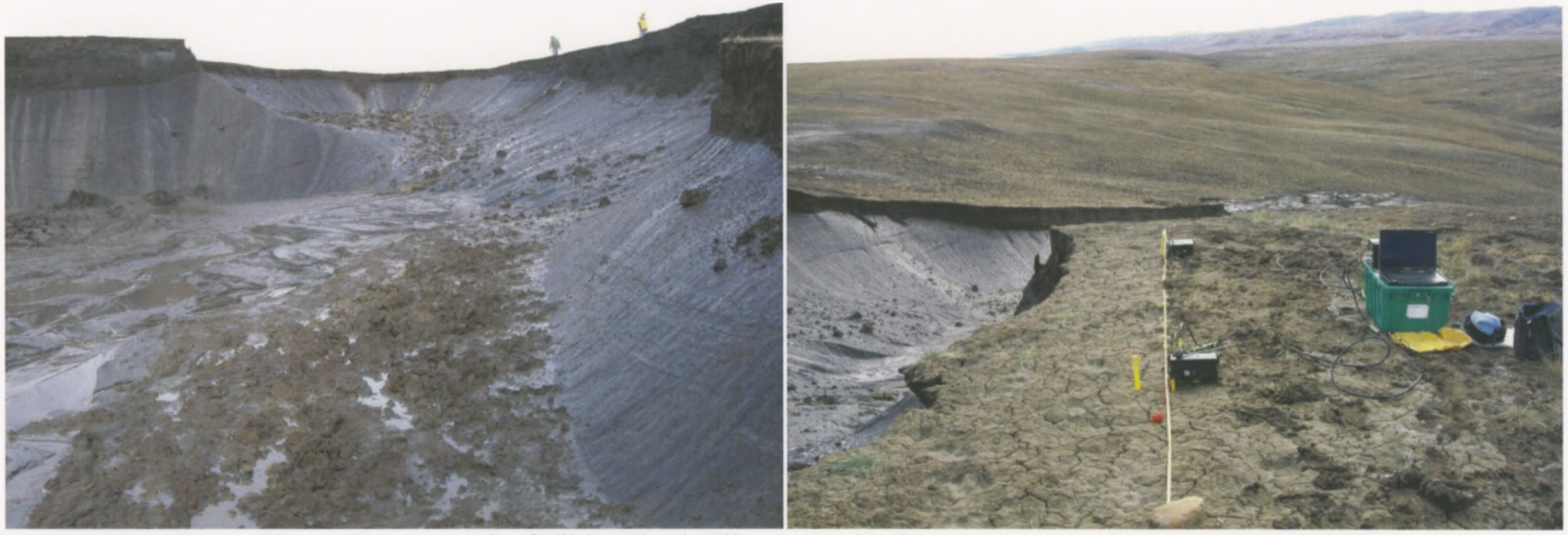

Figure A1-3. Right: Slump feature south of Slidre Fiord, Ellesmere Island with several metres of exposed stratified segregation ice. Left: Location of overburden surveys at the site. This transect line was then excavated for on-ice surveys.

Wolf Slump, Ellesmere Island, Nunavut
79°54'13"N 84°52'01"W

File	Date	Target	Type	Orientation	Freq. (MHz)	Start Pos. (cm)	Final Pos. (cm)	Step Size (cm)	Antenna Sep. (cm)	Stacks	Compass (Tx to Rx)
WOLF2	16-Jul	Active Layer	CO	Reg.	450	25	300	5	25	32	NS
WOLF3	16-Jul	Active Layer	CMP	Rx 90 CW	450	25	200	5	25	32	NS
WOLF4	16-Jul	Active Layer	CMP	Tx 90 CCw	450	25	200	5	25	32	NS
WOLF5	16-Jul	Active Layer	CMP	Tx and Rx	450	25	200	5	25	32	NS

Unfortunately, no photos are available for this site.

Thomas Lee Inlet, Devon Island, Nunavut
75°21'29" N 88°40'52" W

File	Date	Target OVERBURDEN	Type	Orientation	Freq. (MHz)	Start Pos. (cm)	Final Pos. (cm)	Step Size (cm)	Antenna Sep. (cm)	Stacks	Compass (Tx to Rx)
Line00	31-Jul	AB	CO	Reg.	100	1	2000	25	100	128	NS
Line01	31-Jul	AB/EF centred on 5m	CMP	Reg.	100	50	600	50	50	128	NS
Line02	31-Jul	AB/EF Tx on 2m, Rx 2.5m	WA	Reg.	100	50	600	25	50	128	NS
Line03	31-Jul	AB centred on 15m	CMP	Reg.	100	50	650	50	50	128	NS
Line04	31-Jul	AB Tx on 18m, Rx 17.75m	WA	Reg.	100	50	600	25	50	128	NS
Line05	31-Jul	CD	CMP	Reg.	100	50	300	50	50	128	WE
Line06	31-Jul	CD	WA	Reg.	100	50	325	25	50	128	WE
Line07	31-Jul	AB	CO	Reg.	200	0	1950	10	50	128	NS
Line08	31-Jul	AB/EF centred on 5m	CMP	Reg.	200	40	600	20	40	128	NS
Line09	31-Jul	AB/EF Tx on 2m, Rx 2.5m	WA	Reg.	200	40	750	10	40	128	NS
Line10	31-Jul	AB centred on 15m	CMP	Reg.	200	40	600	20	40	128	NS
Line11	31-Jul	AB Tx on 18m, Rx 17.75m	WA	Reg.	200	40	770	10	40	128	NS
Line12	31-Jul	CD	CMP	Reg.	200	40	300	20	40	128	WE
Line13	31-Jul	CD	WA	Reg.	200	40	300	10	40	128	WE
TL1	31-Jul	AB 5-10m transect	CO	Reg.	450	0	1000	5	25	64	NS
TL2	31-Jul	CD	CO	Reg.	450	0	300	2.5	25	64	WE
TL3	31-Jul	CD	CMP	Reg.	450	25	282*	5	25	64	WE
TL4	31-Jul	CD	CMP	Rx 90 CW	450	25	287*	5	25	64	WE
TL5	31-Jul	CD	CMP	Tx 90 CCW	450	25	287	5	25	64	WE
TL6	31-Jul	CD	CMP	Tx and Rx	450	25	287	5	25	64	WE
TL7	31-Jul	CD	WA	Reg.	450	25	305	5	25	64	WE

TL8	31-Jul	CD	WA	Rx 90 CW	450	25	300	5	25	64	WE
TL9	31-Jul	CD	WA	Tx 90 CCW	450	25	300	5	25	64	WE
TL10	31-Jul	CD	WA	Tx and Rx	450	25	300	5	25	64	WE
TL11	31-Jul	CD	WA	Reg. reverse	450	25	300	5	25	64	EW
TL12	1-Aug	EF	CO	Reg.	450	25	300	2.5	25	64	NS
TL13	1-Aug	EF	CMP	Reg.	450	25	300	5	25	64	NS
TL14	1-Aug	EF	CMP	Rx 90 CW	450	25	300	5	25	64	NS
TL15	1-Aug	EF	CMP	Tx 90 CCW	450	25	300	5	25	64	NS
TL16	1-Aug	EF	CMP	Tx and Rx	450	25	300	5	25	64	NS
TL17	1-Aug	EF	WA	Reg.	450	25	300	5	25	64	NS
TL18	1-Aug	EF	WA	Rx 90 CW	450	25	300	5	25	64	NS
TL19	1-Aug	EF	WA	Tx 90 CCW	450	25	300	5	25	64	NS
TL20	1-Aug	EF	WA	Tx and Rx	450	25	300	5	25	64	NS
TL21	1-Aug	EF	WA	Reg. reverse	450	25	300	5	25	64	NS

File	Date	Target ICE	Type	Orientation	Freq. (MHz)	Start Pos. (cm)	Final Pos. (cm)	Step Size (cm)	Antenna Sep. (cm)	Stacks	Compass (Tx to Rx)
TL23	1-Aug	CD	CMP	Reg.	450	25	250	5	25	64	WE
TL24	1-Aug	CD	CMP	Rx 90 CW	450	20	250	5	25	64	WE
TL25	1-Aug	CD	CMP	Tx 90 CCW	450	20	250	5	25	64	WE
TL26	1-Aug	CD	CMP	Tx and Rx	450	20	250	5	20	64	WE
TL27	1-Aug	CD	WA	Reg.	450	25	250	5	25	64	WE
TL32	1-Aug	EF	CO	Reg.	450	12.5	287.5	2.5	25	64	NS
TL33	1-Aug	EF	CMP	Reg.	450	20	305	5	25	64	NS
TL34	1-Aug	EF	CMP	Rx 90 CW	450	20	300	5	25	64	NS
TL35	1-Aug	EF	CMP	Tx 90 CCW	450	20	30	5	25	64	NS
TL36	1-Aug	EF	CMP	Tx and Rx	450	20	300	5	25	64	NS
TL37	1-Aug	EF	WA	Reg.	450	25	300	5	25	64	NS
TL41	1-Aug	EF	WA	Reg. reverse	450	25	300	5	25	64	NS

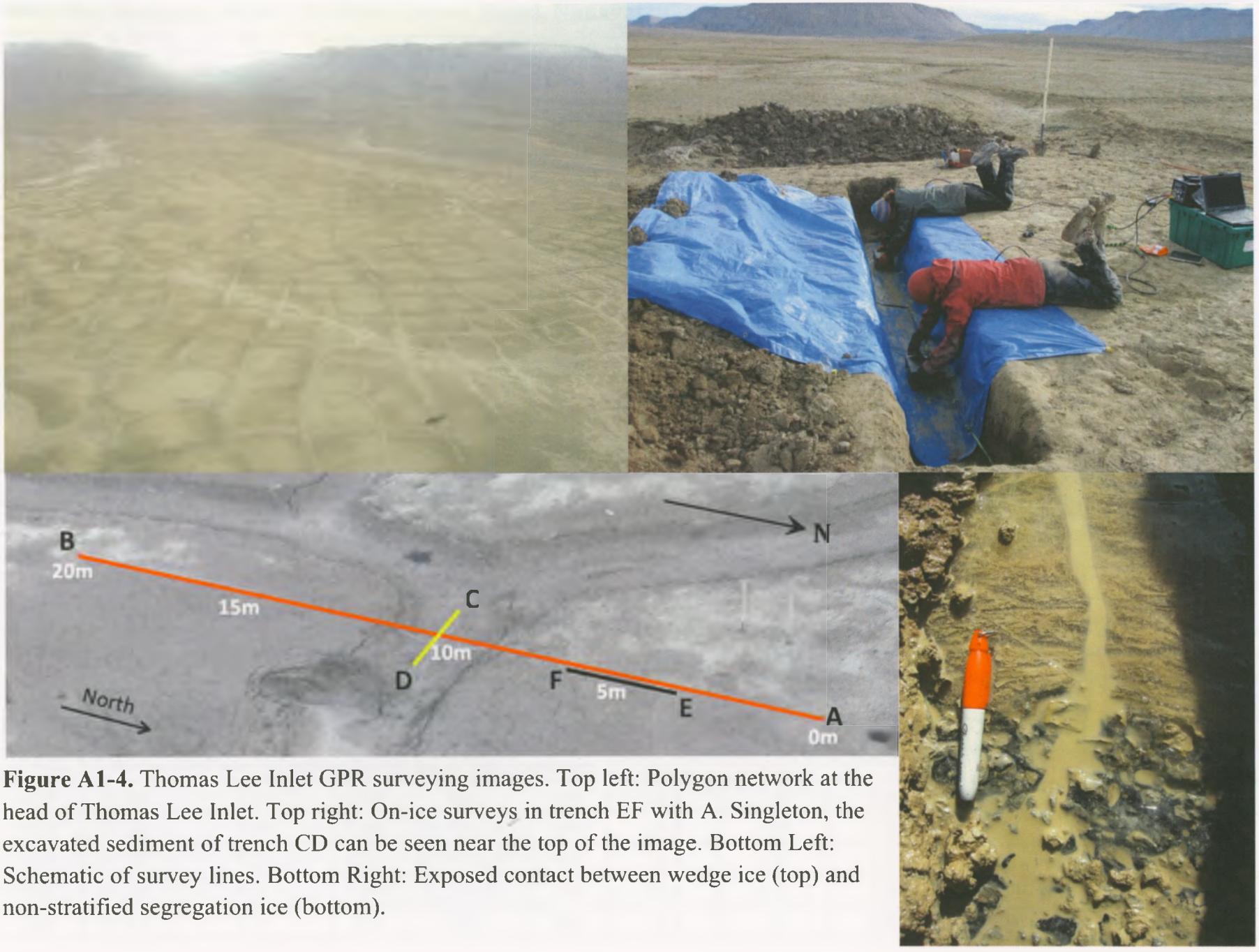

Figure A1-4. Thomas Lee Inlet GPR surveying images. Top left: Polygon network at the head of Thomas Lee Inlet. Top right: On-ice surveys in trench EF with A. Singleton, the excavated sediment of trench CD can be seen near the top of the image. Bottom Left: Schematic of survey lines. Bottom Right: Exposed contact between wedge ice (top) and non-stratified segregation ice (bottom).

Gully site, Haughton impact structure, Devon Island, Nunavut
75°22'06" N 89°31'33" W

File	Date	Target OVERBURDEN	Type	Orientation	Freq. (MHz)	Start Pos. (cm)	Final Pos. (cm)	Step Size (cm)	Antenna Sep. (cm)	Stacks	Compass (Tx to Rx)
G1	30-Jul	AB overburden	CO	Reg.	450	0	995	5	25	128	WE
G2	30-Jul	CD overburden	CO	Reg.	450	0	302.5	2.5	25	128	NS
G3	30-Jul	CD overburden	CMP	Reg.	450	20	300	5	20	128	NS
G4	30-Jul	CD overburden	CMP	Rx 90 CW	450	20	300	5	25	128	NS
G5	30-Jul	CD overburden	CMP	Tx 90 CCW	450	20	300	5	25	128	NS
G6	30-Jul	CD overburden	CMP	Tx and Rx	450	25	300	5	25	128	NS
G7	30-Jul	CD overburden	WA	Reg.	450	25	300	5	25	128	NS
G8	30-Jul	CD overburden	WA	Rx 90 CW	450	25	300	5	25	128	NS
G9	30-Jul	CD overburden	WA	Tx 90 CCW	450	25	300	5	25	128	NS
G10	30-Jul	CD overburden	WA	Tx and Rx	450	25	300	5	25	128	NS
G11	30-Jul	DC overburden	WA	Reg. reverse	450	25	300	5	25	128	NS
G12	30-Jul	AB overburden	CO	Reg.	100	0	2500	25	100	DynaQ	WE
G13	30-Jul	AB overburden	CO	Reg.	50	0	2500	50	100	DynaQ	WE
G14	30-Jul	AB overburden	CO	Reg.	200	0	2500	10	50	DynaQ	WE
G15	30-Jul	CD overburden	WA	Reg.	100	25	300	25	25	128	NS
G16	30-Jul	CD overburden	WA	Reg.	200	25	355	10	10	128	NS

File	Date	Target ICE	Type	Orientation	Freq. (MHz)	Start Pos. (cm)	Final Pos. (cm)	Step Size (cm)	Antenna Sep. (cm)	Stacks	Compass (Tx to Rx)
G17	31-Jul	CD	CO	Reg.	450	12.5	2.875	2.5	25	64	
G18-22	* Shorter CMP surveys were collected due to time constraints										
G18	31-Jul	CD	CMP	Reg.	450	12.5	1.5	2.5	25	64	NS
G19	31-Jul	CD	CMP	Rx 90 CW	450	12.5	1.55	2.5	25	64	NS
G20	31-Jul	CD	CMP	Tx 90 CCW	450	12.5	1.5	2.5	25	64	NS
G21	31-Jul	CD	CMP	Tx and Rx	450	12.5	1.5	2.5	25	64	NS
G22	31-Jul	CD	WA	Reg.	450	12.5	1.5	2.5	25	64	NS

G23-25	* WA surveys at other orientations not run at this site due to time constraints										
G26	31-Jul	CD	WA	Reg. reverse	450	12.5	1.5	2.5	25	64	SN
G27	10-Aug	CD	CO	Reg.	900	7.5	292.5	2.5	15	64	NS
G28	10-Aug	CD	CMP	Reg.	900	15	300	5	15	64	NS
G29	10-Aug	CD	CMP	Rx 90 CW	900	20	300	5	20	64	NS
G30	10-Aug	CD	CMP	Tx 90 CCW	900	20	300	5	20	64	NS
G31	10-Aug	CD	CMP	Tx and Rx	900	25	300	5	25	64	NS
G32	10-Aug	CD	WA	Reg.	900	15	300	5	15	64	NS

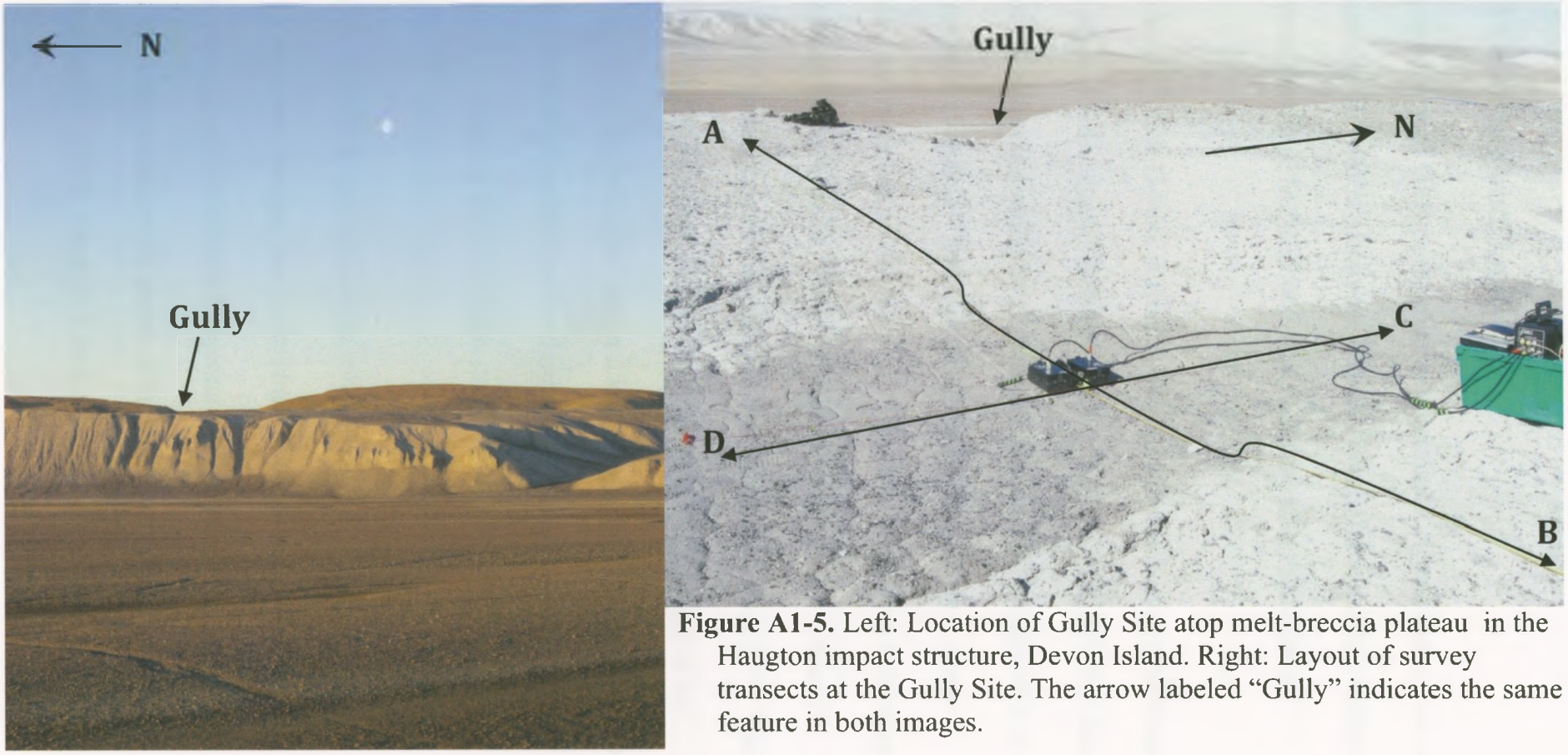

Figure A1-5. Left: Location of Gully Site atop melt-breccia plateau in the Haugton impact structure, Devon Island. Right: Layout of survey transects at the Gully Site. The arrow labeled "Gully" indicates the same feature in both images.

7 APPENDIX 2: GPR Processing and Analysis

This document provides a summary of GPR post-processing methods. Specific attention will paid to those techniques associated with velocity analysis, velocity corrections, and conversion of these results into dielectric permittivity. CMP and WA analysis progressed as follows:

1) In the EKKO_View 2 and EKKO_View Deluxe software, provided by Sensors and Software Ltd., CMP and WA files were studied individually. Before velocity analysis, each file was post-processed to draw out hyperbolic features associated with changes in dielectric permittivity. In nearly all cases, the "Recommended Processing" function provided in the 'Settings' menu of EKKO_View 2 provided suitable enhancement of the features. This function varies according to the dataset, but for all files this function involved a "Dewow" filter to remove low frequency ringing, and most often a SEC2 gain function with Attenuation factors ranging from 5-10, Start Gain values from 1-5, and Maximum Gain values between 200 and 500. Adjustment of the default parameters occurred if the direct wave signal and/or underlying hyperbolic features were present but weak, and these adjustments generally involved increasing the attenuation factor (especially in clay rich settings) or increasing the maximum gain.

2) Once the direct wave and hyperbolic features were clear, velocities were picked. The direct wave velocity was calculated by approximating a line to the slope of the first arrivals (the air wave was non-existent or very weak given that shielded antenna were used). At this point, the time-zero was also checked by assessing whether the slope of the direct wave intersected with the 0-0 mark on the Antenna Separation versus Time plot, and corrected for if necessary using

the Time Zero correction function in EKKO_View Deluxe. These velocities were recorded in a spreadsheet for each CMP and WA file.

3) The "Hyperbola Velocity Calibration" function in the "Tools" menu of Ekko_View was then used to calculate the radar wave propagation velocity associated with each hyperbolic feature. This function allows for manual adjustment of the arrival time and curvature of a hyperbola. Arrival times were always picked from an antenna separation of 0 m, and the curvature was adjusted so that the feature agreed with the strongest and most continuous hyperbolic features in the radargram. For each file, the arrival times and associated velocities of hyperbolic features were recorded chronologically following the direct wave measurements.

4) The continued analysis involved correcting the velocities to account for the effect of wave propagation speeds in overlying layers on the observed velocity of underlying layers, following from the method developed by Tillard and Dubois [2003] (the details of which are described in the first manuscript). For each target, a velocity matrix (Vx) was created where rows referred to different surveys (i.e. CMP and WA surveys at each of the orientations) and columns referred to the successive velocities picked from hyperbolic features in the radargram. Similarly, a matrix of equal dimensions was created for the hyperbolic feature arrival times (Tx). The Matlab script used for correcting the observed velocities using the Dix equation, Vx, and Tx, follows:

```
% GPR Velocity Analysis
% By Laura Thomson, March 25, 2011
% Variables
% Vx - hyperbolic velocities
% Tx - time picks of velocities
% Note size Tx == size Vx

Vx = Vx;
Tx = Tx;
```

```
% Velocity spectrums
Vx

% Squaring Vx
Vrms = Vx.^2;

% Dix Equation, note Vrms values are already squared
% V1 = sqrt(Vrms(1,:));
% V2 = sqrt(((Tx(2,:).*Vrms(2,:)) - (Tx(1,:).*Vrms(1,:))) ./ (Tx(2,:)-
Tx(1,:)));
% V3 = sqrt(((Tx(3,:).*Vrms(3,:)) - (Tx(2,:).*Vrms(2,:))) ./ (Tx(3,:)-
Tx(2,:)));
% etc.

% Written as a loop...
[i,j] = size(Vx);
for a=1:i-1
V1 = sqrt(Vrms(1,:));
Vdix(a,:) = sqrt(abs(((Tx(a+1,:).*Vrms(a+1,:)) - (Tx(a,:).*Vrms(a,:))) ./
(Tx(a+1,:)-Tx(a,:))));
end

VDix = [V1;Vdix]
```

5) The corrected velocities (VDix) were then converted to dielectric permittivities using the following script:

```
% Converting to Dielectric (E) assuming non-magnetic material
Er = (0.3./VDix).^2
```

6) Finally, the true depths of the dielectric horizons were calculated using the observed velocities (true radar wave propagation speeds) and the two-way travel time arrivals in Tx.

7) Given the overall greater quality, according to strength and clarity, of the regular orientation CMP surveys in comparison with both WA surveys and the other antenna orientations, the dielectric profiles from these surveys were most suited for addressing the objectives of manuscript one (Figure A2-1).

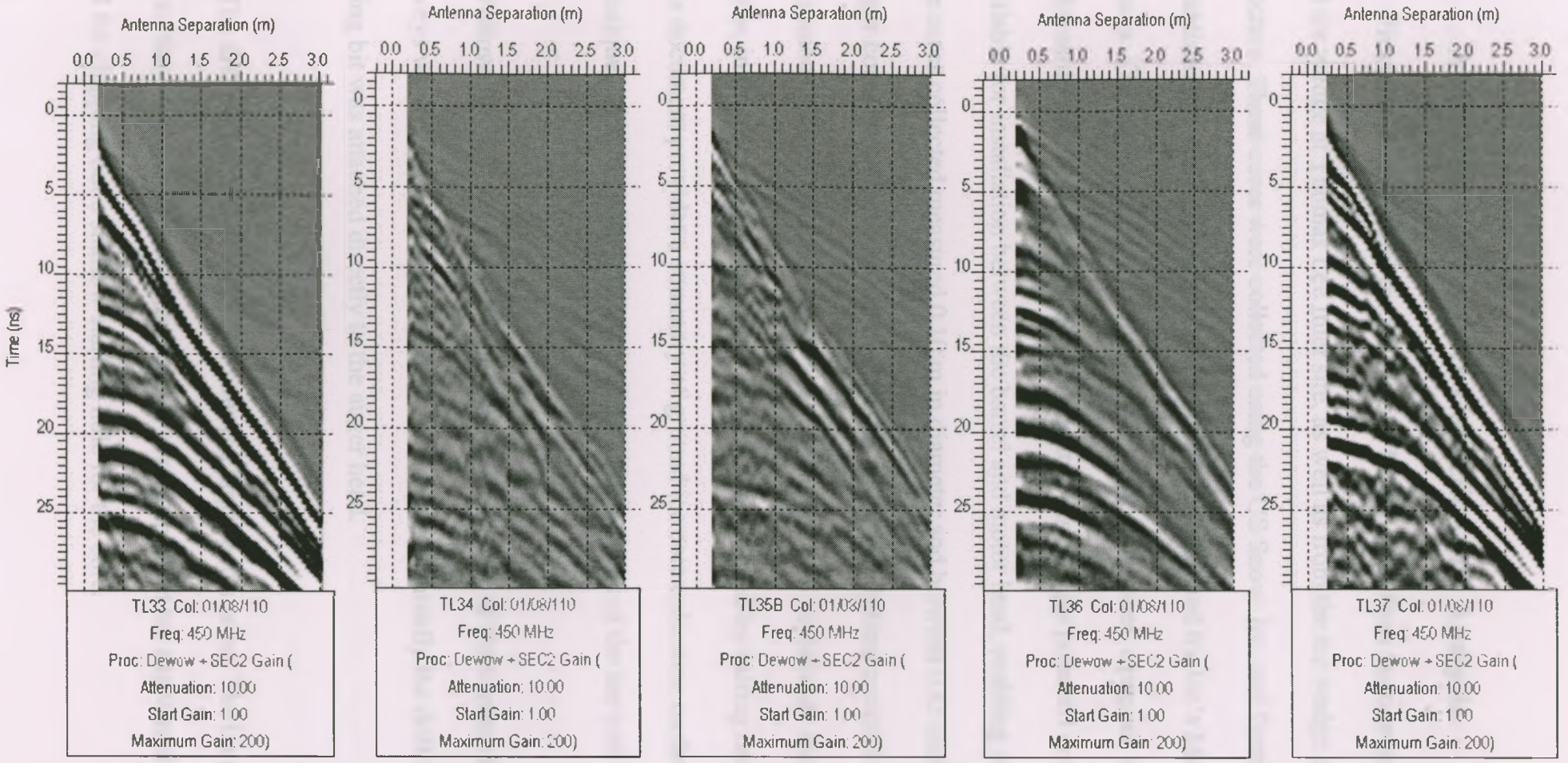

Figure A2-1. On-ice radargrams from the non-stratified segregation ice at Thomas Lee Inlet, Devon Island. From left to right: Regular orientation CMP (TL33); Rx rotated 90° clockwise CMP (TL34); Tx rotated 90° counter-clockwise (TL35B); Tx and Rx rotated 90° clockwise and counter-clockwise, respectively (TL36); and Regular orientation WA (TL37). The above radargrams, having undergone the same post-processing (being a SEC2 Gain with Dewow, Attenuation= 10, Start Gain = 1, and a Maximum Gain = 200), show the relative signal strength and clarity between antenna orientations and survey design.

8 APPENDIX 3: Ice Core Collection and Analysis

Field logistics allowed for ice cores to be collected from the non-stratified segregation ice and ice wedge at Thomas Lee Inlet site, as well as from the ice wedge in the Haughton impact structure. These cores were collected using the US Snow, Ice, and Permafrost Research Establishment (SIPRE) designed core auger, manufactured by Jon's Machine Shop in Fairbanks, Alaska. The auger system in comprised of a 1 m core barrel, equipped with removable and replaceable carbide tip cutting bits, which attaches to a gas powered drive motor. Extensions are available for installation between the barrel and motor head, enabling drilling up to 4m depth. The cores collected measured 0.10 m in diameter and between 0.85 and 0.95 m in length. While longer cores would have been beneficial for the study, drilling methods were inhibited by the continuous collapse of the trench walls. Having the drill bit become stuck, and subsequently frozen, in the permafrost was also a risk that was avoided by halting drilling at a depth of 1 m. This document provides a summary of ground ice core collection methods and analysis techniques used to create physical and chemical profiles of the ice with depth.

1) Following GPR surveys within the trench the middle of the transect line, where the CMP surveys were centred, was cleared of mud and debris. Initially the drill was assembled so that the coring bit was attached directly to the auger head.

2) The drill was held by two people over the target and started. The bit tended to skip across the ice surface before biting into the ice, and in retrospect an ice axe would have been a beneficial tool for chipping out a shallow starting hole for the core.

3) Once the drill was catching, the throttle of the auger was maintained at a constant pace and the weight of the motor head was enough to draw the bit into the ice deposits. After every 20 cm gain in depth (approximately), the drill shaft was rapidly drawn up to just below the surface, so as to clear the flights of ice shavings, and then lowered once again. Ice shaving were cleared away from the drill hole while drilling with our boots so that they did not re-enter the hole.

4) At a depth of approximately 70 cm, it became necessary to remove the drill from the hole so that an extension could be added between the bit and motor head, allowing for deeper drilling. When removed from the hole, the ice core always stayed inside the core shaft so that the core retriever in the drill kit was never needed.

5) To remove the top part of the core from the barrel, the motor head was removed as well as the connector at the top of the drill shaft. As this piece often became engrained with mud, it was often necessary to use a rock hammer to persuade the piece to come off the core barrel. Once removed, the core was pushed backwards out of the drill barrel using the handle of a rock hammer. Again, an ice axe, having a longer handle, would have been helpful.

6) Once removed, the ice core was double bagged in long core bags, labeled according to site, segment, and orientation, subsequently put into PVS core tubes, then stored in a cooler.

7) Coring was then resumed, using an extension if necessary for deeper segments, until a depth of 1 m was reached.

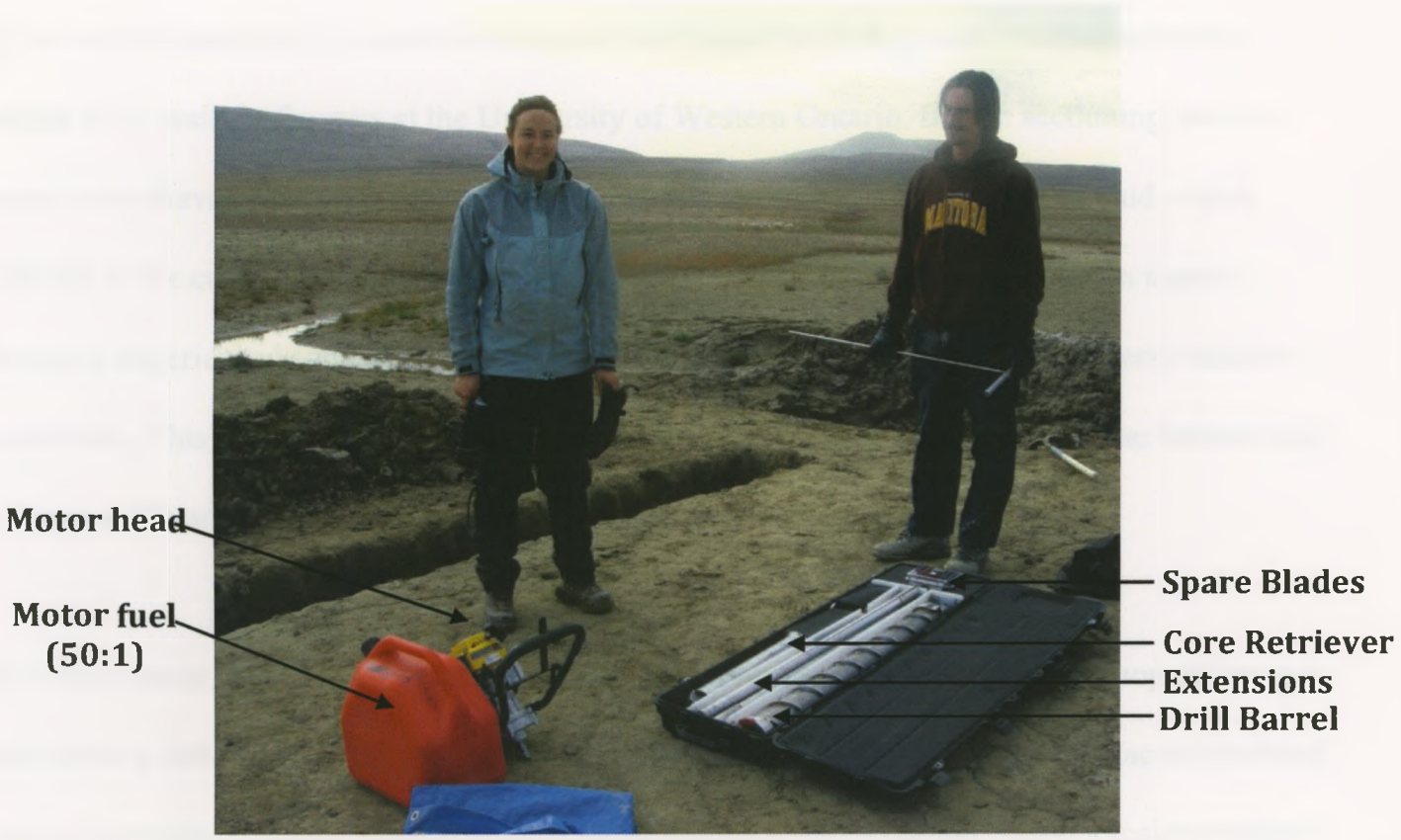

Figure A3-1. Top: Permafrost drill with parts indicated; C. Marion and T. Unrau for scale. Bottom: Drilling with C. Marion in the trench over an ice wedge at Thomas Lee Inlet, Devon Island.

8) As soon as possible, ice cores were moved to a freezer until they were transported to the minus 25°C walk-in freezers at the University of Western Ontario. Before sectioning, the ice cores were shaved along the edges using a hand saw to remove a frozen film of mud, which adhered to the cores during the drilling process. Also, the cores from the Haughton impact structure experienced some thawing during to a five day delay at camp due to adverse weather conditions. This resulted in a small amount of pooled water to be refrozen along the bottom edge of these cores and this feature was also scrapped off using a hand saw.

9) In the freezer, each core was sectioned into 5 cm long segments, starting at the top of the core and moving downwards with increasing depth. The segments were individually placed in labeled plastic bags and weighed (while frozen) with an accuracy of 0.01 grams, using a scale provided by Dr. S. Hicock.

10) The cores segments were then thawed, allowing the sediment to settle to the base of the bags.

11) In the lab of Dr. G. Southam, 250 ml of the clearest melt water was extracted from each bag using a syringe and filtered at 1.2 μm using Whatman GF/C glass microfilters into 250 ml falcon tubes, labeled according to core and segment depth. As such, between 17 to 19 water samples were acquired for each core.

12) Using a calibrated pH probe, H+ levels were measured to an accuracy of 0.01 on the logarithmic scale. Similarly, a conductivity meter was used to measure the conductivity of each

sample to an accuracy of 1 μS. For both measurements, the probes were rinsed with distilled water between samples.

13) The sediments remaining in the sample bags were transferred to labeled aluminum plates, each bag being rinsed with distilled water to ensure all the sediment was transferred, and allowed to dry in a drying oven at 38°C. To ensure that samples were dried sufficiently, samples were weighed each day until weight variation was <0.02 g.

14) Once dried, final sediment weights were taken with the scale tared to the weight of the aluminum pans, assumed to be of statistically similar weights. The methods described in the first manuscript of this thesis describe how the volumetric ice content was derived from the respective ice and sediment weights of each sample.

15) Finally, the pH, conductivity, and volumetric ice content results were compiled for each core in a spreadsheet, for later comparison with the dielectric profiles derived from the GPR data.

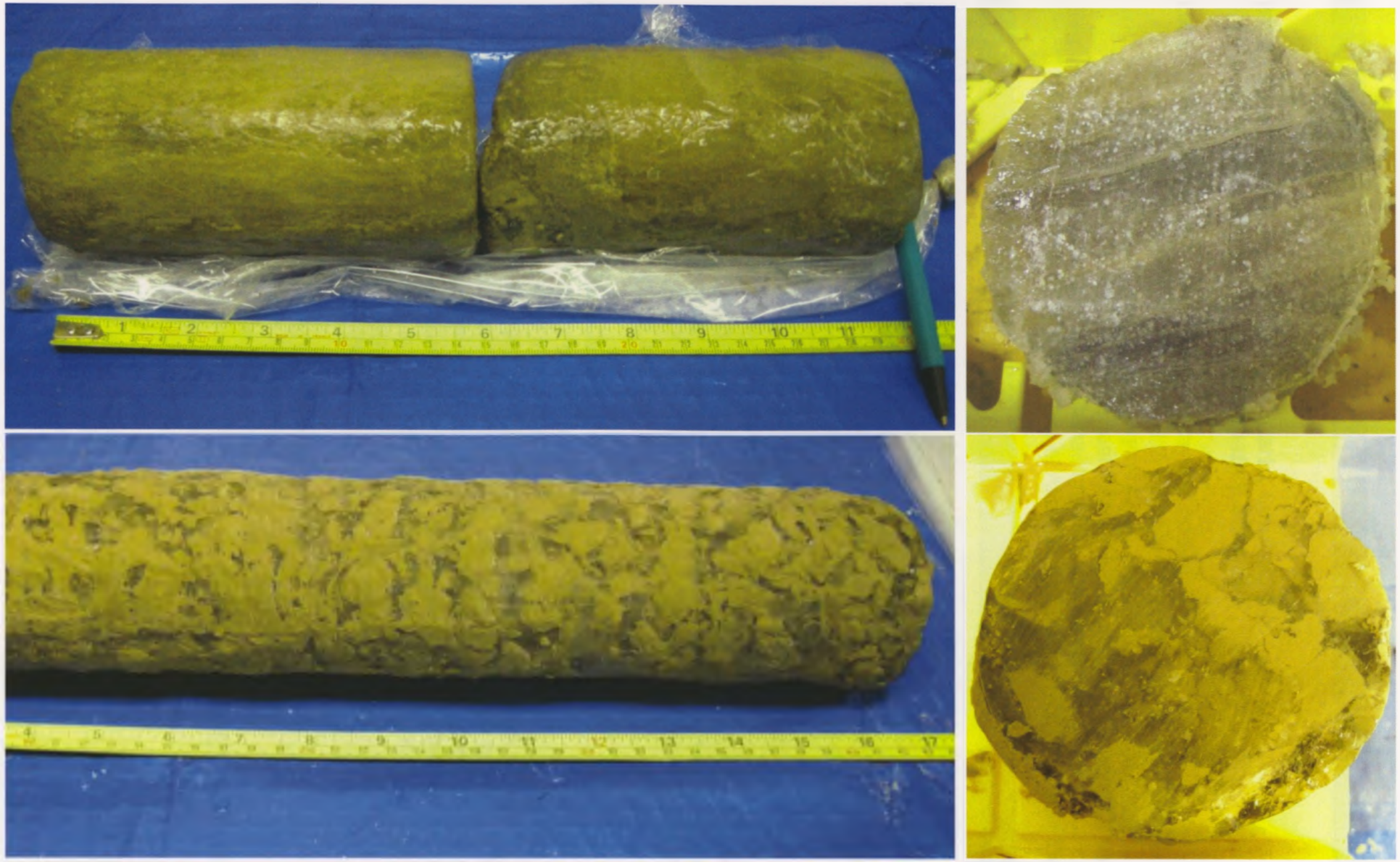

Figure A3-2. Examples of cores collected from Thomas Lee Inlet, Devon Island. Top: Ice wedge core and segment. Bottom: Non-stratified segregation ice core and segment.